# OFFICE OF CIVILIAN RADIOACTIVE WASTE MANAGEMENT
# SPECIAL INSTRUCTION SHEET

1. QA: QA

Page: 1 of: 1

*Complete Only Applicable Items*

**This is a placeholder page for records that cannot be scanned or microfilmed**

| 2. Record Date | 3. Accession Number |
|---|---|
| 6/28/00 | MOL.20000711.0192 |
| **4. Author Name(s)** | **5. Author Organization** |
| BLAIR S, WAGNER R, WILDER DG | N/A |

6. Title
CALCULATION COVER SHEET, CALCULATION OF PERMEABILITY CHANGE DUE TO COUPLED THERMAL-HYDROLOGICAL-MECHANICAL EFFECTS (C)

| 7. Document Number(s) | 8. Version |
|---|---|
| CAL-NBS-MD-000002 | REVISION 00 |
| **9. Document Type** | **10. Medium** |
| DESIGN DOCUMENT | OPTIC, PAPER |

11. Access Control Code
PUB

12. Traceability Designator
SEE BLOCK 7

13. Comments
THIS ONE OF A KIND COLOR RECORD WHICH CAN BE FOUND THRU THE RECORDS PROCESSING CENTER

# OFFICE OF CIVILIAN RADIOACTIVE WASTE MANAGEMENT

## CALCULATION COVER SHEET

1. QA: QA
Page: 1 of: 35

2. Calculation Title

Calculation of Permeability Change Due To Coupled Thermal-Hydrological-Mechanical Effects

3. Document Identifier (including Revision Number)

CAL-NBS-MD-000002 REV 00

| 4. Total Attachments | 5. Attachment Numbers – Number of pages in each: I-8, II-8, III-8, IV-8 |
|---|---|
| 4 | |

| | Print Name | Signature | Date |
|---|---|---|---|
| 6. Originator | Stephen Blair | Stephen C. Blair | 6/28/00 |
| 7. Checker | Ralph Wagner | Ralph Wagner | 27 Jun 00 |
| 8. Lead | Dale Wilder | Dale G. Wilder | 6/28/00 |

9. Remarks

Checker signed before originator because document was finalized on June 27, 2000 in Las Vegas. The author was in LLNL in California and the checker's vacation plans would impede timely delivery of this document .

**Revision History**

| 10. Revision No. | 11. Description of Revision |
|---|---|
| 00 | Initial Issue |

## CONTENTS

## FIGURES

Page

## FIGURES (Continued)

**Page**

# TABLES

**Page**

## ACRONYMS

| | |
|---|---|
| 3D | three-dimensional |
| 3DEC | Three Dimensional Distinct Element Code |
| CRWMS | Civilian Radioactive Waste Management System |
| DIRS | Document Input Reference System |
| DKM | dual permeability model |
| EDA | Enhanced Design Alternatives |
| ESF | Exploratory Studies Facility |
| NFE PMR | Near Field Environment Process Model Report |
| M&O | Management and Operating Contractor |
| OM | order of magnitude |
| QA | Quality Assurance |
| TBV | To Be Validated |
| TH | thermal-hydrological |
| THM | thermal-hydrological-mechanical |
| TM | thermal-mechanical |

# 1. PURPOSE

The purpose of this calculation is to provide a bounding estimate of how thermal-hydrological-mechanical (THM) behavior of rock in the region surrounding an emplacement drift in a Monitored Geologic Repository subsurface facility may affect the permeability of fractures in the rock mass forming the region. The bounding estimate will provide essential input to performance assessment analysis of the potential repository system. This calculation also supports the Near Field Environment Process Model Report (NFE PMR) and will contribute to Site Recommendation.

The geologic unit being considered as a potential repository horizon at Yucca Mountain, Nevada lies within a fractured, densely welded ash-flow tuff located in the Topopah Spring Tuff member of the Paintbrush Group. Fractures form the primary conduits for fluid flow in the rock mass. Considerable analysis has been performed to characterize the thermal-hydrologic (TH) behavior of this rock unit (e.g., CRWMS M&O 2000a, pp. 83-87), and recently the dual permeability model (DKM) has proved to be an effective tool for predicting TH behavior (CRWMS M&O 2000a). The DKM uses fracture permeability as a primary input parameter, and it is well known that fracture permeability is strongly dependent on fracture deformation (Brown, 1995). Consequently, one major unknown is how deformation during heating and cooling periods may change fracture permeability. Opening of fractures increases their permeability, whereas closing reduces permeability. More importantly, shear displacement on fractures increases their permeability, and fractures undergoing shear are likely to conduct fluids. This calculation provides a bounding estimate of how heating and cooling in the rock surrounding an emplacement drift and the resulting mechanical deformation may affect the fracture permeability of the rock.

Procedure AP-3.12Q, Rev. 0, ICN 1, *Calculations*; and the technical development plan for this calculation (CRWMS M&O 2000b) guided the preparation of this calculation document.

# 2. METHOD

The method used in this calculation is to simulate the thermal-hydrological-mechanical (THM) behavior of a region of fractured rock that surrounds a section of a long, horizontal emplacement drift in the Topopah Spring Tuff at Yucca Mountain. This calculation assumes that the major change in rock mass permeability due to thermal-mechanical TM effects will be caused by fracture deformation in the rock mass.

A distinct element numerical code-3DEC (Itasca Consulting Group, 1998) is used in this calculation to simulate TM behavior in a three-dimensional (3D) region of fractured rock surrounding an emplacement drift. The distinct element method was chosen because it allows discrete fractures to be incorporated into the calculation. This is important because deformation of fractures can cause large changes in fracture permeability, and continuum approaches do not provide direct estimates of fracture deformation. Boundary conditions and a thermal field equivalent to that expected in an emplacement drift, based on the EDA-II design (CRWMS M&O 1999a), are imposed on the region.

Fracture deformation values estimated at a series of times are used to compute permeability changes in a cross section perpendicular to the emplacement drift. The permeability changes are then contoured to produce input for the Performance Assessment analysis for the different thermal phases expected over the lifetime of a potential repository and to the NFE PMR.

Electronic management of data, as per AP-SV.1Q, Rev 0, ICN 1 and LLNL QP 3.8 (both procedures are invoked by the TDP, CRWMS M&O 2000b), was conducted as per the checklists completed and shown in CRWMS M&O 2000d, items E and F.

# 3. ASSUMPTIONS

The calculation assumptions discussed in this section were used for the THM calculations discussed in Section 5. General assumptions and the rationales for their use are discussed in Section 3.1 below. Specific assumed values for input parameters are given in Table 1 of Section 5.2. None of the assumptions used for this calculation require confirmation.

## 3.1 GENERAL ASSUMPTIONS FOR THERMAL MECHANICAL MODEL

### 3.1.1 Fracture Distribution

The fracture distribution used in this calculation (see Section 5.1) is based on fractures observed in field mapping studies (Albin et al. 1997, Drawings OA-46-296, OA-46-297, OA-46-298, and OA-46-299). The field studies indicate that fracturing in the middle nonlithophysal unit of the Topopah Spring Tuff can be reasonably represented by three mutually perpendicular fracture sets, with one set of fractures roughly parallel to the emplacement drift orientation. The three fracture sets used in the calculation are shown in Figure 1 and 2

A regional fracture density of 0.1 fractures/m and a local fracture density of 0.5 fracture/m for the near-drift region, extending horizontally and vertically 15 m from the drift, have been assumed in the calculation. The regions of higher fracture density (0.5 fractures/m) were input in such a way as to create a region 30m high by 30m wide by 10m deep (along the drift) that has a block size of 2m x 2m x 2m.

In particular, the higher fracture density is used in a 30m x 30m region parallel to the drift and centered on the drift. In this region both the horizontal fractures and vertical fractures oriented parallel to the drift have a higher fracture density. This higher fracture density is also used for vertical fractures oriented perpendicular to the drift. These fractures have a higher fracture density in a region that extends over the width of the model, and encompasses the central 10m of drift length. These fractures also extend 15m above and below the center of drift.

Other block sizes are shown in Figure 1 and 2. Blocks 2m wide by 2m high by 10m deep are located in the 30m x 30m cross section perpendicular to and centered on the drift. These block sizes occur at the front and back of the model. Blocks 2m deep by 10m wide by 10m high are located in each of the side faces. Finally, 10m x 10m x 10m blocks form the top layer, the bottom two layers and the corner regions of the model.

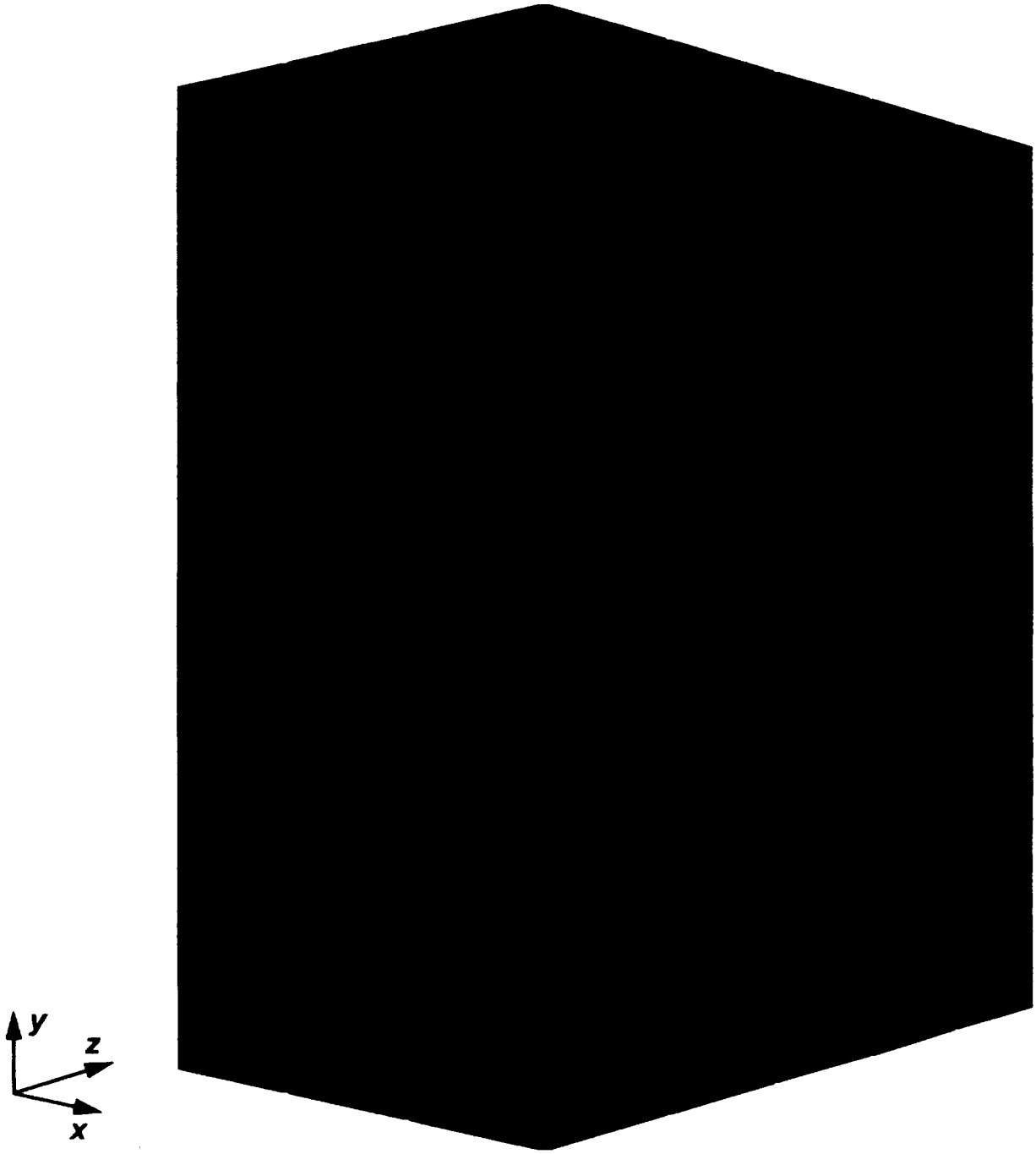


**NOTE**: Rock surrounding a drift is simulated in three dimensions as a rectangular prism 50 m wide (z) by 60 m high (y) by 30 m thick (x).

Figure 1. Geometry of the Simulated Rock Mass.

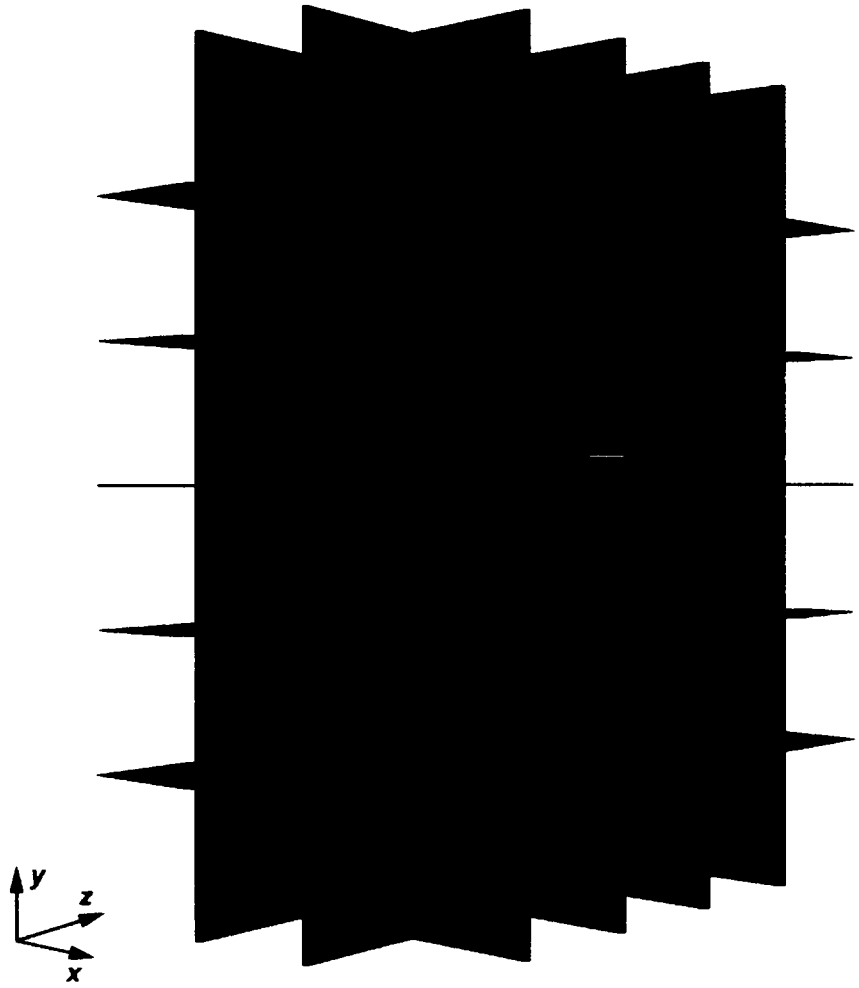


Figure 2. Fracture Sets Used in the Calculation

*Basis*: The assumed fracture densities are lower than those observed in portions of the ESF Main Drift (Albin et al. 1997, p. 25-33) and are lower than those used in an earlier TH modeling effort (CRWMS M&O 2000a), but are appropriate as not all fractures are expected to deform or slide, nor are all fractures expected to conduct fluids. In particular, the fracture densities calculated by Albin et al. (1997; Drawings OA-46-296, OA-46-297, OA-46-298, OA-46-299) include a large number of sealed and partially sealed fractures that are expected to have relatively little effect on mechanical and hydrological properties. Descriptive fracture statistics provided by Albin et al. (1997; p. 82) suggest that approximately 4 out of 5 fractures contain at least some secondary mineral in-filling. In sections of the Main Drift, the mapping studies also included fractures with trace lengths as short as 30 cm (Albin et al., 1997, p. 10). The shorter fractures are expected to have a relatively small impact on the mechanical and hydrological properties. Moreover, similar fracture spacing assumptions were used in a previous THM calculation of the Single Heater Test (Blair et al. 1999, p. 715-719). The spatial distribution of higher fracture density regions in the model was the result of a trade off between the desire for reasonable number of fractures and blocks and constraints imposed by computational capabilities and time required for grid formulation and testing.

### 3.1.2 Boundary Conditions

The mechanical boundary conditions applied to the simulated block (see Section 5.1) are intended to approximate *in situ* conditions and are similar to those used in previous TM modeling (Berge et al. 1998, p. 11). The applied boundary stresses consist of a vertical stress of 7.6 MPa on the top surface of the block. This is equivalent to the lithostatic load at a depth of 337 m, which is approximate depth of potential repository. Horizontal compressive stress equal to 4.85 MPa is imposed normal to each of the vertical faces of the block. A vertical stress gradient of 0.023 MPa/m was applied on the vertical faces of the block to simulate increasing confining stress with depth. The rock density was input to simulate increase of stress with depth in the block. Displacement boundary conditions are imposed on the base of the block which allow horizontal displacements, but not vertical displacements. Collapse of the emplacement drift is not simulated.

*Basis:* The stress boundary conditions used in the simulation (Table 1) are based on measured stress values (Stock et al. 1985, Table 2. p. 8697; Lee and Haimson 1999, p. 749) and calculated stress values (Berge et al. 1998, p. 11). Horizontal displacements are allowed at the base of the block. The bottom of the simulated region was anchored in the vertical direction to be consistent with the natural environment in which the surface is unconfined and can expand upward with thermal expansion due to heating. The boundary stresses increase with depth due to gravitational loading. Simulation of drift collapse and corresponding changes of permeability is possible with a distinct element code, such as 3DEC, but is beyond the scope of the current calculation.

It is assumed that the distinct element software used for this calculation properly employs constitutive equations for both the matrix (block) material and for the fractures. A linearly elastic constitutive equations was used for the matrix, which allows for purely elastic deformation of the individual blocks comprising the simulated rock mass, and a Coulomb-slip constitutive relation was used to represent the fractures. The latter constitutive relation allows the fractures to close under normal stress, open under tension, and slide under imposed shear stresses. Shear behavior is assumed elastic until the fracture shear strength is reached, after which permanent shear deformation (hysteresis) can occur.

### 3.1.3 Drift Geometry

The rock mass surrounding an emplacement drift (see Section 5.1) is simulated in three dimensions as a rectangular prism 50 m wide by 60 m high by 30 m thick. A horizontal, cylindrical drift 5.5 m in diameter is assumed to be excavated through the region in the x direction (see Figure 1), perpendicular to the narrow dimension of the prism.

*Basis:* The drift geometry is based on EDA II drift dimensions specified in the License Application Design Selection Report (CRWMS M&O 1999b, Section 5.3.2).

### 3.1.4 Heating Parameters

The thermal calculations in the 3DEC code are based on a simple thermal conduction model incorporating an infinite set of point heat sources and/or sinks in an infinite medium (see Section 5.1). This calculation assumes that the radioactive waste thermal output can be approximated by a series of point heat sources distributed uniformly along a line, centered on, and parallel to the

emplacement drift. As the calculation is intended to simulate the EDA-II design, identical heat sources were also placed 81 m to the north and south of the tunnel heater array and are assumed to represent neighboring emplacement drifts. A simple step function was used to simulate the EDA-II design thermal power history.

*Basis:* This approach provides a bounding case for the heat input to the system. Heat transfer is assumed to be due solely to uniform, isotropic conduction. Consequently, model temperatures near the drift wall are expected to exceed those predicted with more sophisticated thermohydrologic (TH) codes. However, the temperatures from this calculation are expected to match temperatures predicted with TH codes well enough at distances a few meters from the drift wall for use in this bounding calculation. Because this is a bounding calculation, the elevated peak temperatures near the drift wall (210°C in this calculation vs. <200°C in CRWMS M&O 1999b, Table 5-4), and higher cooling rate at late times (due to the smaller heated region in a real repository) are of minor concern.

### 3.1.5 Permeability Changes

#### 3.1.5.1 Cause of Permeability Change

Rock mass permeability changes are attributed to changes in fracture aperture and/or slip along fractures (see Section 5.1).

*Basis:* The assumption is justified because the matrix permeability is small with respect to fracture permeability and is relatively insensitive to changes in pressure and temperature over the appropriate range of values (DTN: LB990861233129.001).

#### 3.1.5.2 Magnitude of Permeability Change

Local fracture permeability changes are assumed to be proportional to normal (perpendicular to fracture plane) and shear (parallel to fracture plane) fracture displacements at a given location (see Section 5.1). Specifically, at each location where shear slip is predicted, the ratio of new permeability to initial permeability is assumed to equal ten multiplied by the number of millimeters of slip at the location. A similar relation is used for locations where normal opening or closing is predicted. If closure is predicted, permeability is reduced by a factor of ten multiplied by the amount of closure in millimeters. If opening is predicted, permeability is increased by a factor of ten multiplied by the amount of opening in millimeters. The ratio of the initial fracture permeability, $k_0$, to the fracture permeability at time $t$ due to TM effects, $k_t$, can be related to $df$, the magnitude of fracture displacement in mm (shear or normal), as

$$\bar{k} = k_t / k_0 = 1 + 10\ df \qquad \text{(Eq. 1)}$$

Using this relation, shear deformation always produces an increase in permeability, while normal deformation will increase permeability if the fracture opens ($df > 0$) and will decrease permeability if the fracture closes ($df < 0$).

Using equation 1, permeability is assumed to increase if fracture apertures increase and/or shear slip occurs; permeability will decrease only if fracture apertures decrease without shear slip (Olsson and Brown 1993, pp. 849-850).

*Basis.* Two types of fracture deformations contribute to THM coupling: normal displacement perpendicular to a fracture plane and shear displacement parallel to a fracture plane. A straightforward linear approximation of permeability change as a function of deformation was made because the relationship between shear slip and permeability change is poorly known. Moreover, Barton et. al (1997) presented convincing evidence that fractures and faults that are near or at critical levels of shear stress are the ones that conduct fluids. This implies that shear deformation may strongly influence fracture permeability.

The use of the linear relation between changing permeability and shear slip is consistent with the results of laboratory studies by Olsson and Brown (1993, pp. 849-850), who observed shear-induced fracture dilatancy and increased permeability with rotary shear slip, and by Esaki et al. (1999, p. 650) who observed permeability increases of 1.2 to 1.6 orders of magnitude for the first 5 mm of lateral shear slip.

For simplicity, the same relationship is used for both normal and shear deformations. Our approach is also consistent with numerical modeling work by Lee (CRWMS M&O 2000a, p. 80-82) who found that increasing fracture permeability by two orders of magnitude, to simulate the opening of vertical fractures, was required to provide realistic temperature predictions in the Large Block Test. Fracture opening displacements in the Large Block Test were on the order of a few mm (CRWMS M&O 2000c, p 3-154, Fig 3-78).

Future revisions to project documents may provide an opportunity to evaluate different approaches. For instance, a relationship based on the "cubic" law (Raven and Gale 1985, p.257) could be used to estimate the effect of normal opening/closing of fractures on permeability, and a non-linear relation between shear displacement and permeability change could be used. Recent experimental evidence suggests that shear displacements may affect flow anisotropy (Yeo et al. 1999, p. 1069). Development and implementation of these more complex relationships is beyond the scope of this report.

## 3.2 SPECIFIC ASSUMPTIONS FOR THERMAL MECHANICAL CALCULATION: ASSUMED VALUES FOR MODEL INPUTS

### 3.2.1 Thermal Assumptions

#### 3.2.1.1 Initial Temperature

The initial temperature of rock simulated in the calculation (see Section 5.1) is assumed to be 20°C.

*Basis.* Temperature measurements at repository depth show in situ temperature to be at approximately 25°C (CRWMS M&O 2000a, p. 48). The calculation THM effects depends more on temperature change than absolute temperature and the use of 20°C rather than 25°C as the initial in situ temperature will not significantly affect the result of this bounding calculation.

### 3.2.1.2 Thermal Expansion Coefficient ($°C^{-1}$)

A value of 3.0 E-6/°C was assumed for the thermal expansion coefficient and used in Section 5.1 of this calculation.

*Basis*: The model thermal expansion coefficient is based on three field measurements obtained in the Single Heater Test (CRWMS M&O, 1999c, Section 9, p.11, Table 9-3). A relatively low thermal expansion value was chosen to incorporate implicitly a major effect of fractures on mechanical behavior. This is desirable, as it is impractical to incorporate explicitly large numbers of fractures.

### 3.2.1.3 Thermal Capacitance J/($cm^3$-°C)

A value of 2.10 J/($cm^3$-°C) was assumed for the rock thermal capacitance and used in Section 5.1 of this calculation.

*Basis*. The source of the thermal capacitance data is Table 4-8 of Brodsky et al. (1997). Table 4-8 lists mean thermal capacitance values as a function of temperature at 25° C intervals for TSw2 tuff. The mean thermal capacitance values range from 1.8 to 2.5 J/($cm^3$ -°C) and are based on 7 samples. The temperature range of interest extends from 25 to 150 ° C, and the assumed value is the average of the first six table entries, 2.10 J/($cm^3$-°C).

### 3.2.2 Joint Properties

To date few data on the joint properties used in the 3DEC model have been collected. The values assumed for this calculation and listed below are taken from laboratory tests or calculated from laboratory test results. Additional work is required to assess the range of variability in the joint properties, and the model sensitivity to these parameters.

### 3.2.2.1 Joint Normal Stiffness (GPa/m)

A value of 73.5 GPa/m was assumed for the rock joint normal stiffness parameter (see Section 5.1).

*Basis*: Joint normal stiffness for TSw2 is given in Table 5-39 of CRWMS M&O 1997 (Section 5, p. 146). This value was obtained from 11 laboratory tests on natural and artificial fractures. These tests were conducted an applied normal stress of 2.5 MPa and are appropriate for use in this calculation.

### 3.2.2.2 Joint Shear Stiffness (GPa/m)

A value of 150 GPa/m was assumed for the joint shear stiffness parameter (see Section 5-1).

*Basis*: The joint shear stiffness parameter was estimated from data provided by Olsson and Brown (1994). The data were obtained form seven NRG-4 and NRG-6 core samples using a rotary shear apparatus and experimental procedures described in Section 2 of their report. Shear stiffnesses were calculated by Olsson and Brown (1994, p.3) from measurements of fracture slip over a range of applied shear stresses under normal loads of 5-10 Mpa. Measurements were

made on seven samples, and were repeated on one sample, so that eight results are available. Olsson and Brown (1994) plotted shear stiffness as a function of shear stress in Figures 2d, 4d, 7d, 9d, 12d, 15d, 18d, and 21d of their report. Numerical values were estimated from these figures as follows. Shear stiffness is inversely related to shear stress and the stiffness value of interest for this calculation is the maximum shear stiffness, which is obtained at zero shear stress, and which must be estimated from small slip displacements induced by low shear loads. Maximum shear stiffness for each of the eight tests reported in the above referenced figures was determined by estimating the low shear stress asymptote. These values spanned a range from approximately 30 to 400 Mpa/mm. The median value of the eight estimates was computed to be 150 Mpa/mm (150 Gpa/m). This median value is used in this calculation in order to reduce the influence of outliers on the estimate.

### 3.2.2.3 Joint Friction Angle

A value of 41° was assumed for the joint friction angle parameter (see Section 5-1).

*Basis*: This value was taken from Table 5-40 of CRWMS M&O 1997, Section 5, p. 146. This value is based on 12 laboratory tests on natural and artificial fractures of TSw2.

### 3.2.2.4 Joint Cohesion

A value of 0.86 MPa was assumed for the joint cohesion parameter (see Section 5-1).

*Basis*: This value was taken from Table 5-40 of CRWMS M&O 1997, Section 5, p. 146. This value is based on 12 laboratory tests on natural and artificial fractures of TSw2.

### 3.2.2.5 Joint Tensile Strength (MPa)

A value of 1.0 MPa was assumed for the joint tensile strength parameter (see Section 5-1).

*Basis*: No direct measurements of joint tensile strength were found. Joint tensile strength is expected to be low. A lower bound for joint tensile strength is value of 0 MPa. which implies no strength. An upper bound can be estimated using the ratio of the joint cohesion, c, to the tangent of the joint friction angle (Itasca Consulting Group, 1998; p. 3-83, equation 3-18):

$$\sigma^{t}_{max} = c/\tan\phi. \qquad \text{(Eq.2)}$$

Values for the tangent of the joint friction angle (41°) and joint cohesion (0.86 MPa) were taken from CRWMS M&O 1997 (Table 5-40, Section 5, p. 146). The values are based on 12 tests on samples from unit TSw2. The estimated upper bound on joint tensile strength is 1.0 MPa and the default value of 0 MPa provides a suitable lower bound. The upper bound provides a conservative estimate of fracture opening under tension.

## 4. USE OF COMPUTER SOFTWARE

The software used in this calculation was appropriate for its application. The software subject to the requirements of AP-SI-1Q, *Software Management* was obtained from configuration management and was used within the range of validation. The qualification status of the software

is indicated in the Document Input Reference System (DIRS). No previously developed models were used in the calculation.

## 4.1 SOFTWARE APPROVED FOR QUALITY ASSURANCE (QA) WORK

3DEC version 2.0, (STN: 10025-2.00-00) is a specialized commercially available software application developed by Itasca Consulting Group, Inc. (Itasca Consulting Group, 1998) to perform discontinuum modeling in three dimensions based on the distinct element method. 3DEC simulates the behavior of discontinuous media, such as a jointed rock mass, in response to either static or dynamic loads. The discontinuous media are modeled as an assemblage of discrete blocks that behave as either rigid or deformable material. The discontinuities are treated as boundary conditions between the blocks, along which large displacements and rotations are allowed to model joint behavior. 3DEC was used for all of the numerical calculations. The calculations were performed on a Dell Optiplex GX1 computer running the Windows NT 4.0 operating system.

Noesys software, which is used in this calculation, is exempt from AP-SI.1Q requirements because it is commercially available software used only for visual display of output data.

## 4.2 SOFTWARE ROUTINE

No mesh generators, other than that built into 3DEC, were used.

The routine "ds_joints.pl" (STN: 10293-1.0-00) is a perl script that extracts joint normal displacement and joint shear displacement from a 3DEC log file. It also finds the maximum normal and shear displacement value at any X for a given (Y, Z) pair and writes an output file to be displayed using Noesys.

# 5. CALCULATION

## 5.1 CALCULATION OF PERMEABILITY CHANGE FOR FRACTURES.

The rock mass surrounding an emplacement drift is simulated in three dimensions as a rectangular prism 50 m wide by 60 m high by 30 m thick (Figure 1), as described in Section 3.1.3. A cylindrical drift 5.5 m in diameter is excavated through the region in the x direction. The drift is horizontal and oriented perpendicular to the narrow dimension of the prism. The prism is intersected by three sets of fractures as defined in Section 3.1.1 Two fracture densities are assumed for each set of fractures: a low fracture density (0.1 fractures/m) for regions more than 15 m from the drift, and a high fracture density (0.5 fractures/m) for regions within 15 m of the drift. Figure 2 is a perspective view of the fracture sets used in this calculation. Boundary stresses discussed in Section 3.1.2 are imposed on the sides and top of the prism. The base of the prism is fixed in the vertical direction, but displacements are allowed in the horizontal directions.

The thermal field imposed by the emplacement of nuclear waste containers is simulated using a conduction-only TM software code that calculates temperatures, thermally-induced stresses, and displacements in a half-space. The thermal calculation is weakly coupled to the distinct-element mechanical calculation in that thermal stresses and displacements are incorporated into the predicted stress and displacement fields.

The calculation is intended to evaluate rock behavior for a cross section perpendicular to an emplacement drift, for which the emplaced waste containers act as a line heat source. To simulate this effect, the heater array extends approximately 30 m in the x direction beyond the boundaries of the simulated fractured block in both the positive and negative directions (Figure 3a). The calculation is intended to simulate the EDA-II design (CRWMS M&O, 1999b, Section 5.3.2); thus identical heat sources are placed at 81 m to the north and south of the tunnel heater array as shown in Figure 3b.

This thermal simulation is an isotropic, uniform, conduction-only calculation, and thus the estimated temperatures are expected to be elevated near the drift wall compared to those predicted using more sophisticated TH software codes. Overall, at locations more than a few meters away from the drift, the temperatures match TH predictions well enough for use in this bounding calculation. Because this is a bounding calculation, the elevated temperatures near the drift wall are of minor concern. Thermal assumptions and heating parameters in this calculation are discussed in Section 3.1.4, 3.2.1, and Table 1.

The thermal load of the model is based on the thermal power history calculated for the EDA-II design, in which ventilation is used to remove heat from the emplacement drift for the first 50 years after emplacement. The EDA-II design shows a "spike" in the pillar temperature starting at 50 years, when ventilation ceases, followed by a substantial amount of cooling before 100 years.

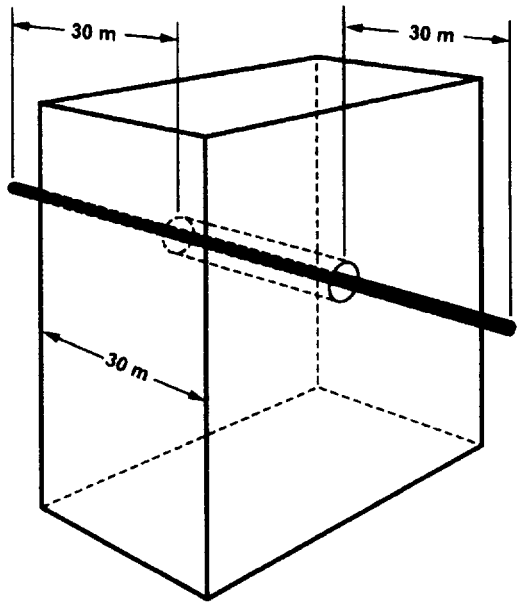


(a)

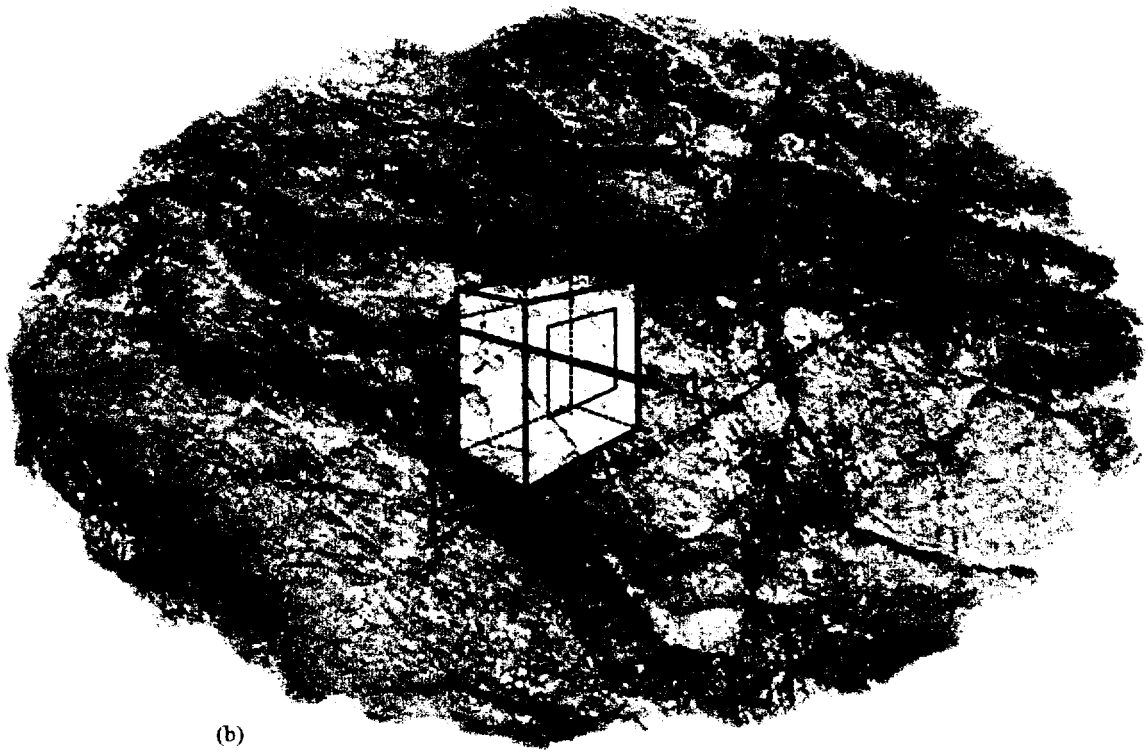

(b)

NOTE: a. The heater array extends approximately 30 m beyond the boundaries of the mechanical model in both the + and – directions.
b. Identical heat sources are placed at 81 m to the north and south of the tunnel heater array.

Figure 3. Heater Geometry

A simple step function was used for the thermal power input in 3DEC (Figure 4). Power was supplied at a constant level of 460 Watts/m for 50 years to simulate the ventilation phase, then raised to 615 Watts/m and held constant for 100 years to simulate the non-ventilated phase, then reduced to zero. This heating schedule produced peak pillar temperatures of 90°C similar to the maximum EDA-II pillar temperature of <96°C (CRWMS M&O 1999b, Table 5-4), but over a longer time, followed by a rapid cool down.

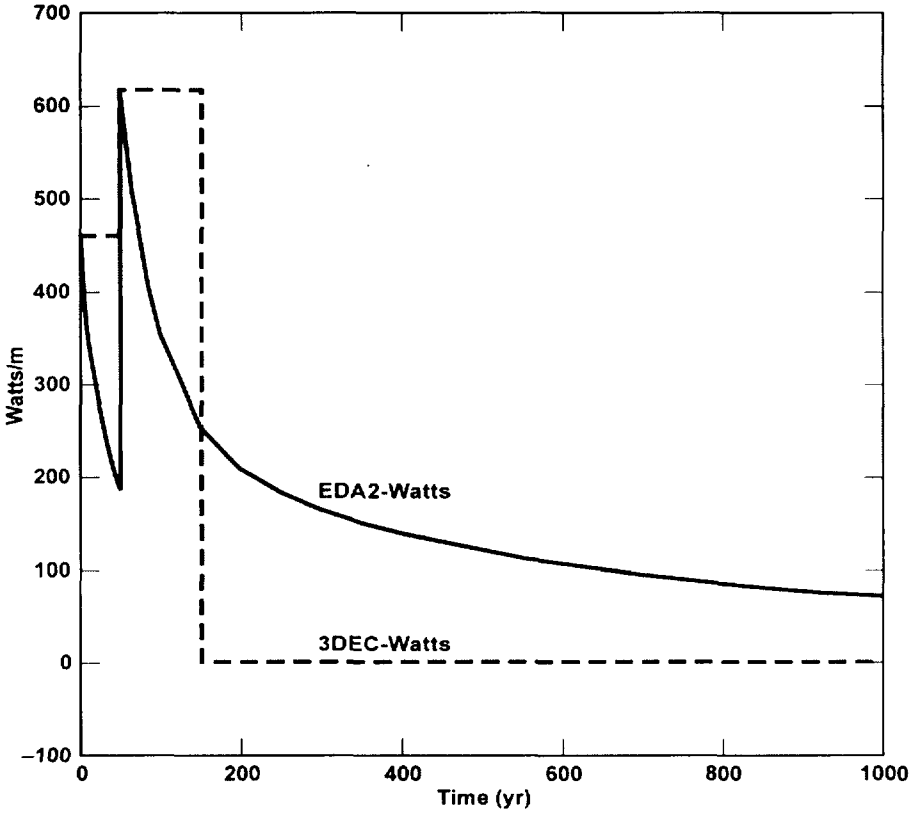


Figure 4. Thermal Power History Used in Calculation

The prism is aligned with the principal stress directions so that only one nonzero normal stress component acts upon each face. The sign convention is that negative stresses are compressive.

The software code was used to calculate stresses and deformations in the block at a series of times, as discussed in Section 5.3. The calculated joint deformations, using joint properties presented in Section 3.2.2 and mechanical properties provided in Table 1, were used to compute permeability changes in a cross section perpendicular to the emplacement drift. Maximum shear and normal deformation values were computed along an array of lines parallel to the drift, then projected onto a plane perpendicular to the drift. The displacements were then used to estimate permeability changes with the proportionality relationship given in Equation (1) as discussed in Section 3.1.5.2.

Cross sections for permeability changes, due to both shear and normal deformation, were then produced from the deformation data (see assumptions in Section 3.1.5). Files containing the

permeability change data from Equation (1) are in the form y, z, $\bar{k}$ for a plane perpendicular to the simulated drift. This file is read into the *Transform* module of the Noesys software package. Within *Transform* the data were resampled to evenly populate a 100 x 100 matrix. Values for the unfilled sites in the matrix were then computed using the "kernel" smoothing algorithm contained in the *Transform* software routine.

Values computed by the smoothing routine were then plotted or written to an output file.

## 5.2 INPUT PARAMETERS

The sources for input parameters used in this calculation are presented in Table 1.

Table 1. Input Parameters Used in the Calculation

| Line # | DTN Data Tracking Number | Description | Value | Units |
|---|---|---|---|---|
| 1 | MO9808RIB00041.000 | Tensile Strength | 8.6E+06 | Pa |
| 2 | MO9808RIB00041.000 | Young's Modulus | 33.0E+09 | Pa |
| 3 | MO9808RIB00041.000 | Poisson's Ratio | 0.21 | none |
| 4 | LL980805704243.023 | Bulk Modulus | 19.0E+09 | Pa |
| 5 | LL980805704243.023 | Shear Modulus | 13.6E+09 | Pa |
| 6 | MO9808RIB00041.000 | Dry Bulk Density | 2270 | $kg/m^3$ |
| 7 | MO0004RIB00036.001 | Thermal Conductivity | 1.66 | W/(m-K) |

Note: Refer to DIRS for qualification status of input parameters.

## 5.3 CALCULATION TIMES

The 3DEC code was used to estimate stress and deformation values in the block at times of 10, 50, 55, 150, 155, 200, and 1000 years. These times were chosen for the following reasons. The 10-year time represents conditions during initial heating phase when drift wall temperature and stress gradients are highest. The 50-year time represents temperature conditions just before the end of ventilation. The 55-year time represents conditions during the rapid rise in drift wall temperatures that occurs after ventilation stops (CRWMS M&O 1999a). The 150-year time is the end of heating in this model; the 155-year time represents conditions early on the cooldown period. The 200-year time was chosen to assess the time dependence of cool-down effects. Finally, the 1000 year time was chosen at it represents permanent changes in fractures after the rock has cooled back to near ambient conditions (give the accelerated cooling due to the limited heat source area.

A listing of the input files used for this calculation is presented in DTN LL000509612312.010.

## 5.4 CALCULATION OUTPUT

The primary results of this calculation are presented as two-dimensional spatial distributions of permeability multiplier values, calculated at times of 10, 50, 55, 150, 155, 200 and 1000 years after heating. Temperature distributions in the YZ plane, perpendicular to the drift, and in the XY plane, parallel to the drift, are given for each calculation time in Attachment I. All of the cross-sections are centered on the simulation mid-plane. Permeability multiplier values were

calculated for the code output values of both normal and shear displacements, and are presented below. Attachments II-IV present supporting information for the permeability multiplier calculations. Plots of principal stresses calculated at each time for the YZ and XY planes are given in Attachment II. Plots of normal and shear displacements at each time for the YZ and XY planes are given in Attachments III and IV, respectively. The DTN for the output of this calculation is LL000313504243.036.

### 5.4.1 Permeability Multipliers for Normal Displacement on Fractures

This section presents two-dimensional images of permeability multipliers calculated from predicted fracture normal displacements. Figures 5a through 5g present results for normal displacement calculations at each of the selected times. Note the color bar is adjusted to show the spatial detail at each time, and colors were not compatible from figure to figure.

Figure 5a shows that after 10 yr. of heating the largest changes in permeability are calculated for regions within one drift diameter of the emplacement drift. These include a decrease in permeability (multiplier values <1) in the drift walls, and regions of increased permeability (multiplier values >1) above and below the drift. This is consistent with closing of vertical fractures in the drift wall, and opening of vertical fractures above and below the drift as the rock tries to expand in the horizontal direction due to increasing temperature. It is important to note that overall the magnitude of the calculated increase is relatively small (less than 2x) and that a multiplier near one is estimated for much of the rock mass. This figure also shows that a slight increase in permeability is calculated for horizontal fractures at distances greater than two drift diameters. This is attributed to thermal expansion of the rock in the near-drift region. Again, note that generally the calculated increase in permeability is small (<2x).

Permeability multiplier values calculated for 50 years of heating (Figure 5b) are very similar to those obtained for 10 years of heating (Figure 5a) indicating that, when heat is applied at a constant rate, the transient period of the normal displacement TM response occurs during the first few years in which temperature gradients are the highest. Figure 5c presents the results after 55 years of heating. This plot shows values very similar to those shown in Figures 5a and 5b, indicating that the increase in thermal load on the rock caused by closure of the drift (end of ventilation) does not have a major TM effect on the normal deformation of fractures in the rock mass.

Figure 5d shows permeability multiplier values due to normal displacement after 150 years of heating, just before the heat source are turned off in the calculation. This figure is very similar to those for 10, 50, and 55 years of heating. Figure 5e shows the values of the permeability multiplier, based on normal displacement, calculated for 155 years, five years after the heating was stopped in the simulation. This figure shows similar features to the previous four permeability multiplier plots with the exception that there is no region of reduced permeability in the drift walls. Thus the lowest values are approximately one. The regions of highest multiplier values are still above and below the drift, and the values have increased to between 2x and 3x. These are still very low values.

Figure 5f shows the values of the permeability multiplier calculated for 200 years based on normal displacement. This figure is similar to Figure 5e (155 years) but shows that the region of

increased permeability above the drift extends upward to about 15 m from the drift center. This upward extension is roughly as wide as the drift and may be associated with the change in principal stress orientation that is shown for this time. This figure also shows a widening of the region of increased permeability below the drift. The maximum permeability increase calculated for this time is about 2.5x.

Figure 5g shows permeability multiplier values calculated for normal displacements on fractures at 1000 years (850 years after heating ceased in the calculation). This figure shows development of vertical zones extending above and below the drift in which permeability may have increased about 1.7x. This may be caused by thermal contraction of the rock near the drift. The zones of increased permeability immediately above and below the drift, seen at 200 years (Figure 5f), have widened and extended to 15 m on either side of the drift. A summary tabulation of the maximum permeability multipliers for normal displacement is provided in Table 2.

Table 2. Maximum Permeability Multiplier

| Time (Years) | Maximum Permeability Multiplier | |
|---|---|---|
| | Normal Displacement | Shear Displacement |
| 10 | <1 | 3 to 6.5 |
| 50 | <1 | 3 to 6.5 |
| 55 | <1 | 3 to 6.5 |
| 150 | <1 | 3 to 6.5 |
| 155 | 2 to 3 | 4 to 7.5 |
| 200 | 2.5 | 7 to 10 |
| 1000 | 1.7 | 8 to 11 |

### 5.4.2 Permeability Multipliers for Shear Displacements on Fractures

This section presents two-dimensional images of permeability multipliers calculated from shear displacements on simulated fractures. After 10 years of heating, shear displacements may increase permeability as much as 3 to 6.5x in the region within one drift diameter (Figure 6a). Permeability multiplier values calculated for times of 50, 55, and 150 years (Figures 6b, 6c and 6d) are very similar to those for 10 years (Figure 6a), indicating that most shear deformation occurs early in the heating phase and is not impacted by the cessation of the ventilation. Figure 6e presents permeability multiplier values at 155 years, five years after the end of the heating phase, based on shear displacements. The results are very similar to those of the earlier times (Figures 6a-6d), but the values are higher, with an increase of nearly one order of magnitude (OM).

Figure 6f shows the permeability multiplier values, based on shear displacements, for 200 years, 50 years after the end of heating. This figure shows a region of increased permeability about 10 m wide and 20 m high centered on the drift. The permeability multiplier values in this region are greater than 7x and range as high as 10x (1 OM). Two other vertical zones of high multiplier values are also shown. These are located at the interfaces between 0.5 fractures/m and 0.1 fractures/m fracture densities, and have multiplier values of around 5x. These zones are likely a computational artifact of the distinct element size discontinuity at these locations. The permeability multiplier values calculated from shear displacements predicted for 1000 years are

presented in Figure 6g. The results are similar to those of Figure 6f, but the permeability multiplier values are higher. Values in the region within two drift diameters of the drift wall are about 8x, with a maximum of 11x (1.1 OM). Figures 6f and 6g indicate that vertical fractures may be activated during the cool down phase, increasing fracture permeability significantly. A summary tabulation of the maximum permeability multipliers for shear displacement is provided in Table 2.

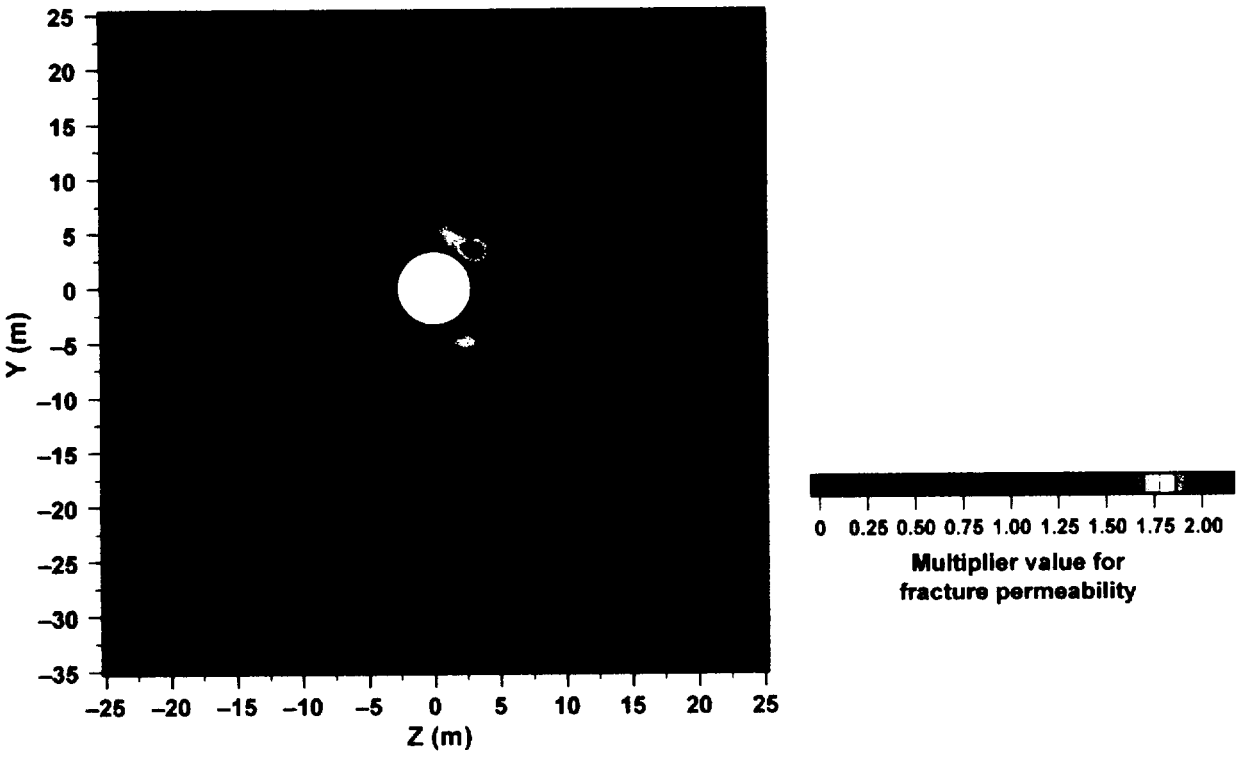


(a) 10-year

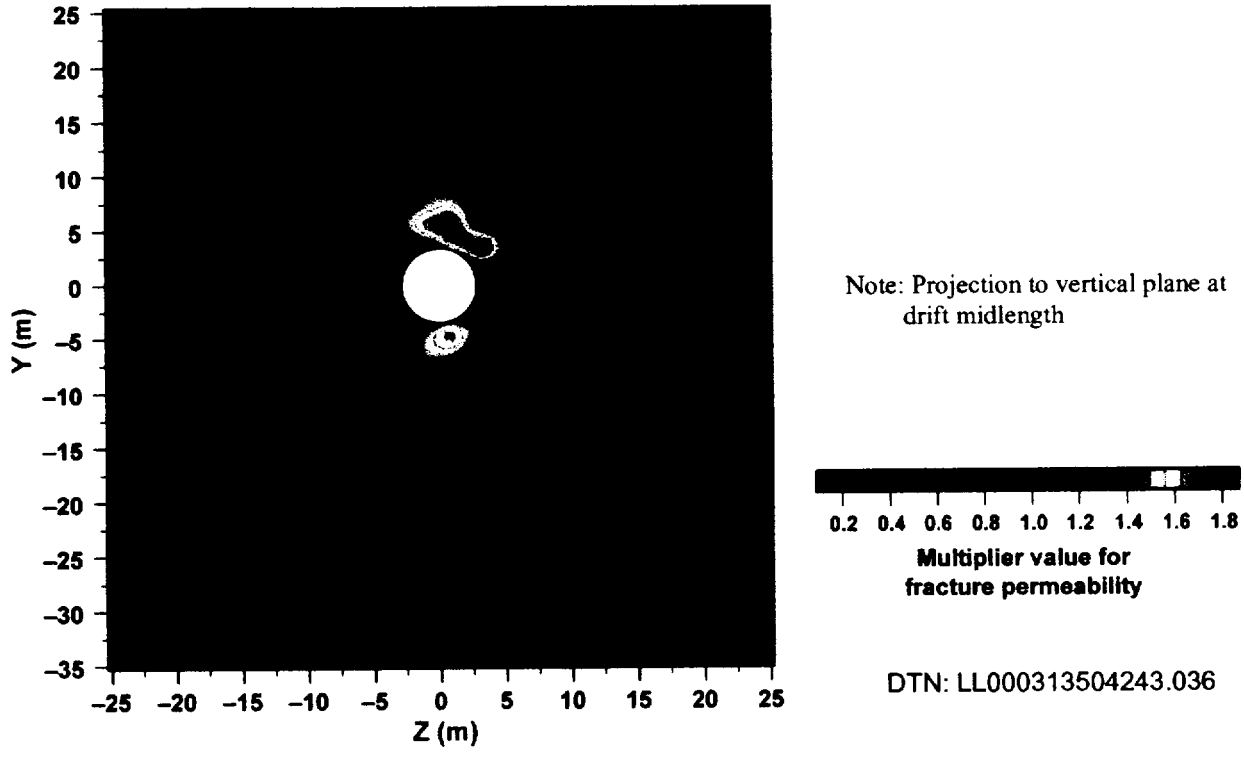


(b) 50-year

Note: Projection to vertical plane at drift midlength

DTN: LL000313504243.036

Figure 5. Estimate of Permeability Change Due to Normal Displacement at (a) 10 and (b) 50 years

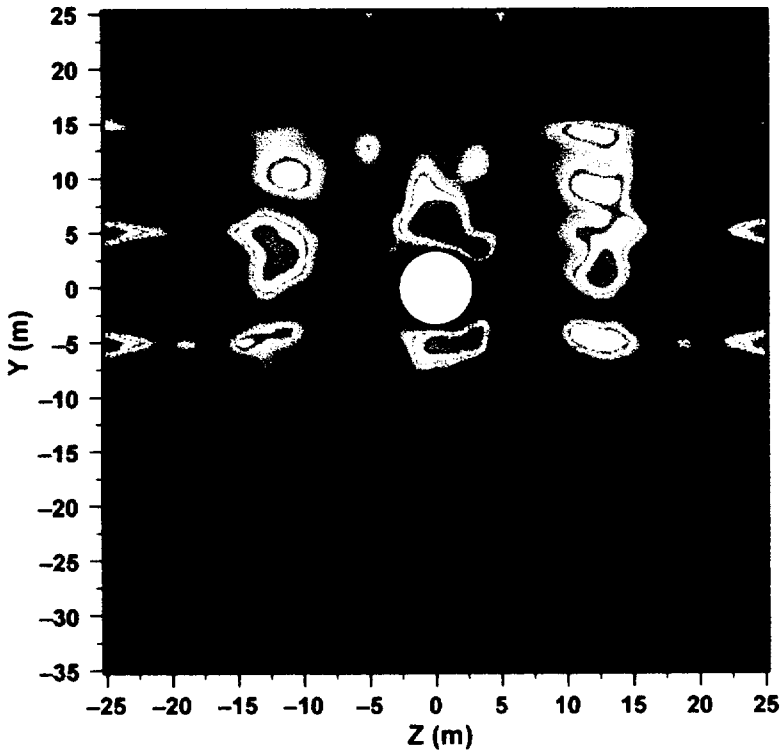


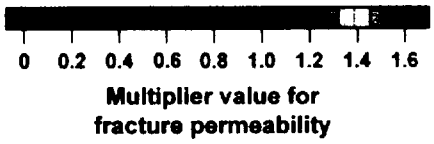


(c) 55-year

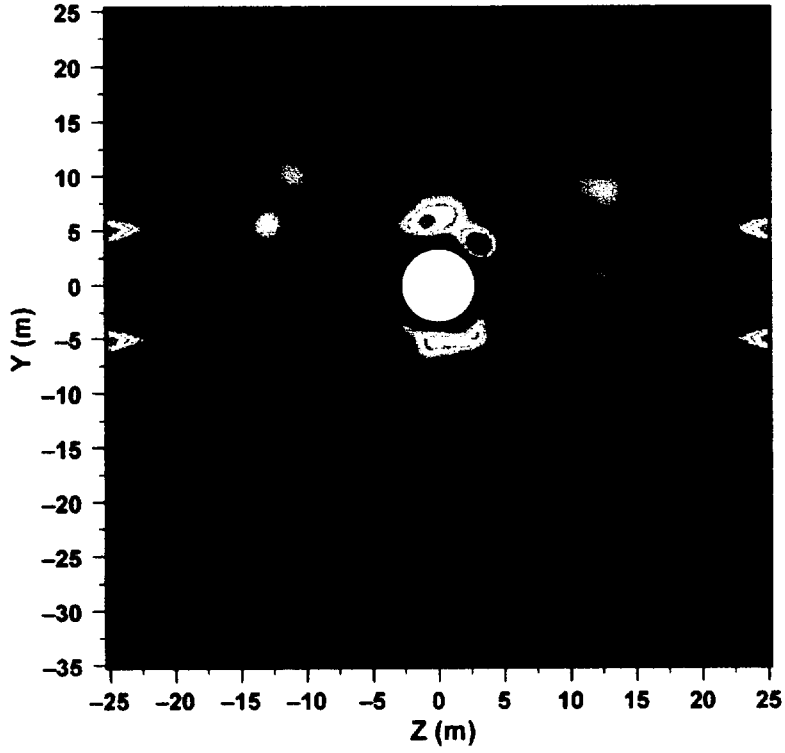


Note: Projection to vertical plane at drift midlength

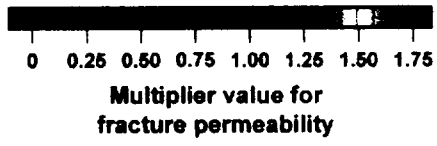


DTN: LL000313504243.036

(d) 150-year

Figure 5. Estimate of Permeability Change Due to Normal Displacement at (c) 55 and (d) 150 years (Continued)

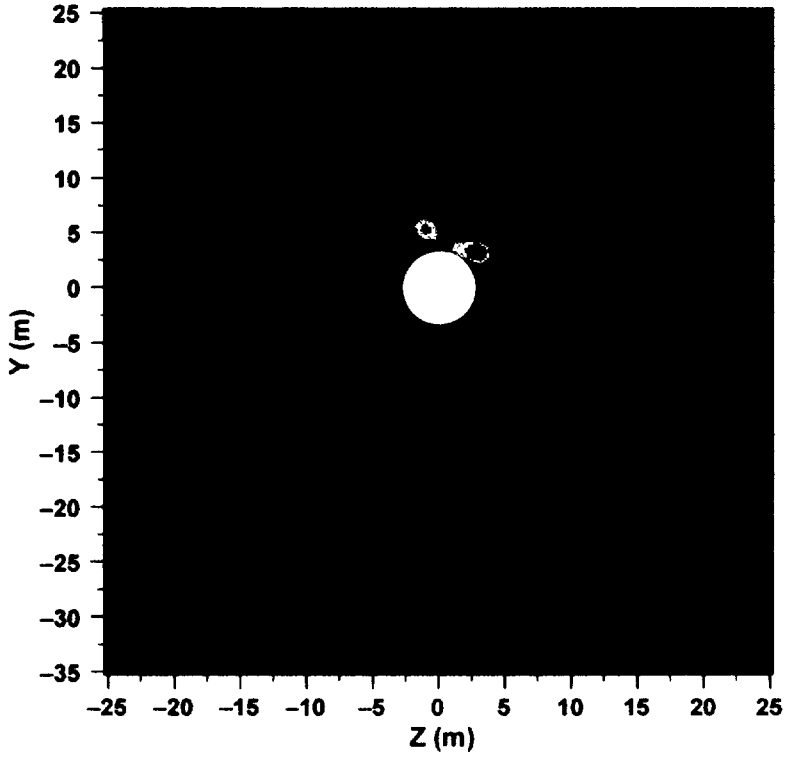


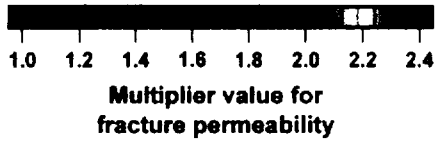


(e) 155-year

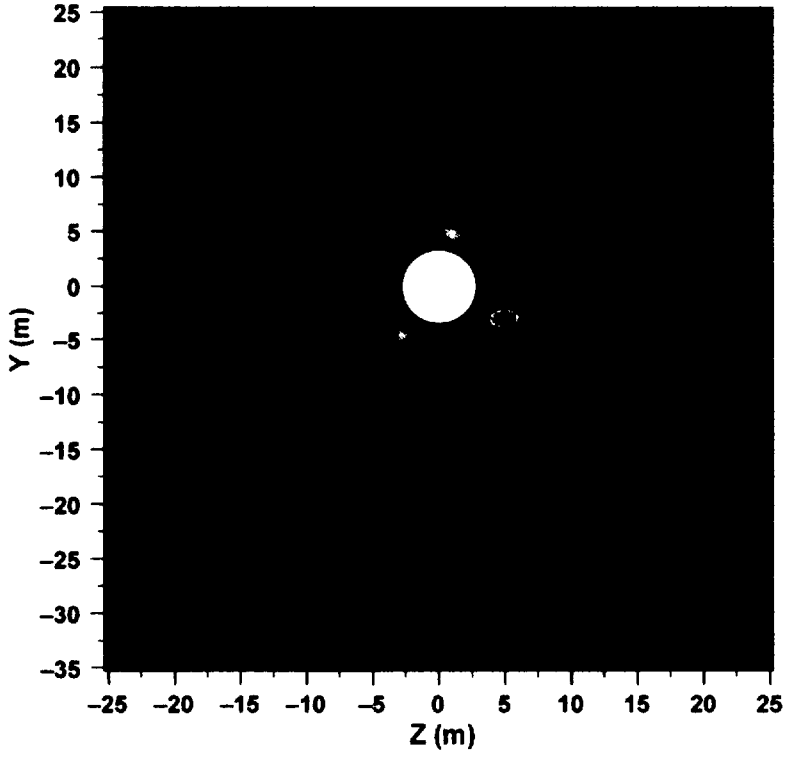


Note: Projection to vertical plane at drift midlength

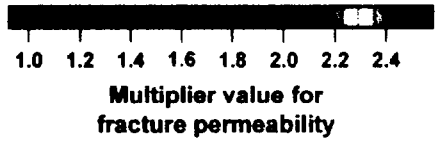


DTN: LL000313504243.036

(f) 200-year

Figure 5. Estimate of Permeability Change Due to Normal Displacement at (e) 155 and (f) 200 years (Continued)

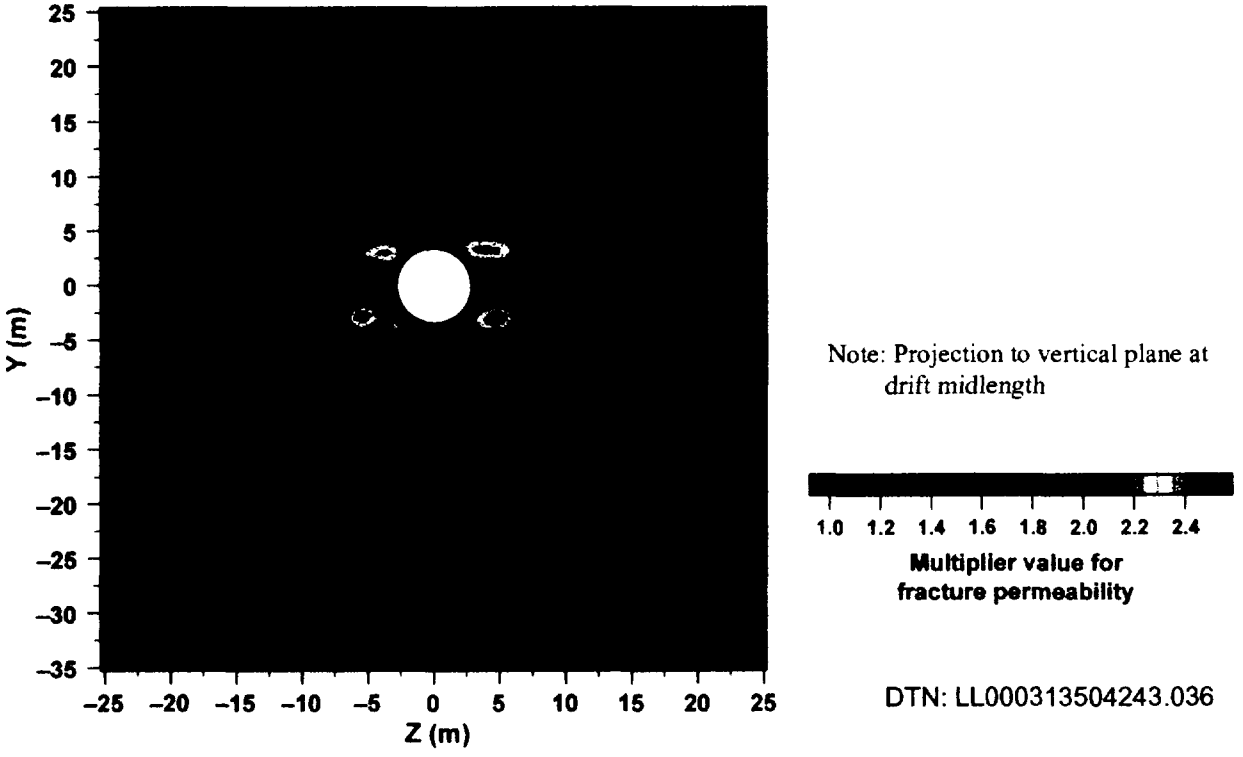


(g) 1000-year

Figure 5. Estimate of Permeability Change Due to Normal Displacement at (g) 1000 years (Continued)

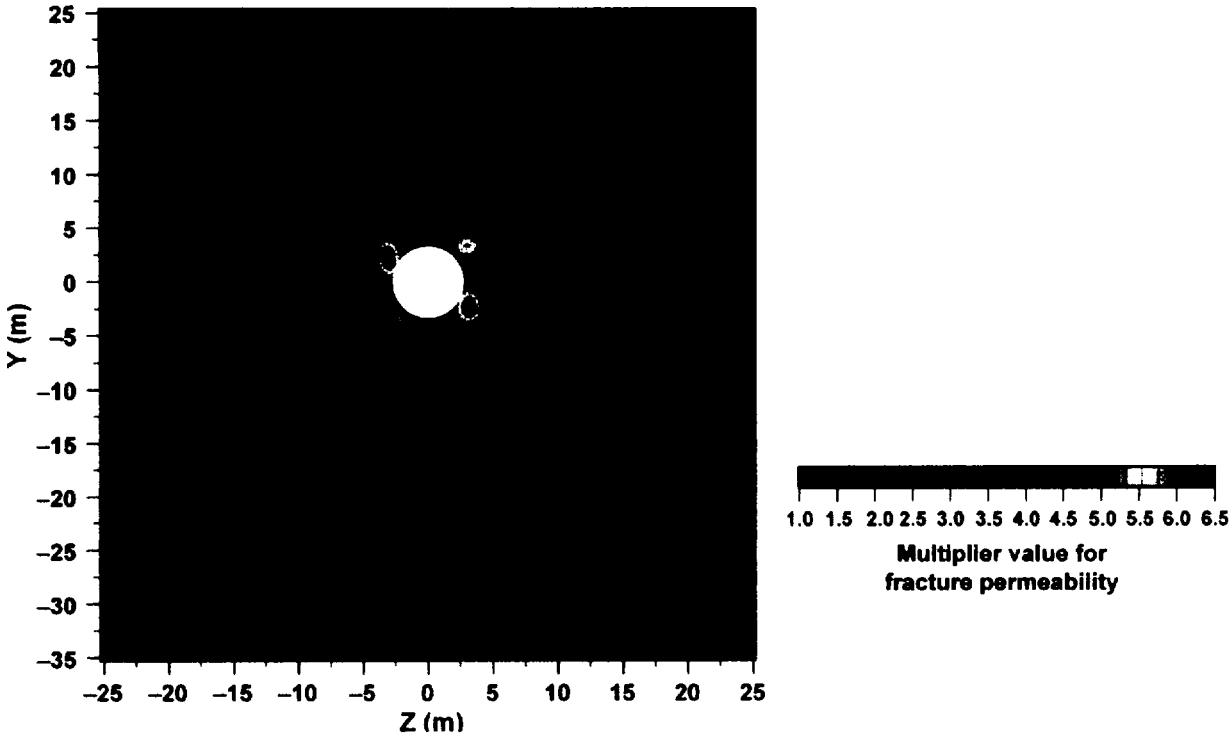


(a) 10-year

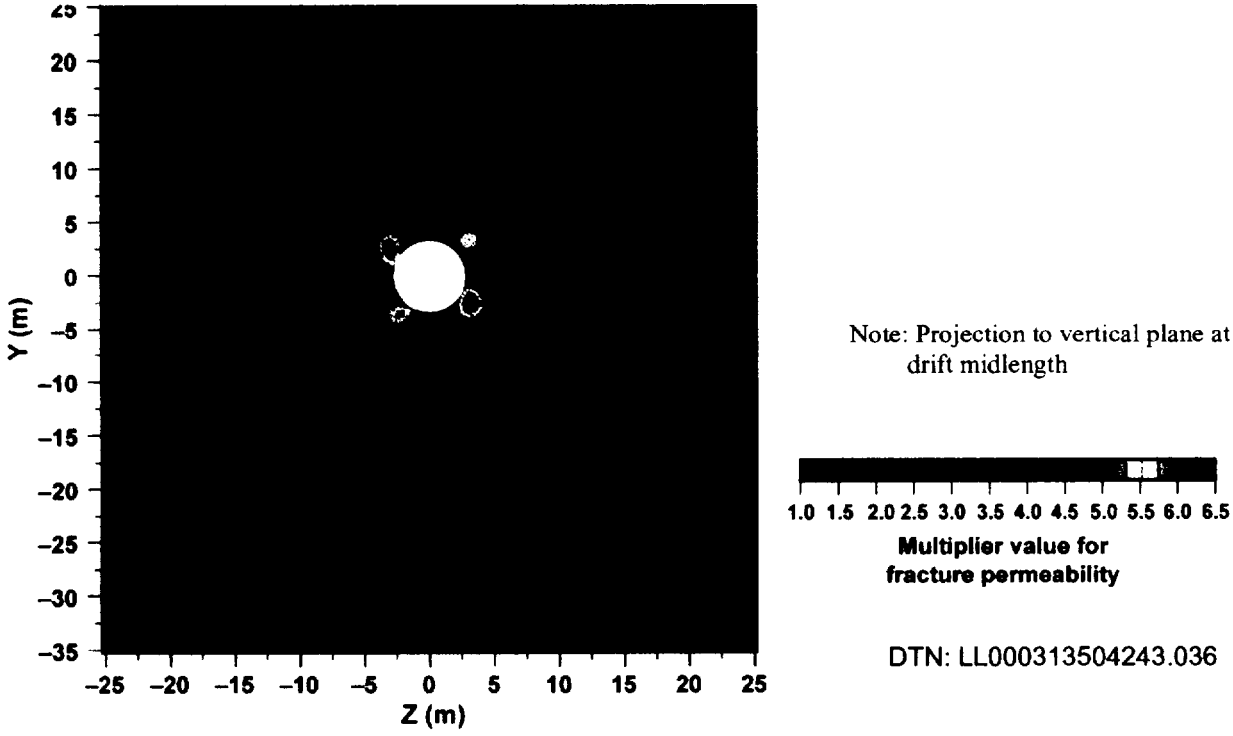


(b) 50-year

Figure 6. Estimate of Permeability Change Due to Shear Displacement on Fractures at (a) 10 and (b) 50 years

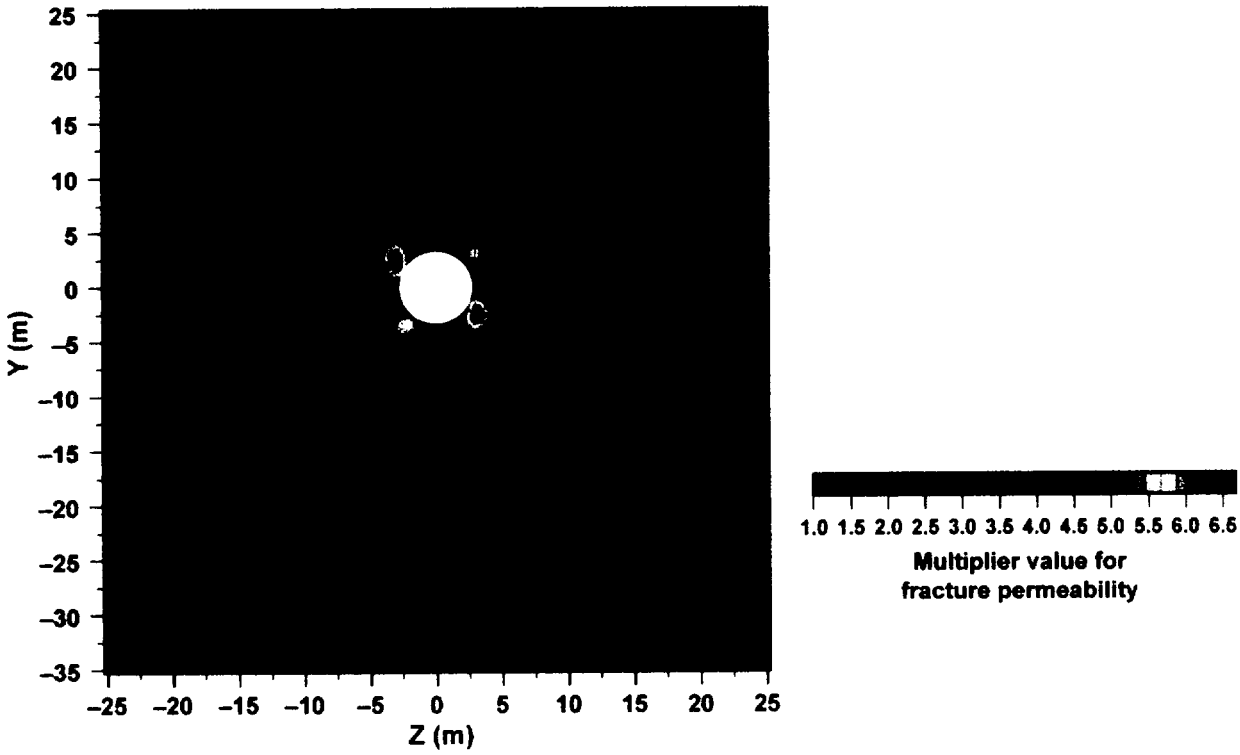


(c) 55-year

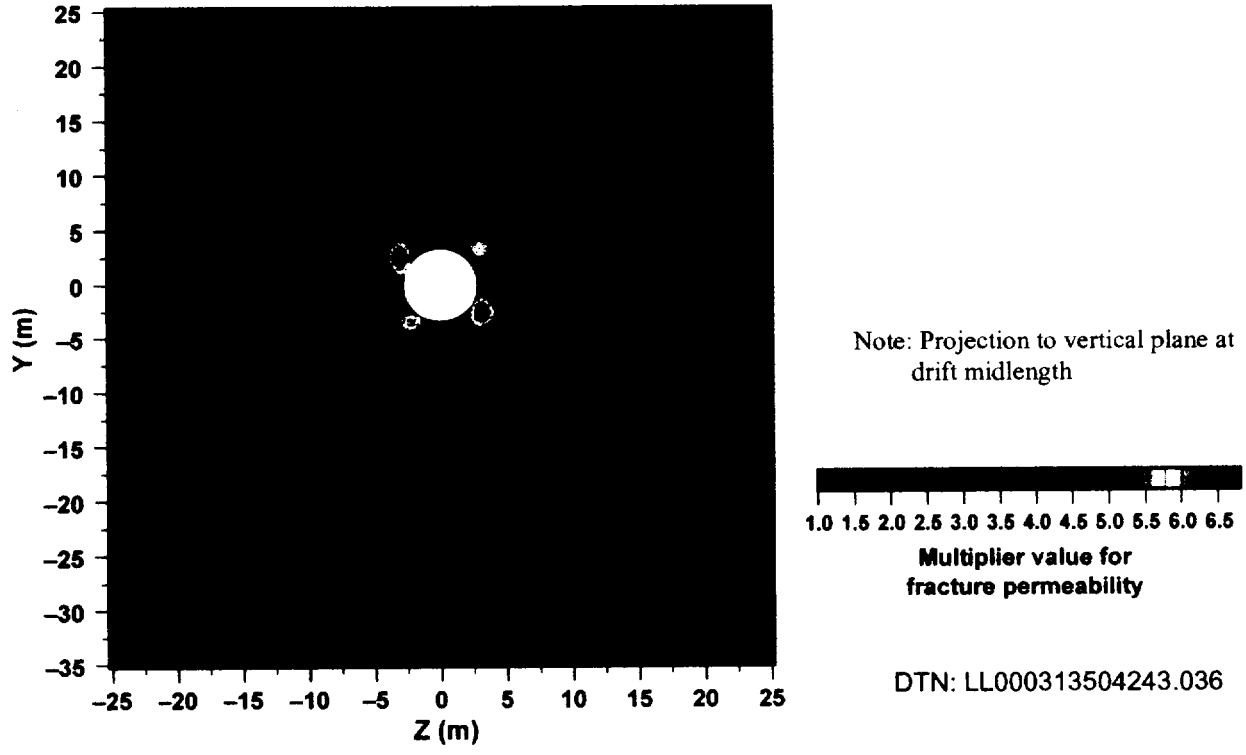


(d) 150-year

Figure 6. Estimate of Permeability Change Due to Shear Displacement on Fractures at (c) 55 and (d) 150 years (Continued)

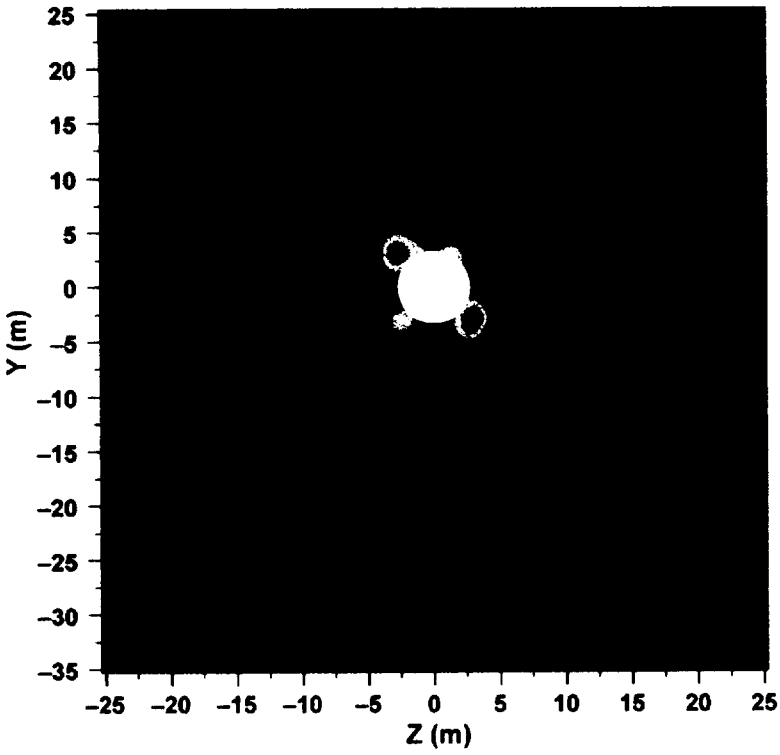


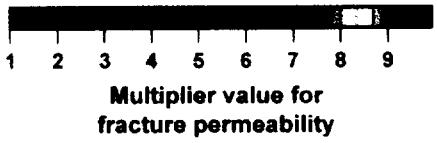


(e) 155-year

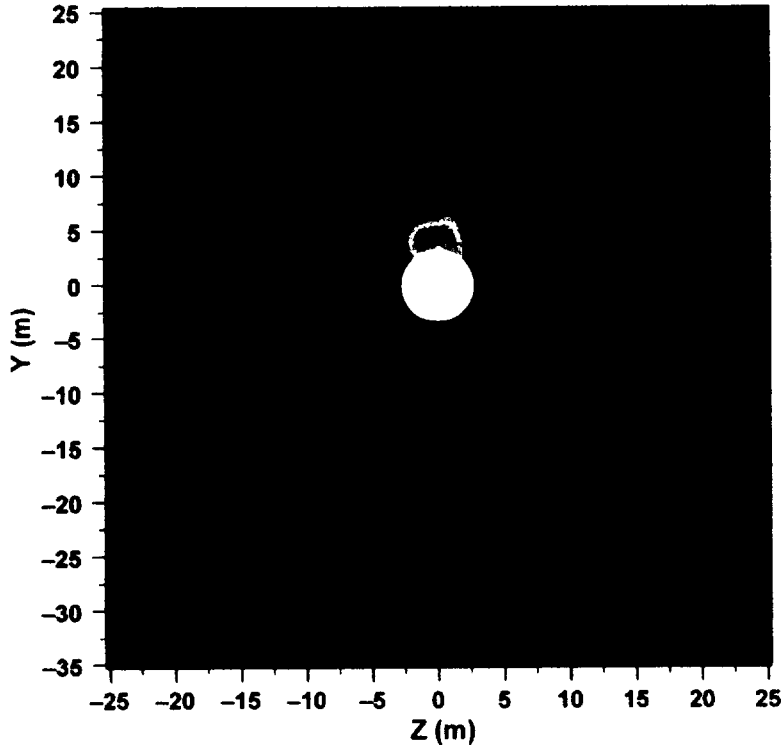


Note: Projection to vertical plane at drift midlength

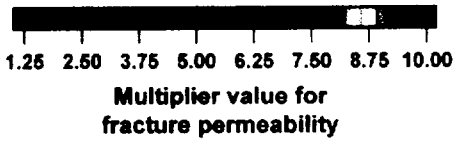


DTN: LL000313504243.036

(f) 200-year

Figure 6. Estimate of Permeability Change Due to Shear Displacement on Fractures at (e) 155 and (f) 200 years (Continued)

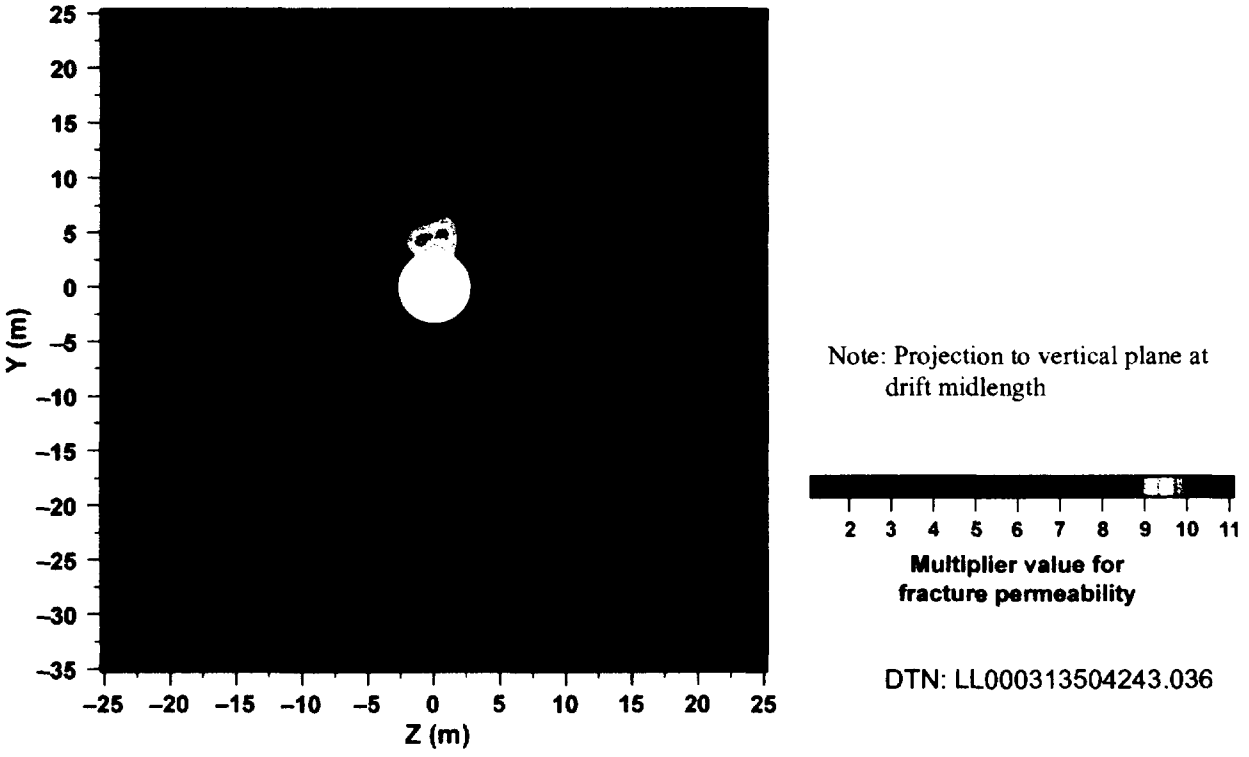


(g) 1000-year

Figure 6. Estimate of Permeability Change Due to Shear Displacement on Fractures at (g) 1000 years (Continued)

## 6. RESULTS

A bounding calculation has been conducted of how TM behavior of rock in the region surrounding an emplacement drift in a Monitored Geologic Repository subsurface facility may affect the permeability of fractures in the near-field.

Results of this calculation indicate that the major TM effect on fracture permeability occurs during cool down for both shear and normal deformation. Moreover, the results indicate that shear deformation of fractures during the cool down of a potential geologic repository may cause permeability of the fractures in a region within two drift diameters of a drift wall to increase in permeability as much as an order of magnitude (10x). Specifically, shear deformation on vertical fractures during cool down produces the maximum amount of permeability change, and increases in permeability of 5x may occur on vertical fractures at distances beyond two drift diameters from the drift wall.

Results indicate that opening of fractures from normal deformation may cause permeability to increase as well, but to a lesser extent than shear deformation. Normal closure of fractures during heating may cause permeability to decrease significantly within one drift diameter of the drift wall. During cool down, vertical fractures above and below the drift may open increasing the permeability by up to a factor of two.

# REFERENCES

## 7.1 DOCUMENTS CITED


Albin, A.L.; Singleton, W.L.; Moyer, T.C.; Lee, A.C.; Lung, R.C.; Eatman, G.L.W.; and Barr, D.L. 1997. Geology of the Main Drift—Station 28+00 to 55+00, Exploratory Studies Facility, Yucca Mountain Project, Yucca Mountain, Nevada. Denver, Colorado: Bureau of Reclamation and U.S. Geological Survey. ACC: MOL.19970625.0096.

Barton, C.A.; Hickman, S.; Morin, R.; Zoback, M.D.; Finkbeiner, T.; Sass, J.; and Benoit, D. 1997. "Fracture Permeability and Its Relationship to In Situ Stress in the Dixie Valley, Nevada, Geothermal Reservoir." Proceedings from Twenty-Second Workshop on Geothermal Reservoir Engineering, January 27-29, 1997. 210-215. Stanford, California: Stanford University. TIC: 237673.

Berge, P.A.; Wang, H.F.; and Blair, S.C. 1998. Estimated Bounds on Rock Permeability Changes from THM Processes. UCRL-ID-131492. Livermore, California: Lawrence Livermore National Laboratory. ACC: MOL.19981109.0302.

Blair, S.C.; Lin, W.; Ramirez, A.L.; Daily, W.D.; and Buscheck, T.A. 1999. "Coupled THM Analysis of the Single Heater Test at Yucca Mountain." Proceedings of the 37th U.S. Rock Mechanics Symposium, Vail Colorado, June 6-9, 1999, Rock Mechanics for Industry. Amadei, B.; Kranz, R.L.; Scott, G.A.; and Smeallie, P.H., eds. 2, 715-719. Rotterdam, The Netherlands: Balkema. TIC: 247482.

Brodsky, N.S.; Riggins, M.; Connolly, J.; and Ricci, P. 1997. Thermal Expansion, Thermal Conductivity, and Heat Capacity Measurements for Boreholes UE25 NRG-4, UE25 NRG-5, USW NRG-6, and USW NRG-7/7A. SAND95-1955. Albuquerque, New Mexico: Sandia National Laboratories. ACC: MOL.19980311.0316.

Brown, S.R. 1995. "Simple Mathematical Model of a Rough Fracture." Journal of Geophysical Research, 100, (B4), 5941-5952. Washington, D.C.: American Geophysical Union. TIC: 237570.

CRWMS M&O 1997. Yucca Mountain Site Geotechnical Report. B00000000-01717-5705-00043 REV 01. Two volumes. Las Vegas, Nevada: CRWMS M&O. ACC: MOL.19971017.0736; MOL.19971017.0737.

CRWMS M&O 1999a. Enhanced Design Alternative II Report. B00000000-01717-5705-00131 REV 00. Las Vegas, Nevada: CRWMS M&O. ACC: MOL.19990712.0194.

CRWMS M&O 1999b. License Application Design Selection Report. B00000000-01717-4600-00123 REV 01 ICN 01. Las Vegas, Nevada: CRWMS M&O. ACC: MOL.19990908.0319.

CRWMS M&O 1999c. Single Heater Test Final Report. BAB000000-01717-5700-00005 REV 00 ICN 1. Las Vegas, Nevada: CRWMS M&O. ACC: MOL.20000103.0634.

CRWMS M&O 2000a. Thermal Tests Thermal-Hydrological Analysis/Model Report. ANL-NBS-TH-000001 REV 00. Las Vegas, Nevada: CRWMS M&O. Submit to RPC URN-0212

CRWMS M&O 2000b. Calculation of Permeability Change Due to Coupled Thermal-Hydrological-Mechanical Effects. Development Plan TDP-NBS-MD-000008 REV 00. Las Vegas, Nevada: CRWMS M&O. ACC: MOL.20000328.0592.

CRWMS M&O 2000c. Near-field Environment Process Model Report. TDR-NBS-MD-000001 REV 00. Las Vegas, Nevada: CRWMS M&O. Submit to RPC URN-0124

Esaki, T.; Du, S.; Mitani, Y.; Ikusada, K.; and Jing, L. 1999. "Development of a Shear-Flow Test Apparatus and Determination of Coupled Properties for a Single Rock Joint." International Journal of Rock Mechanics and Mining Sciences, 36, 641–650. New York, New York: Elsevier Science. TIC: 247483.

Itasca Consulting Group 1998. 3DEC, Three Dimensional Distinct Element Code User's Guide, Version 2.0. Minneapolis, Minnesota: Itasca Consulting Group, Inc. TIC: 247503.

Lee, M.Y. and Haimson, B.C. 1999. "Initial Stress Measurements in the Exploratory Studies Facility Yucca Mountain, Nevada." Rock Mechanics for Industry, Proceedings of the 37th U.S. Rock Mechanics Symposium, Vail/Colorado/USA/6-9 June 1999 Rock Mechanics for Industry. Amadei, B.; Kranz, R.L.; Scott, G.A.; and Smeallie, P.H., eds. 2, 743-750. Rotterdam, The Netherlands: A.A. Balkema. TIC: 247086.

Olsson, W.A. and Brown, S.R. 1993. "Hydromechanical Response of a Fracture Undergoing Compression and Shear." International Journal of Rock Mechanics, Mining Sciences & Geomechanics Abstracts, 30, (7), 845-851. New York, New York: Pergamon Press. TIC: 234100.

Olsson, W.A. and Brown, S.R. 1994. Mechanical Properties of Seven Fractures from Drillholes NRG-4 and NRG-6 at Yucca Mountain, Nevada. SAND94-1995. Albuquerque, New Mexico: Sandia National Laboratories. ACC: MOL.19941007.0081.

Raven, K.G. and Gale, J.E. 1985. "Water Flow in a Natural Rock Fracture as a Function of Stress and Sample Size." International Journal of Rock Mechanics and Mining Sciences & Geomechanics Abstracts, 22, (4), 251-261. Oxford, United Kingdom: Pergamon Press. TIC: 235724.

Reshel TJ 2000. *Table Of Contents For TDP-NBS-MD-000008, Calculation Of Permeability Change Due To Coupled Thermal-Hydrologic-Mechanical Effects Author: Steve Blair (C).* Livermore, California: Lawrence Livermore National Laboratory. ACC: MOL.20000606.0436.

Stock, J.M.; Healy, J.H.; Hickman, S.H.; and Zoback, M.D. 1985. "Hydraulic Fracturing Stress Measurements at Yucca Mountain, Nevada, and Relationship to the Regional Stress Field." Journal of Geophysical Research, 90, (B10), 8691-8706. Washington, D.C.: American Geophysical Union. TIC: 219009.

Yeo, I.W.; De Freitas, M.H.; and Zimmerman, R.W. 1999. "Effect of Shear Displacement on the Aperture and Permeability of a Rock Fracture." International Journal of Rock Mechanics and Mining Sciences, 35, (8), 1051-1070. Oxford, United Kingdom: Pergamon. TIC: 247484.

## 7.2 CODES, PROCEDURE, AND STANDARDS

AP-3.12Q, Rev. 0, ICN 1. Calculations. Washington, D.C.: U.S. Department of Energy, Office of Civilian Radioactive Waste Management. ACC: MOL.20000512.0065

AP-SI.1Q, Rev. 2, ICN 4. *Software Management.* Washington, D.C.: U.S. Department of Energy, Office of Civilian Radioactive Waste Management. ACC: MOL.20000223.0508

AP-SV1Q, Rev. 0, ICN 1. *Control of Electronic Management Data.* Washington, D.C.: U.S. Department of Energy, Office of Civilian Radioactive Waste Management. ACC: MOL.20000512.0068

QP 3.8, Rev. 1, *Control Of The Electronic Management Of Data,* Washington, D.C.: U.S. Department of Energy, Office of Civilian Radioactive Waste Management. ACC: MOL.20000511.0148

## 7.3 SOFTWARE CODES AND ROUTINES

Itasca Consulting Group 1998. Software Code, 3DEC, V2.0, STN: 10025-2.00-00. 1998.

Lawrence Livermore National Laboratory. Software routine: ds_joints.pl. V1.0, STN: 10293-1.0-00, 2000

## 7.4 SOURCE DATA, LISTED BY DATA TRACKING NUMBER

LB990861233129.001. Drift Scale Calibrated 1-D Property Set, FY99. Submittal date: 08/06/1999.

LL000509612312.010. Calculation of Permeability Change Due to Coupled Thermal-Hydrologic-Mechanical Effects. Submittal date: 05/09/2000. Submit to RPC

LL980805704243.023. Estimated Bounds on Rock Permeability Changes from THM. Submittal date: 8/13/1998.

MO0004RIB00036.001. Rock Thermal Conductivity. Submittal date: 04/07/2000. Imaging in Process

MO9808RIB00041.000. Reference Information Base Data Item: Rock Geomechanical Properties. Submittal date: 08/05/1998.

## 7.5. OUTPUT DATA, LISTED BY DATA TRACKING NUMBER

LL000313504243.036. Calculation of Permeability Change Due to Coupled Thermal-Hydrologic-Mechanical Effects. Submittal date: 03/10/2000.

# 8. ATTACHMENTS

Attachment I: Temperatures

Attachment II: Principal Stresses

Attachment III: Joint Normal Displacements

Attachment IV: Joint Shear Displacements

# ATTACHMENT I

# TEMPERATURES (PAGES I-1 TO I-8)

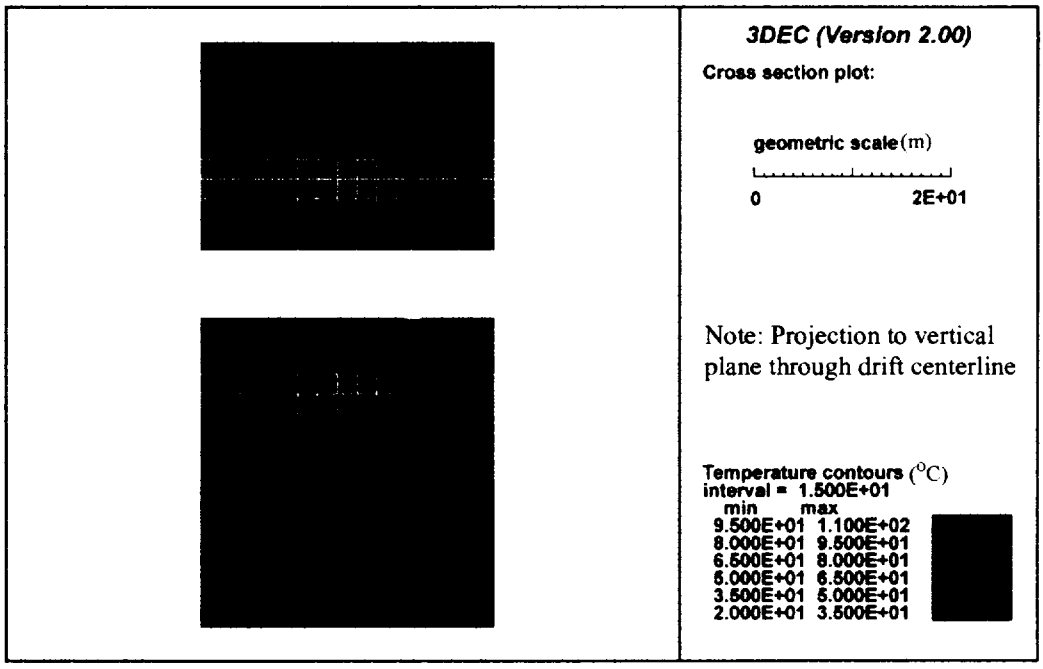


(a) XY Plane

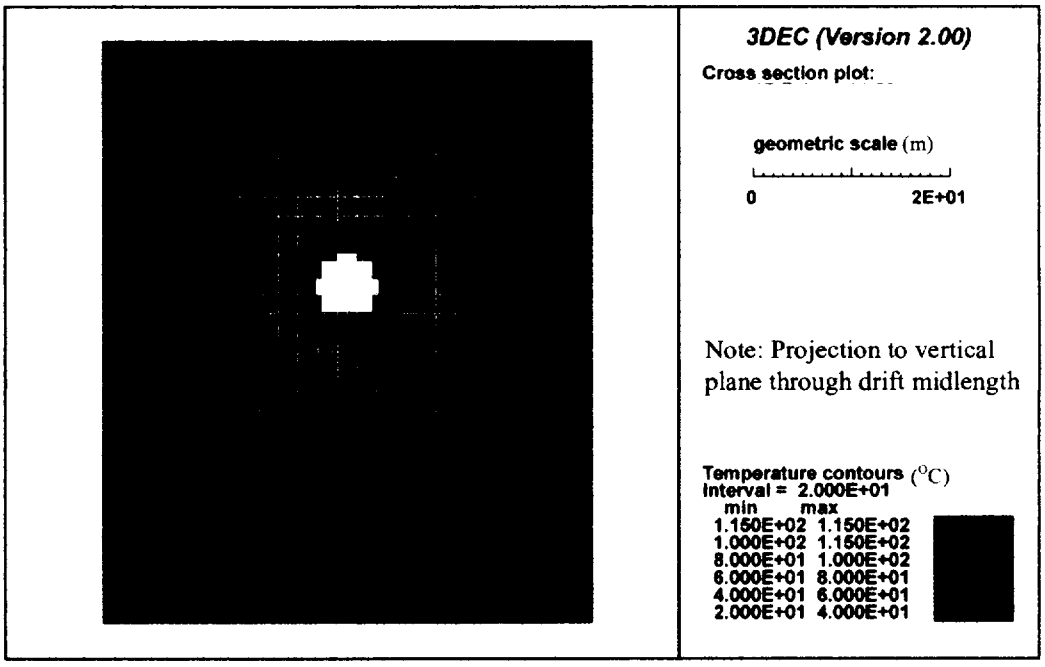


(b) YZ Plane DTN: LL000313504243.036

Figure I-1. Temperature distribution (°C) at 10 years, early ventilation phase

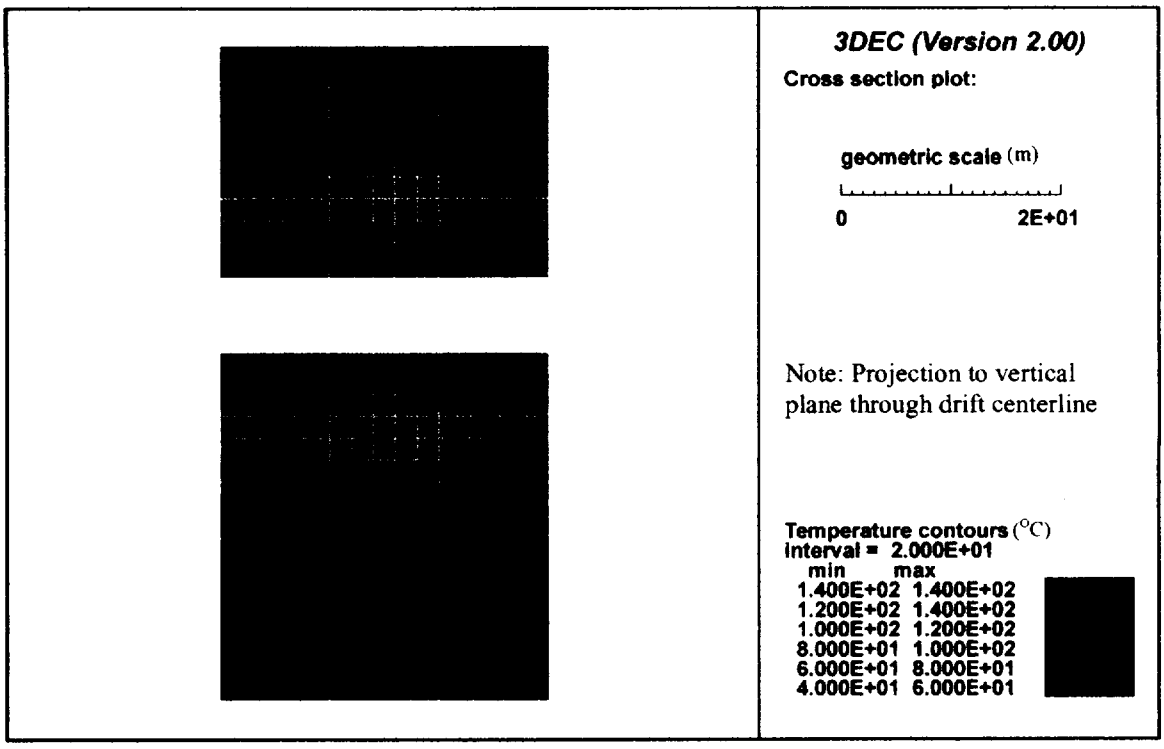


(a) XY Plane

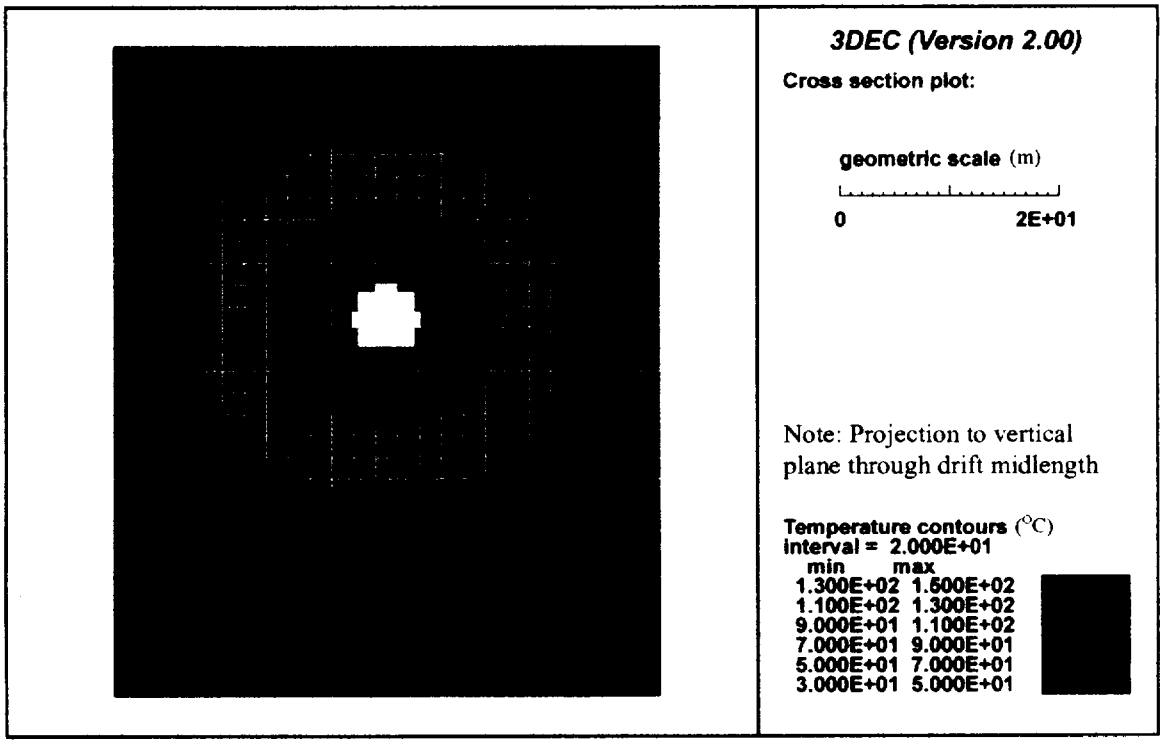


DTN: LL000313504243.036

(b) YZ Plane

Figure I-2. Temperature distribution (°C) at 50 years, late ventilation phase

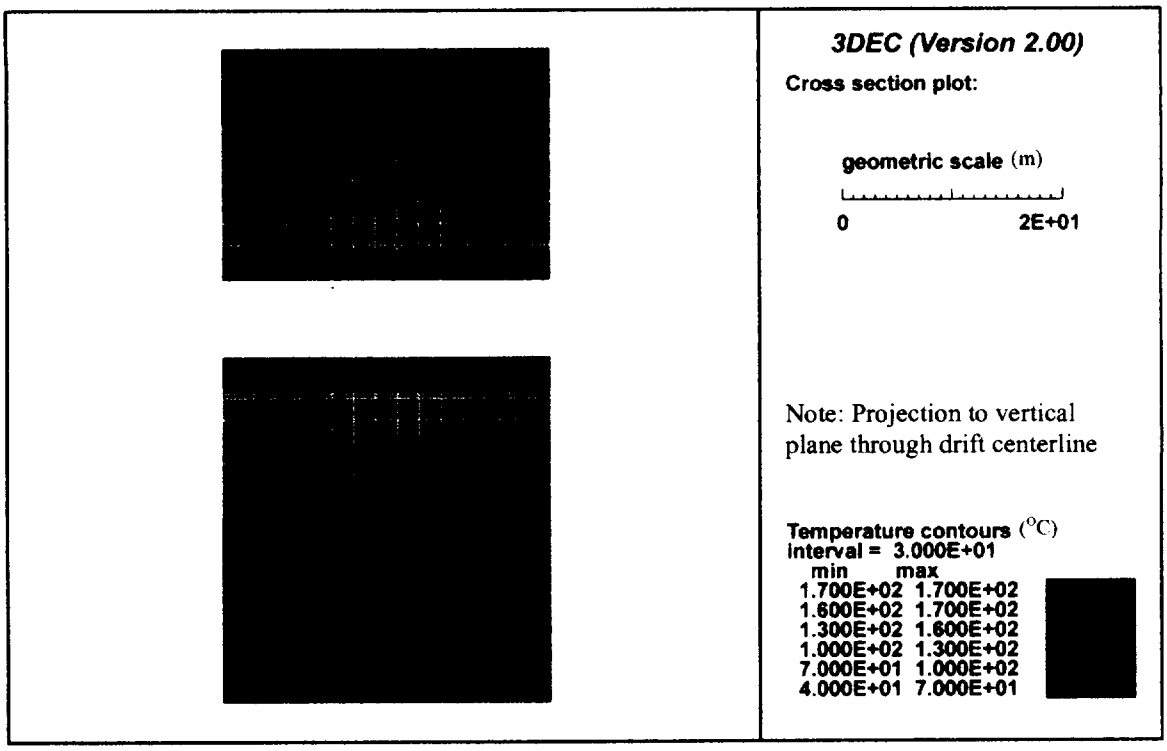


(a) XY Plane

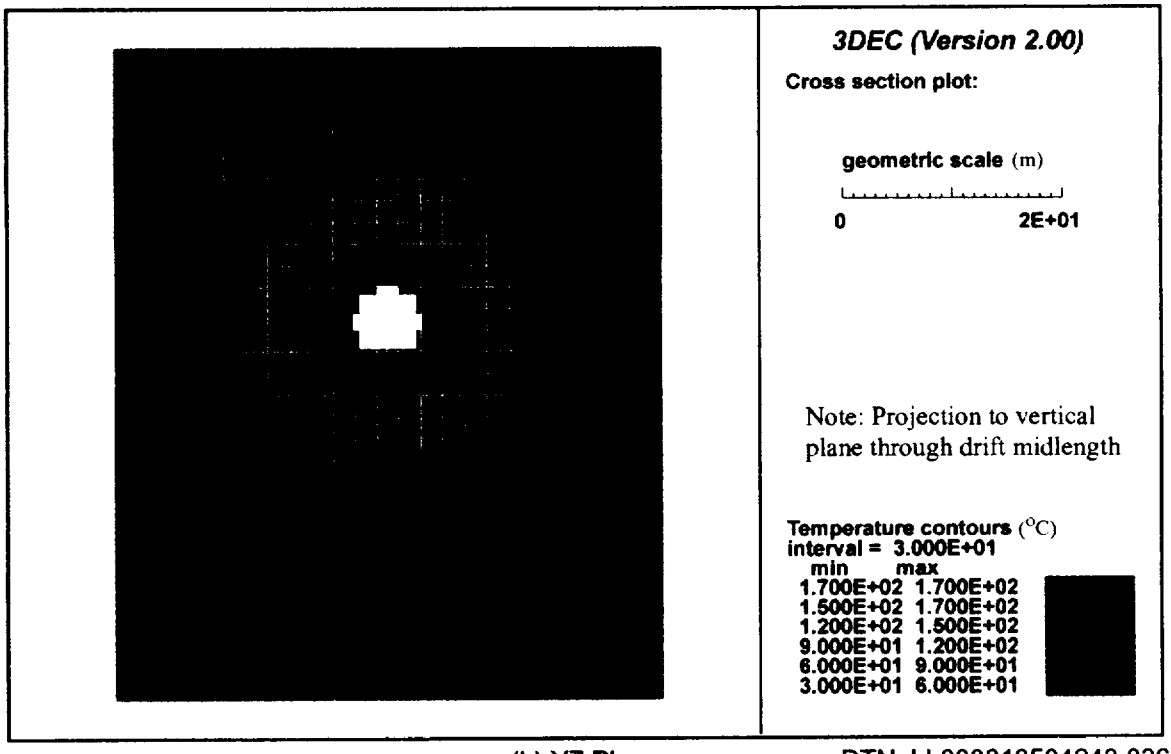


(b) YZ Plane

DTN: LL000313504243.036

Figure I-3. Temperature distribution (°C) at 55 years, early post-ventilation heating phase

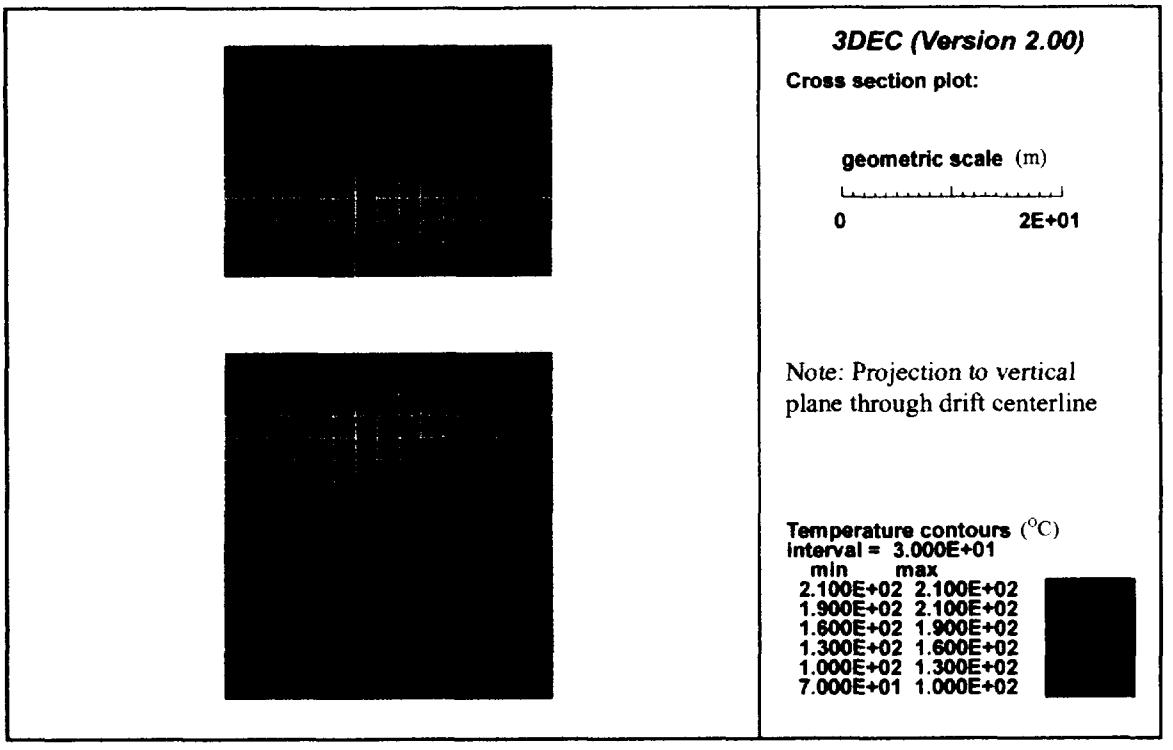


(a) XY Plane

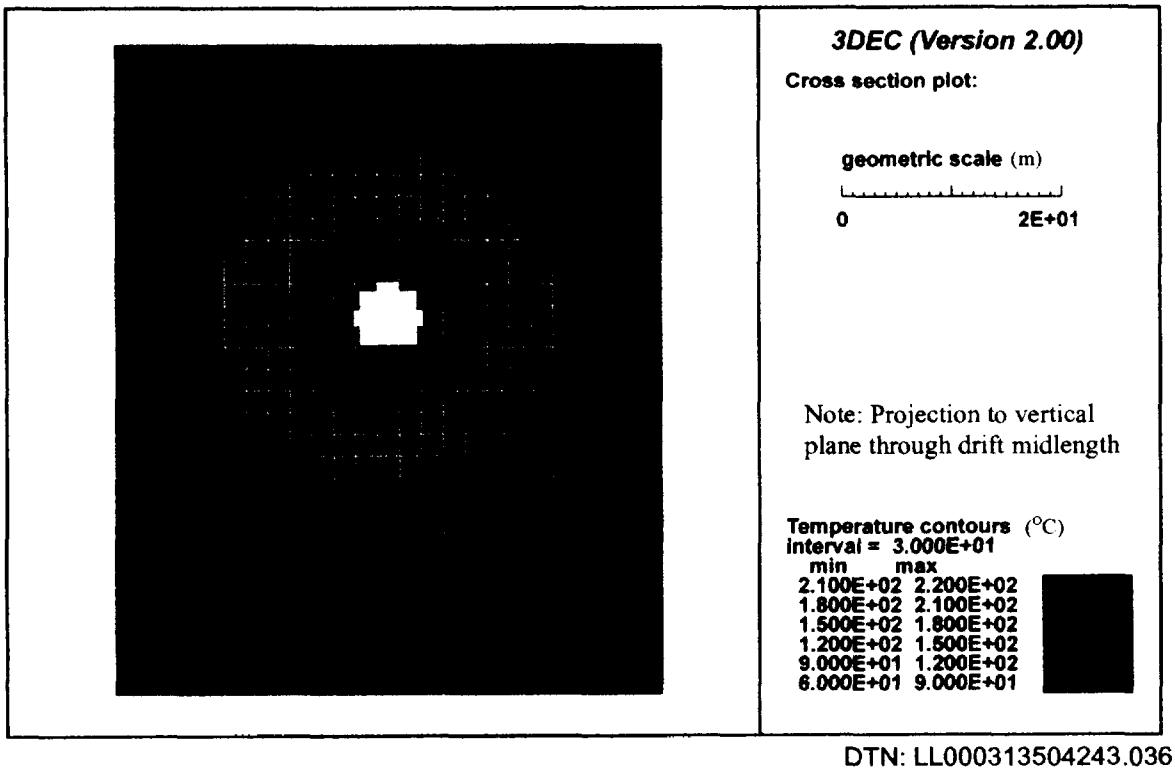


DTN: LL000313504243.036

(b) YZ Plane

Figure I-4. Temperature distribution (°C) at 150 years, late post-ventilation heating phase

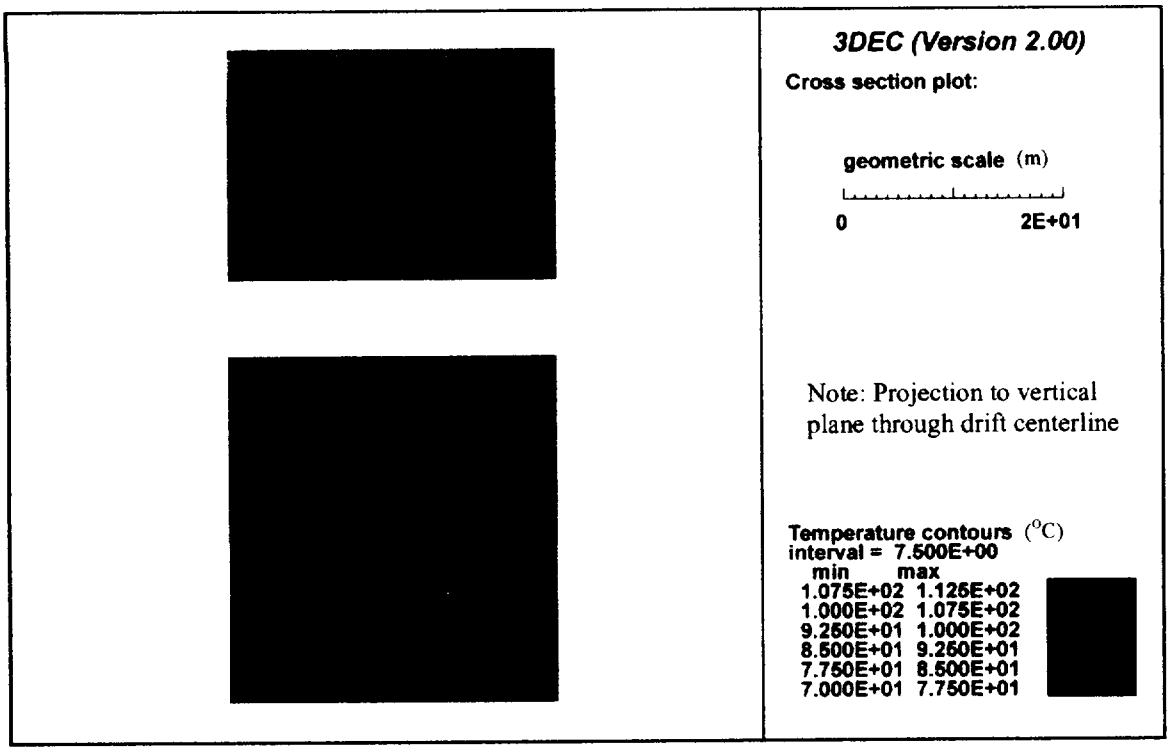


(a) XY Plane

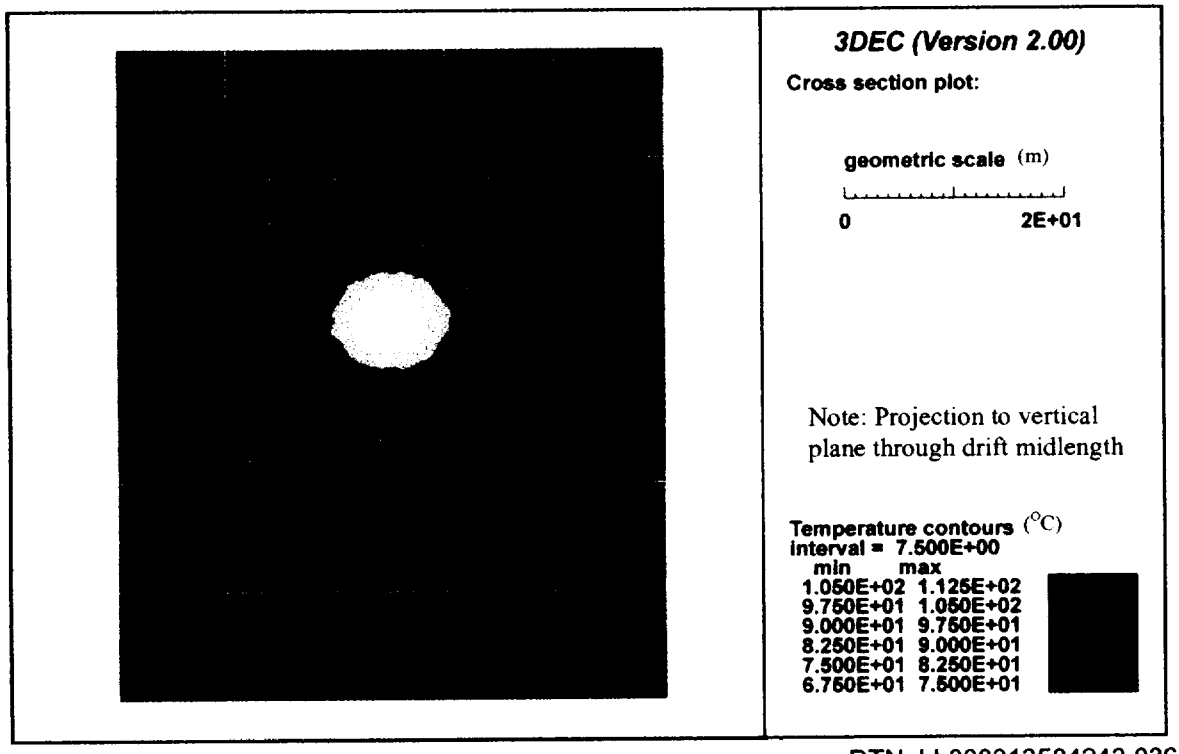


(b) YZ Plane

DTN: LL000313504243.036

Figure I-5. Temperature distribution (°C) at 155 years, early cool-down phase

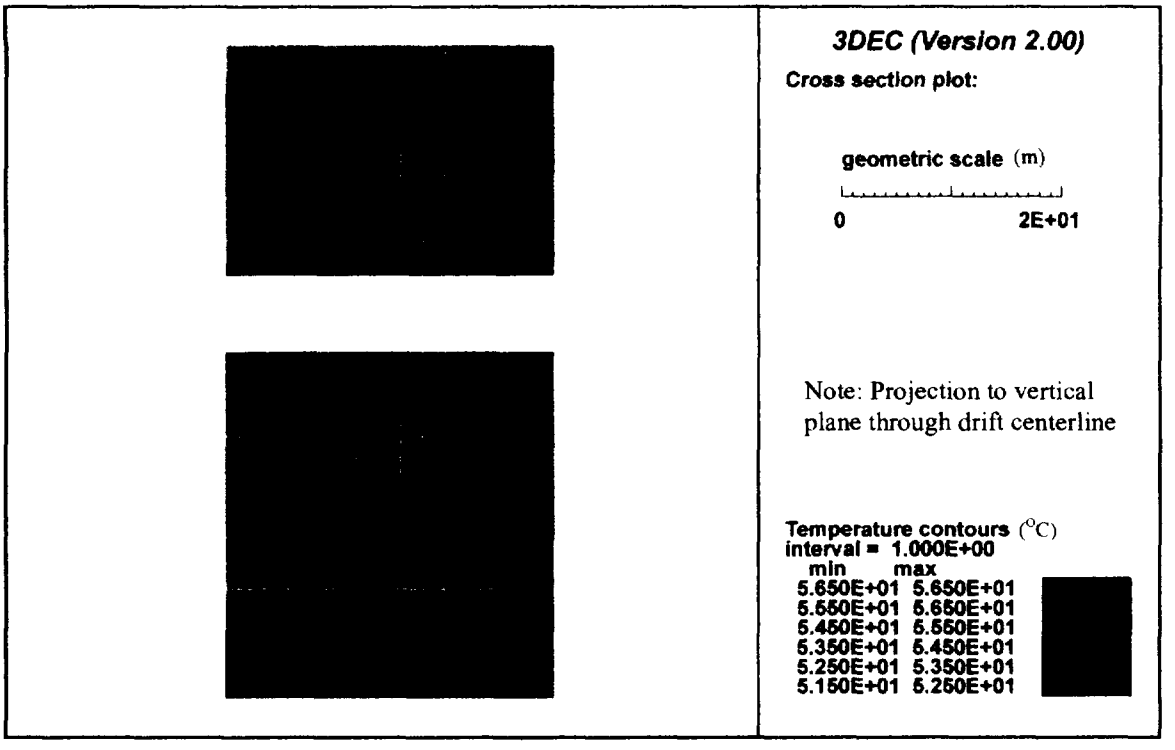


(a) XY Plane

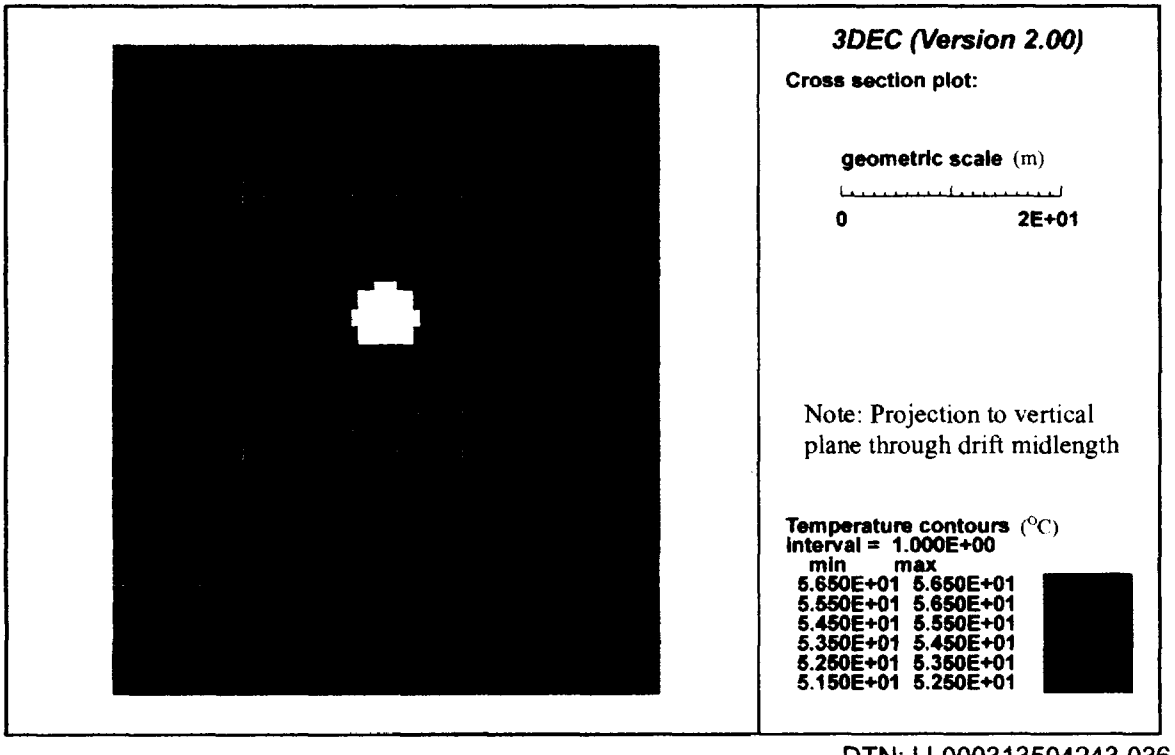


DTN: LL000313504243.036

(b) YZ Plane

Figure I-6. Temperature distribution (°C) at 200 years, middle cool-down phase

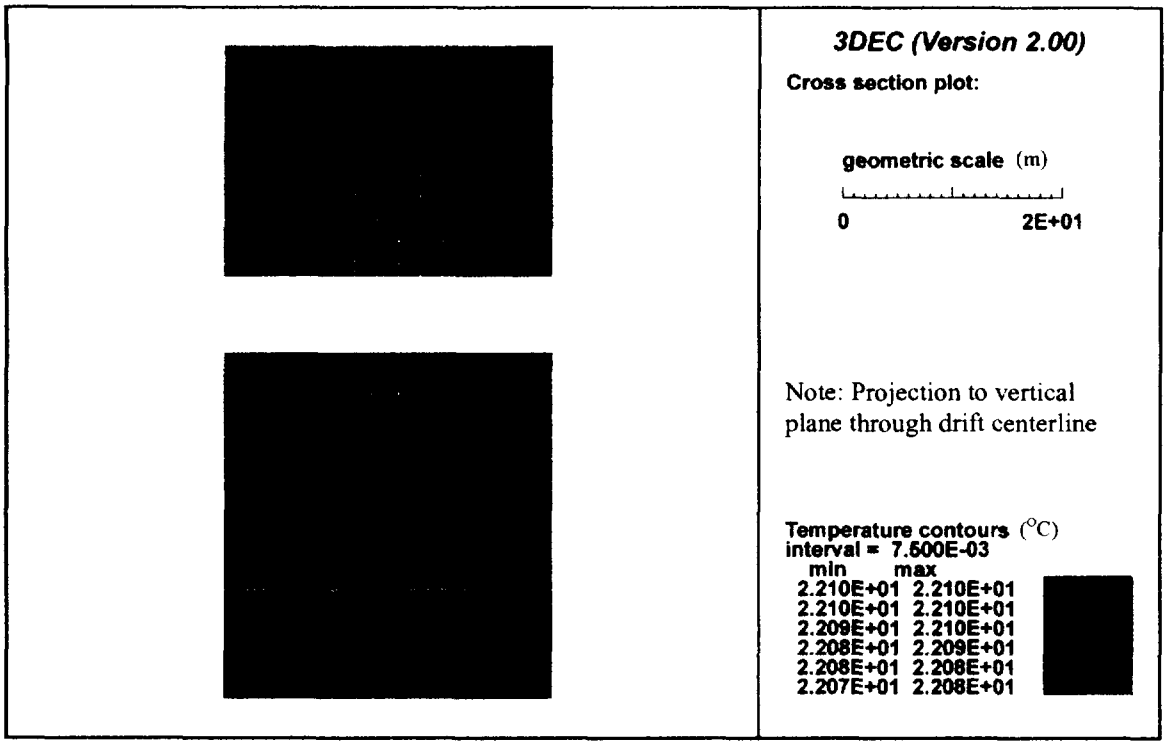


(a) XY Plane

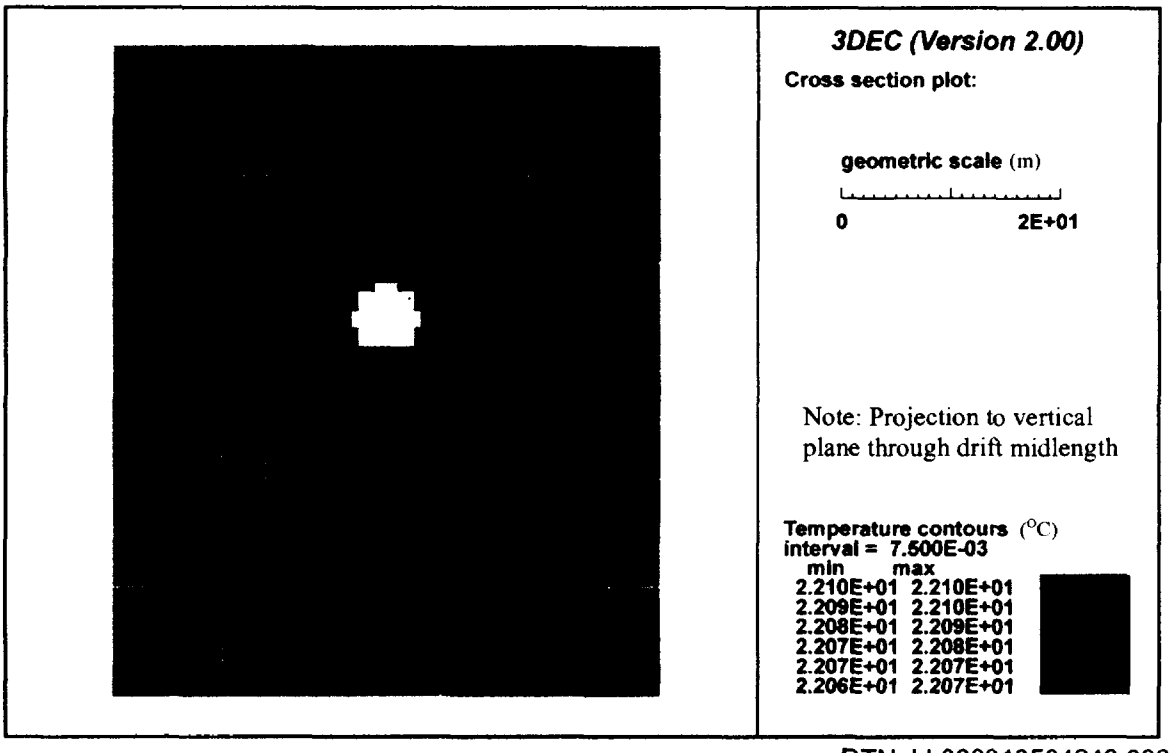


DTN: LL000313504243.036

(b) YZ Plane

Figure I-7. Temperature distribution (°C) at 1000 years, late cool-down phase

# ATTACHMENT II

# PRINCIPAL STRESSES (PAGES II-1 TO II-8)

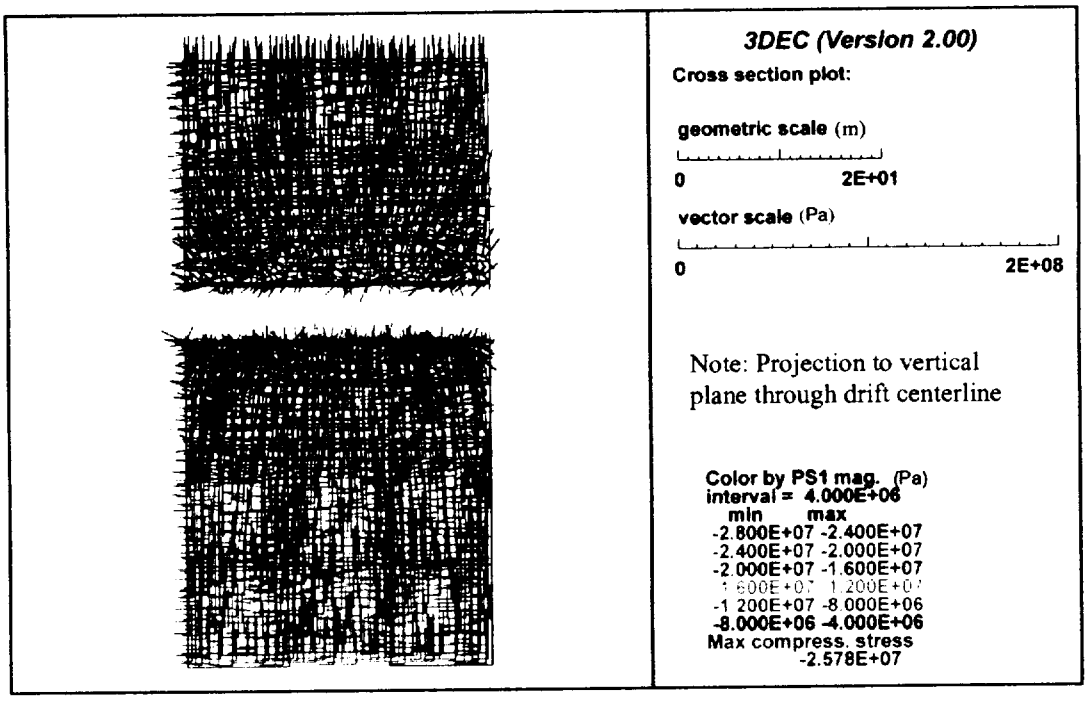


(a) XY Plane

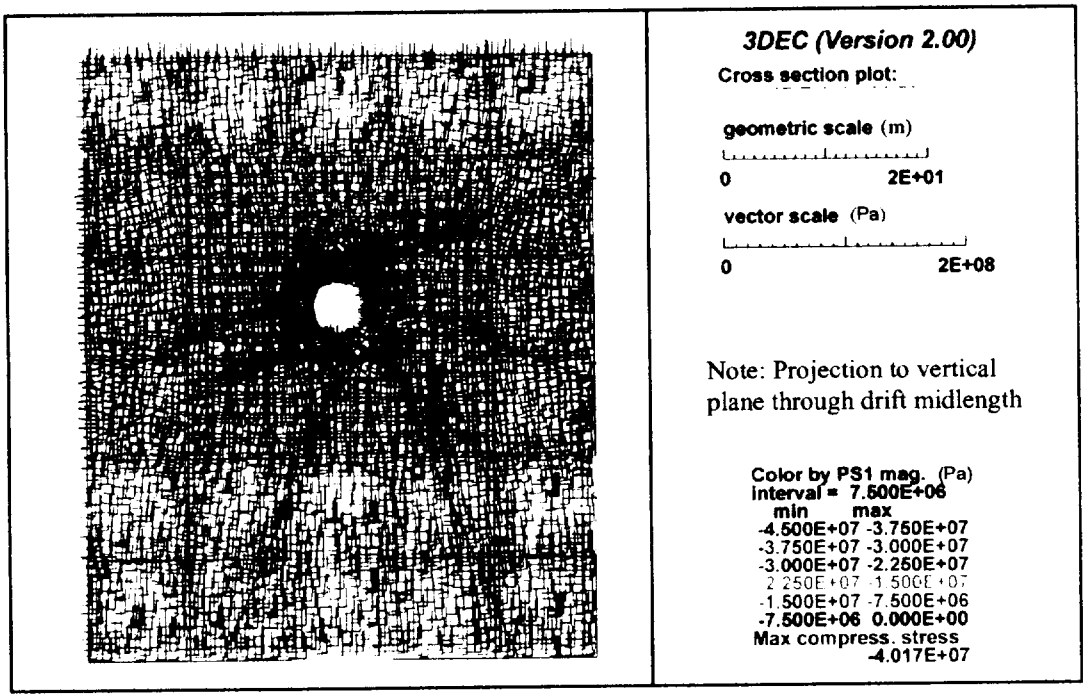


(b) YZ Plane

DTN: LL000313504243.036

Figure II-1. Principal stress distribution at 10 years, early ventilation phase

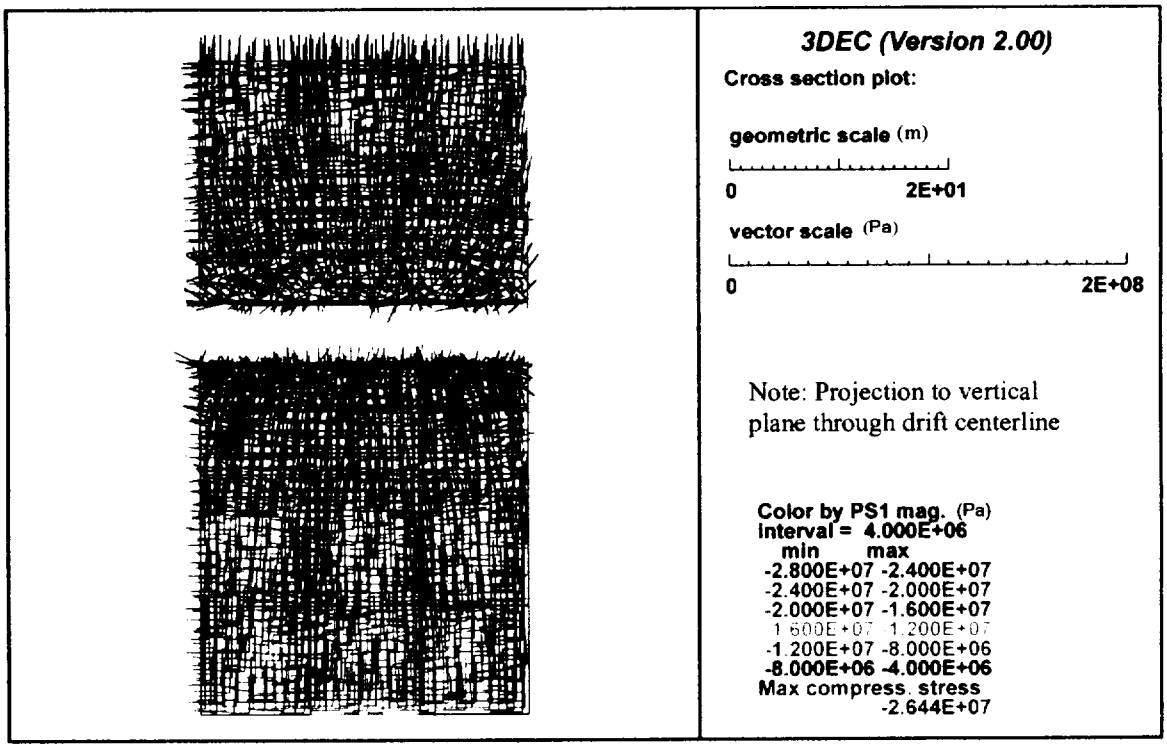


(a) XY Plane

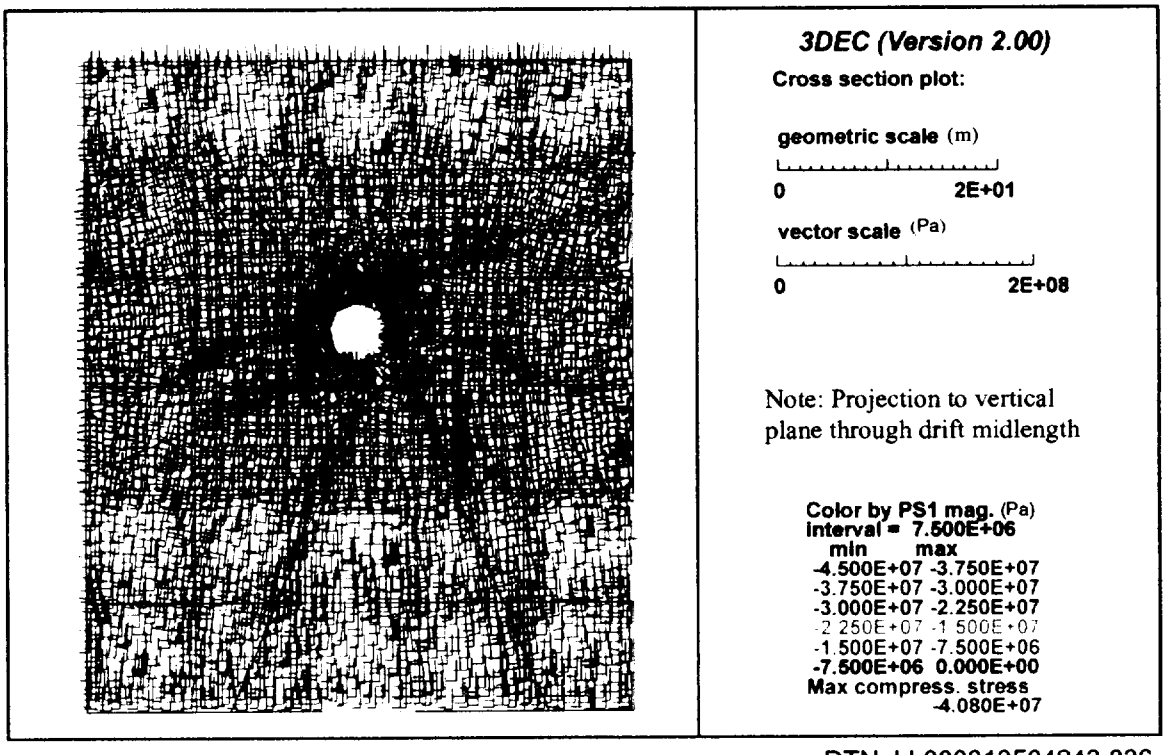


(b) YZ Plane

DTN: LL000313504243.036

Figure II-2. Principal stress distribution at 50 years, late ventilation phase

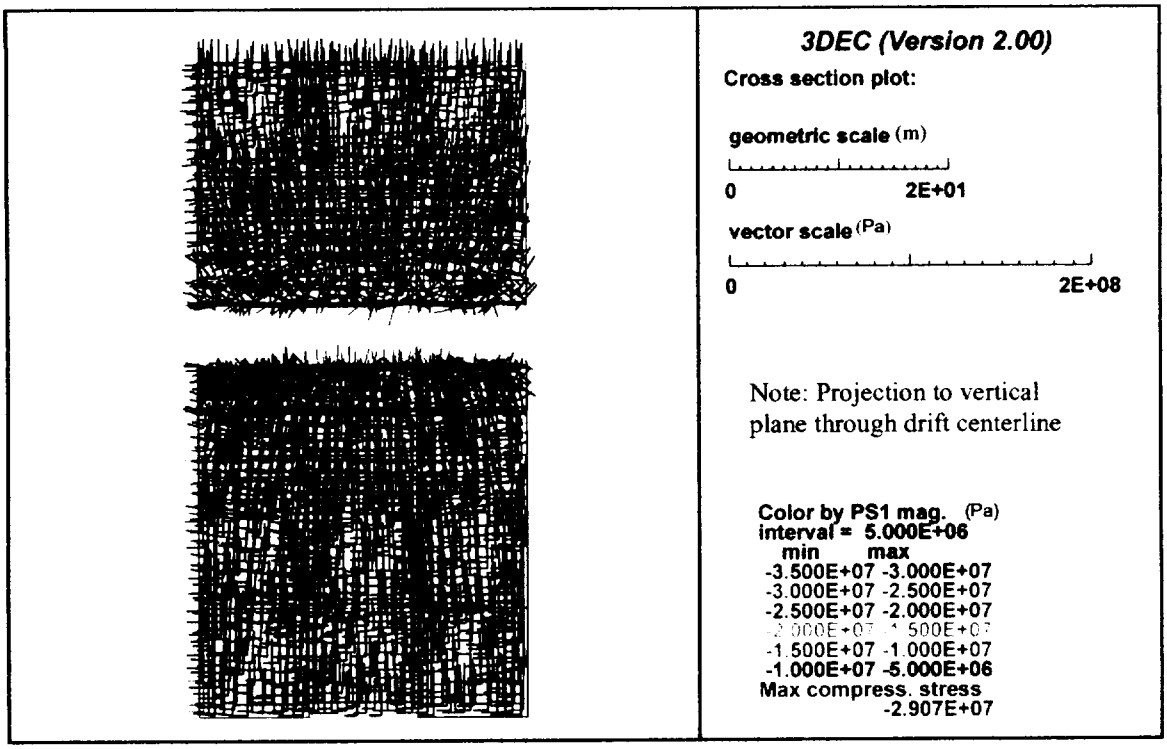


(a) XY Plane

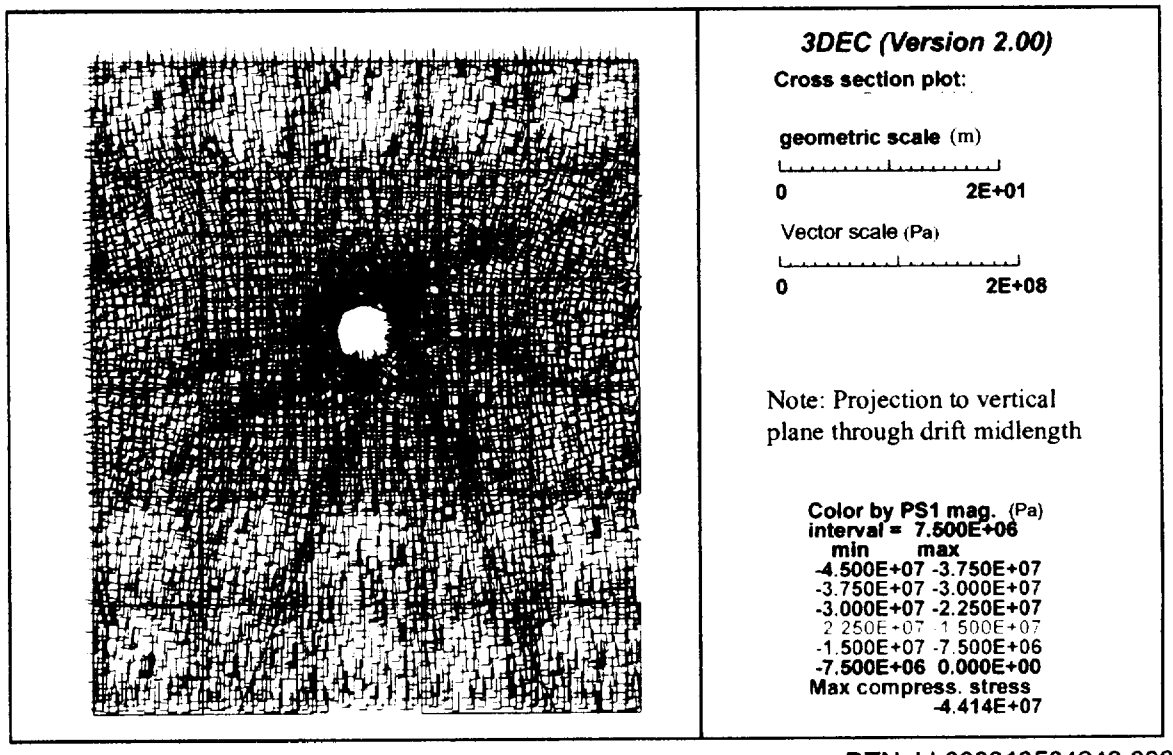


(b) YZ Plane

DTN: LL000313504243.036

Figure II-3. Principal stress distribution at 55 years, early post-ventilation heating phase

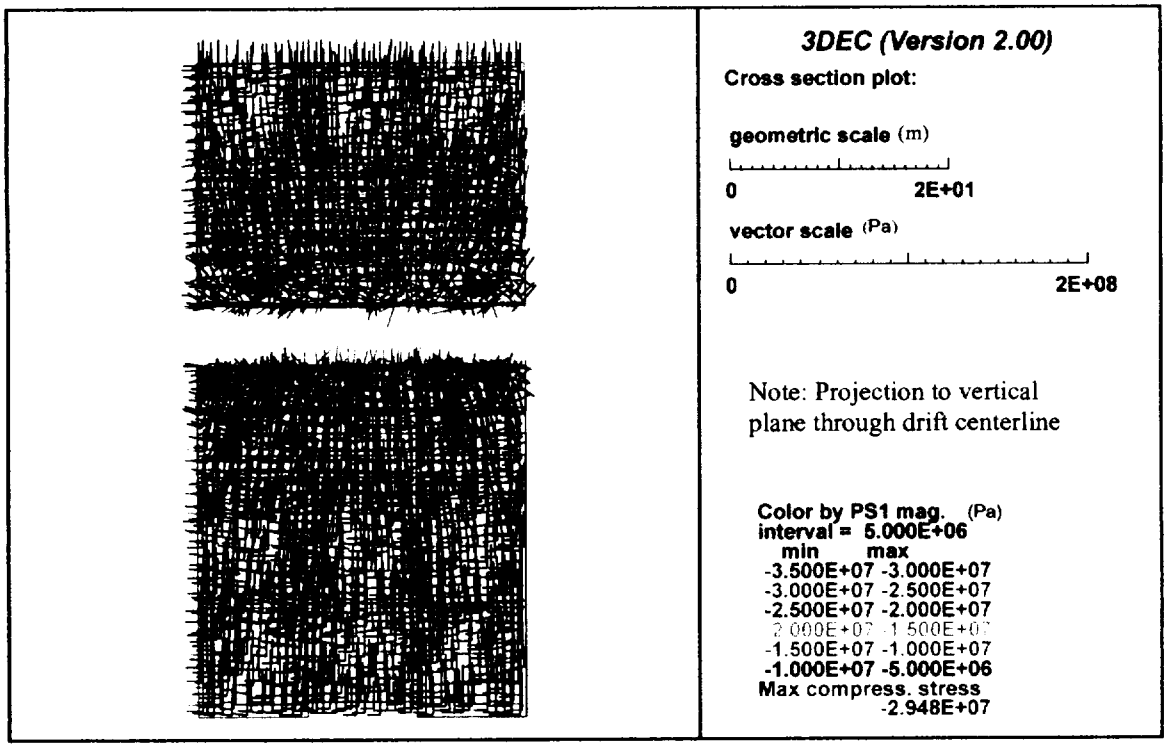


(a) XY Plane

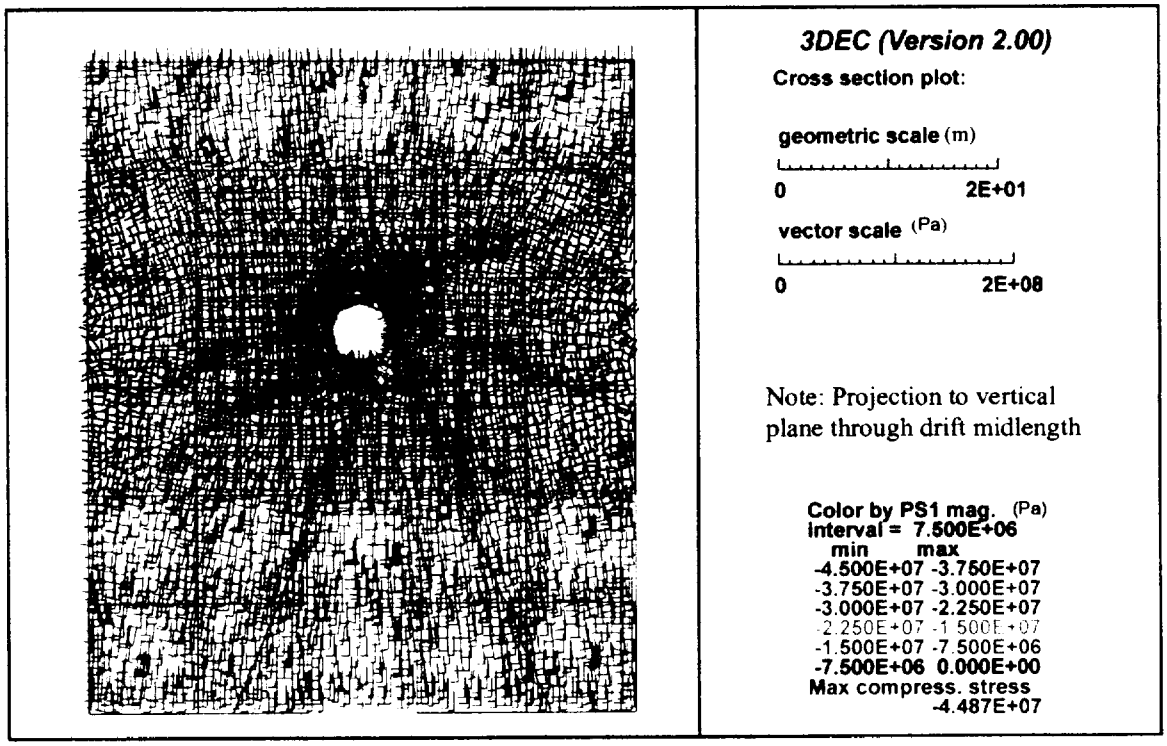


(b) YZ Plane DTN: LL000313504243.036

Figure II-4. Principal stress distribution at 150 years, late post-ventilation heating phase

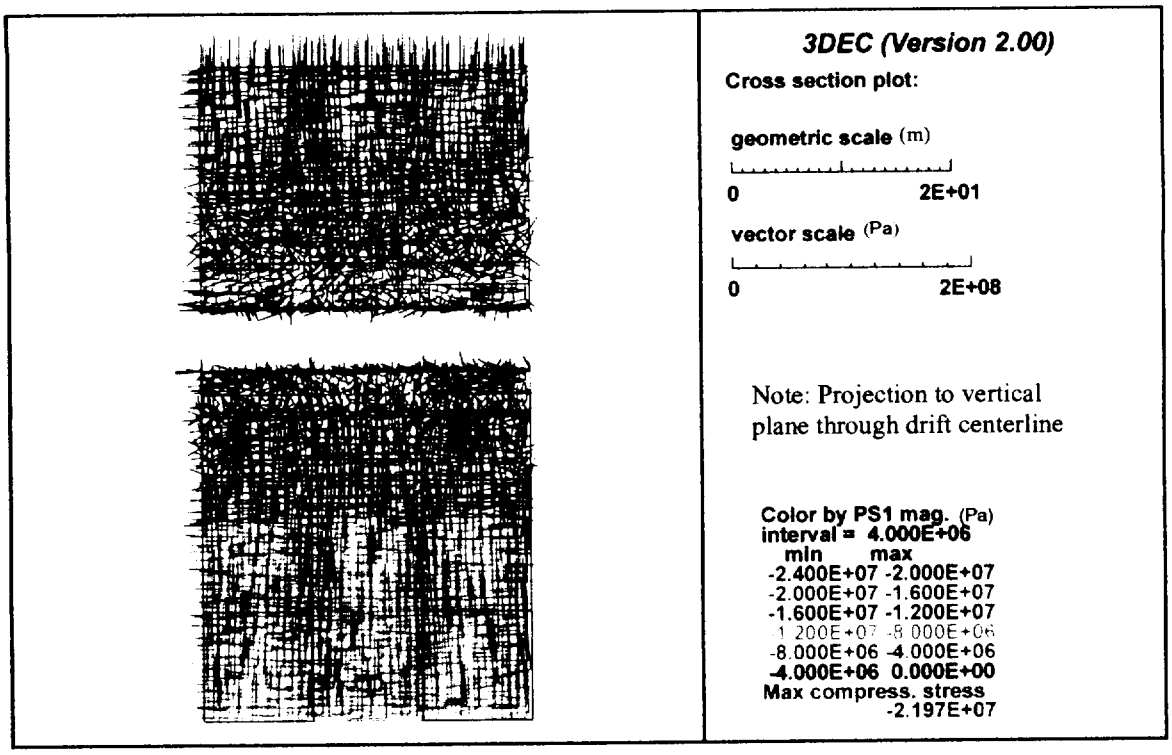


(a) XY Plane

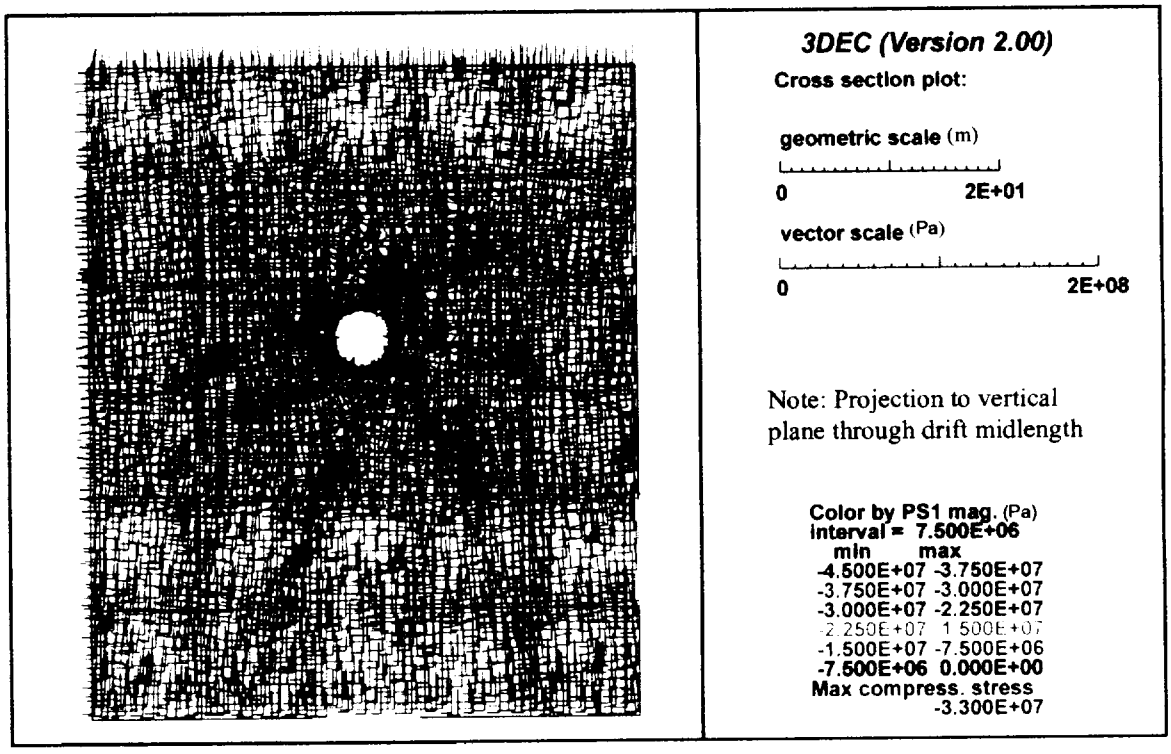


(b) YZ Plane

DTN: LL000313504243.036

Figure II-5. Principal stress distribution at 155 years, early cool-down phase

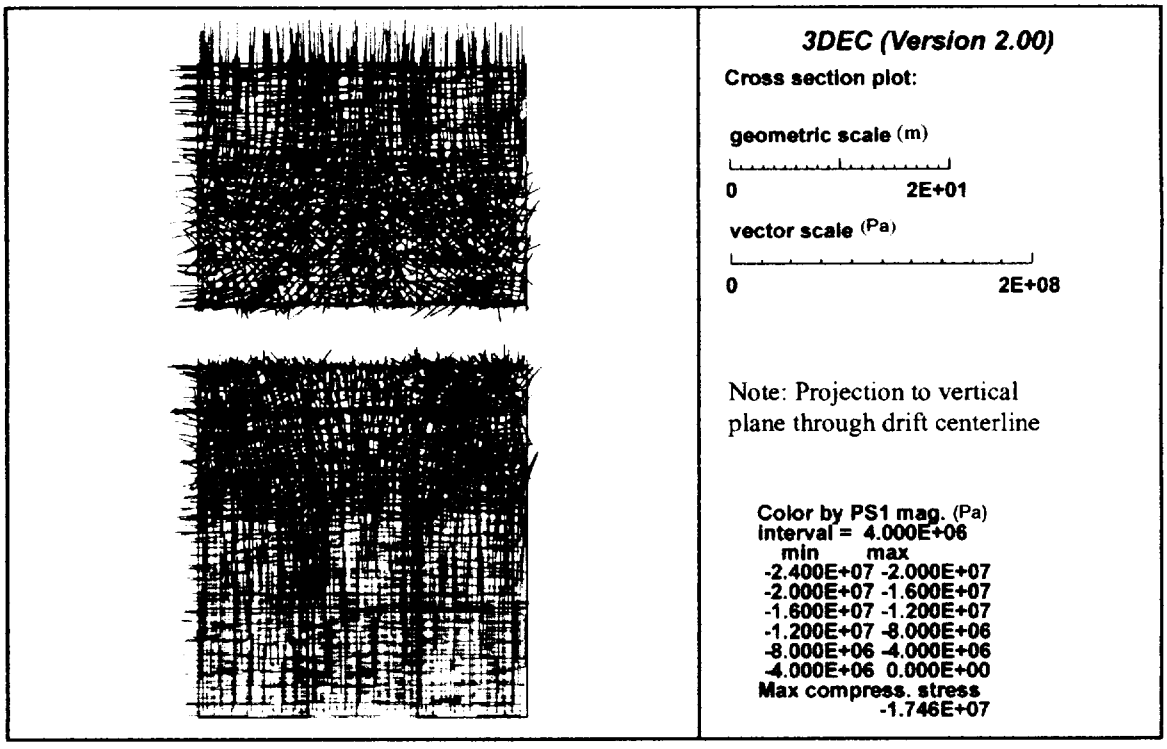


(a) XY Plane

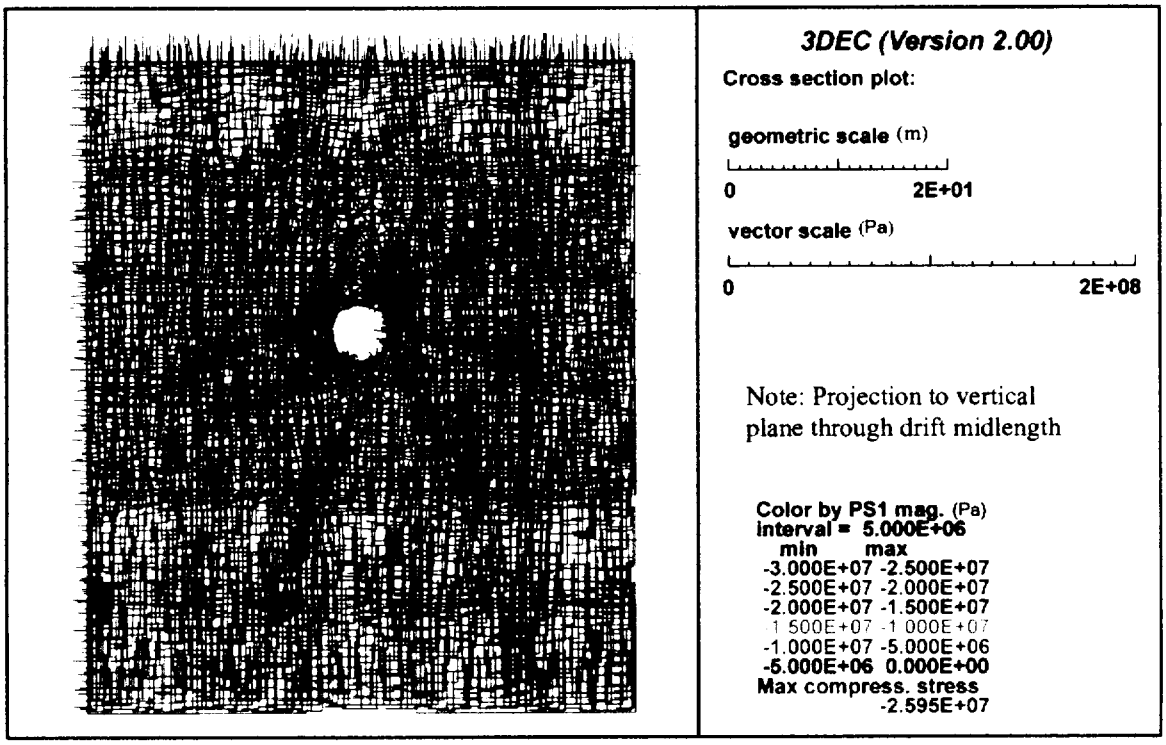


(b) YZ Plane

DTN: LL000313504243.036

Figure II-6. Principal stress distribution at 200 years, middle cool-down phase

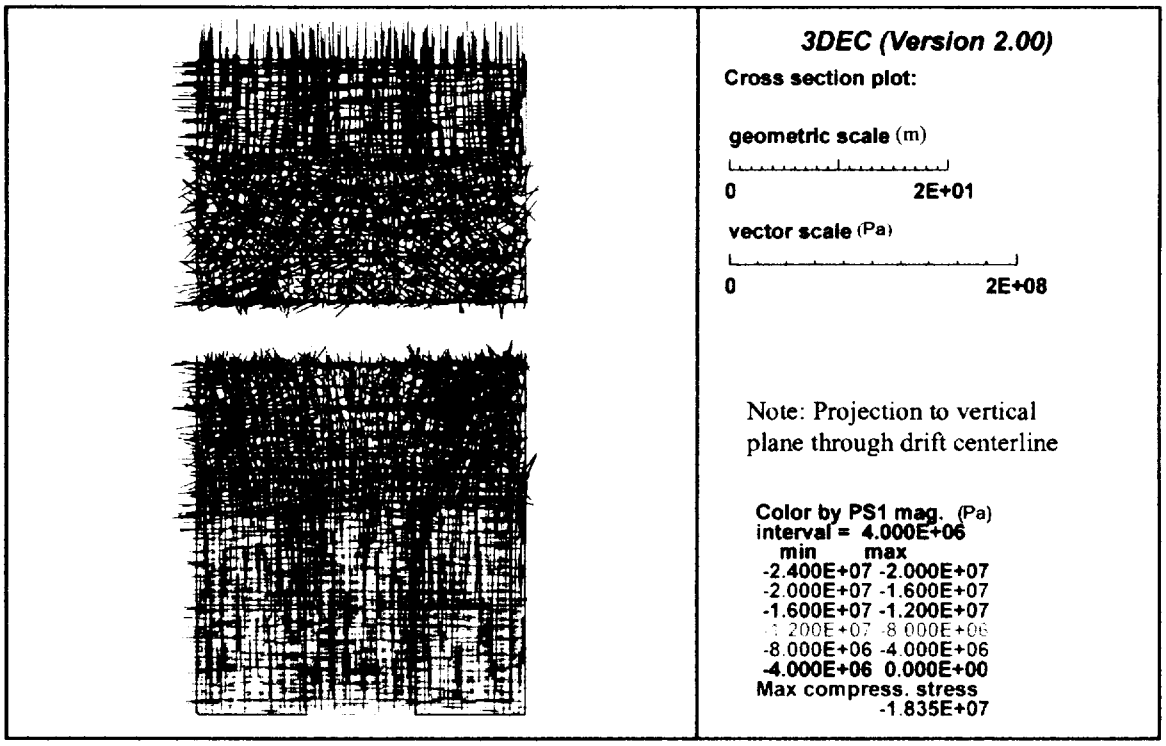


(a) XY Plane

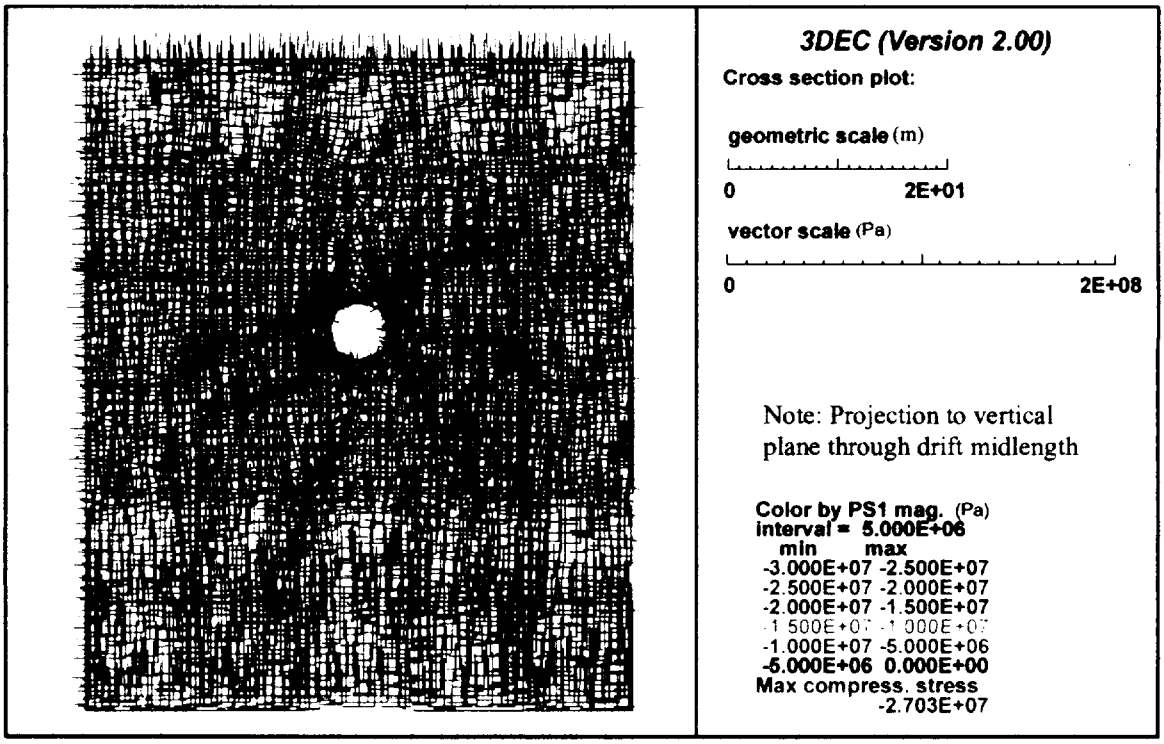


(b) YZ Plane

DTN: LL000313504243.036

Figure II-7. Principal stress distribution at 1000 years, late cool-down phase

## ATTACHMENT III

## JOINT NORMAL DISPLACEMENTS (PAGES III-1 TO III-8)

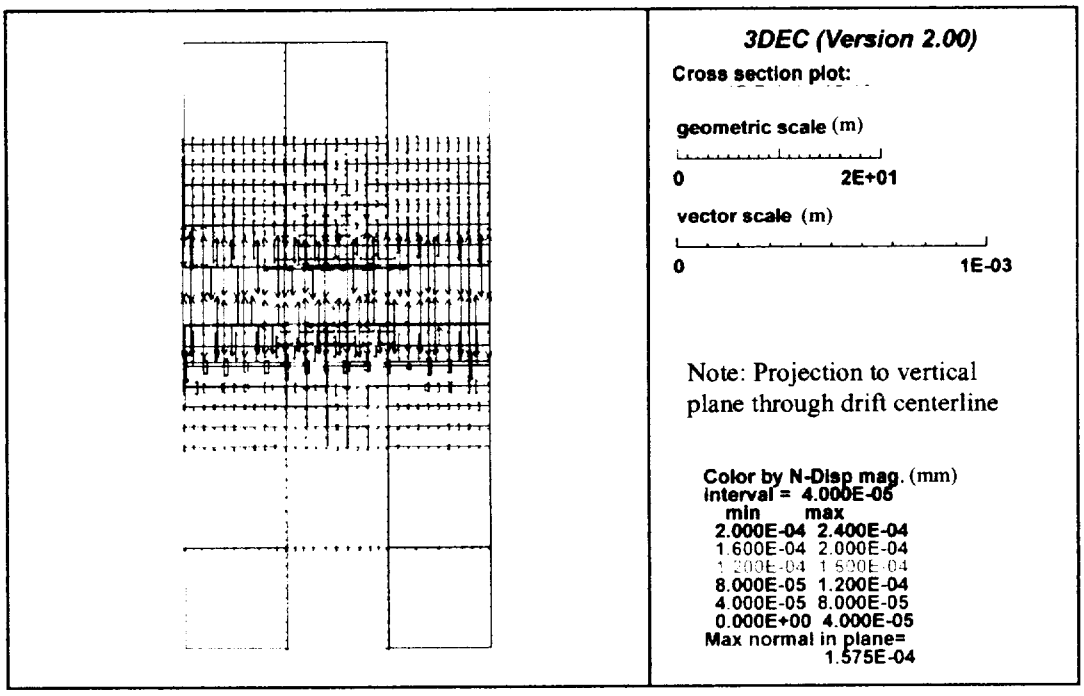


(a) XY Plane

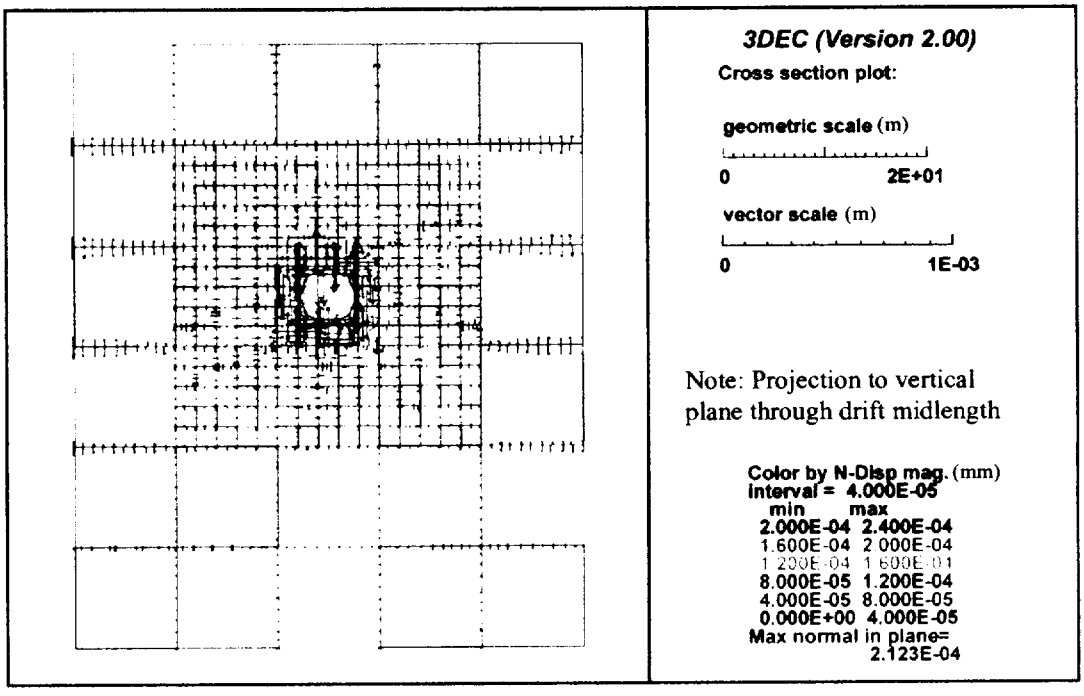


DTN: LL000313504243.036

(b) YZ Plane

Figure III-1. Joint normal displacements at 10 years, early ventilation phase

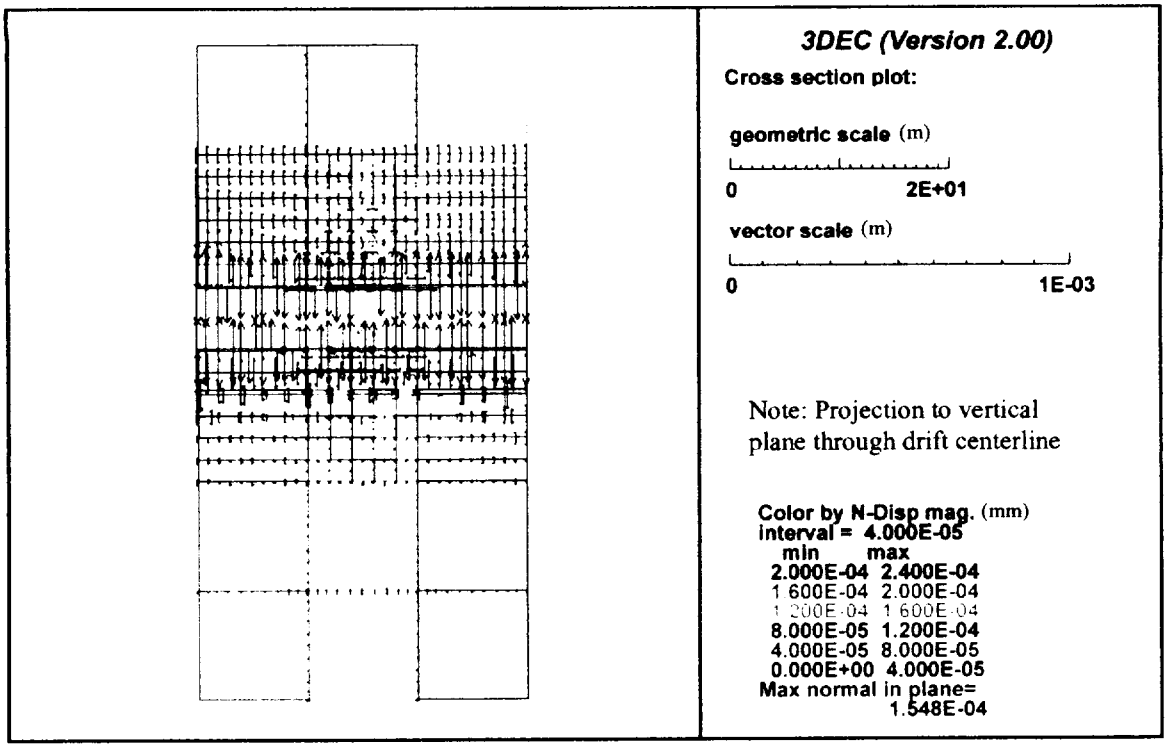


(a) XY Plane

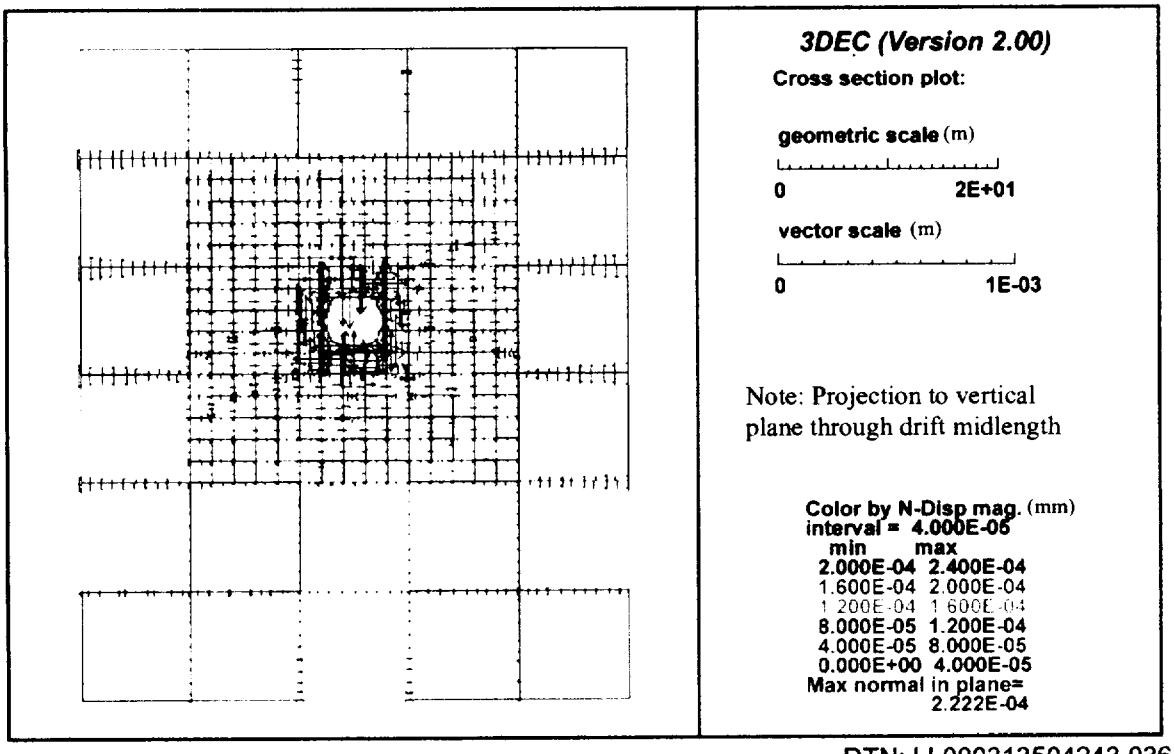


DTN: LL000313504243.036

(b) YZ Plane

Figure III-2. Joint normal displacements at 50 years, late ventilation phase

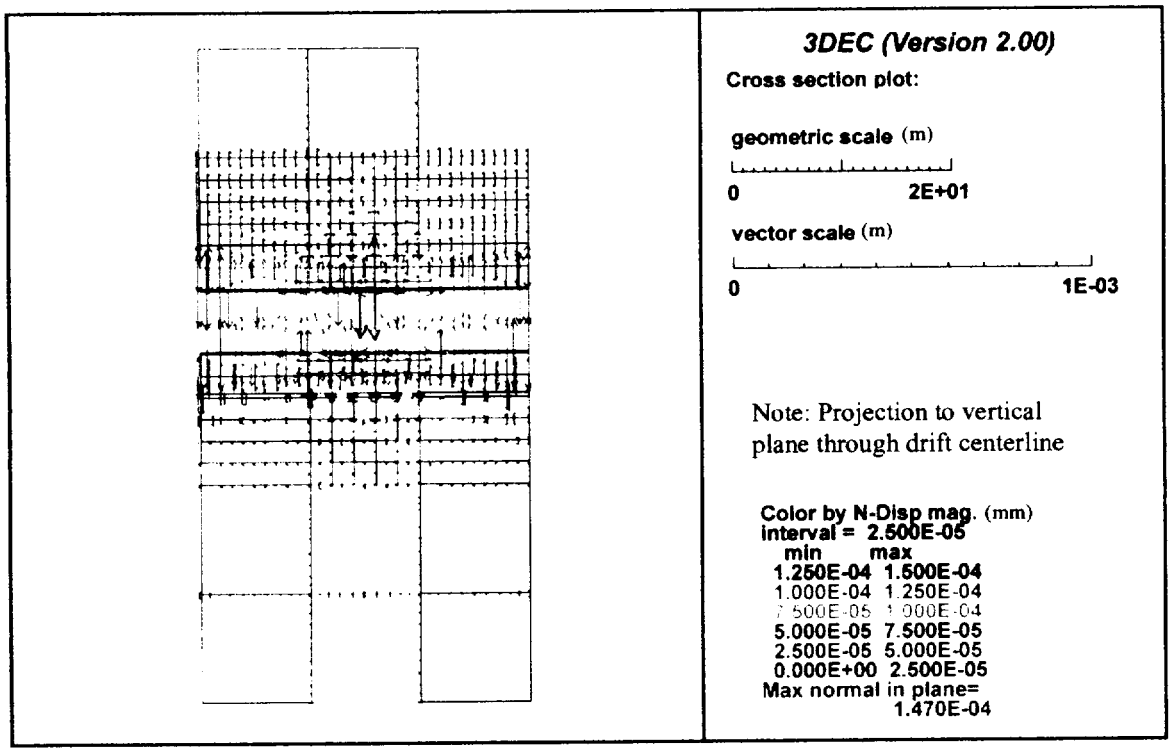


(a) XY Plane

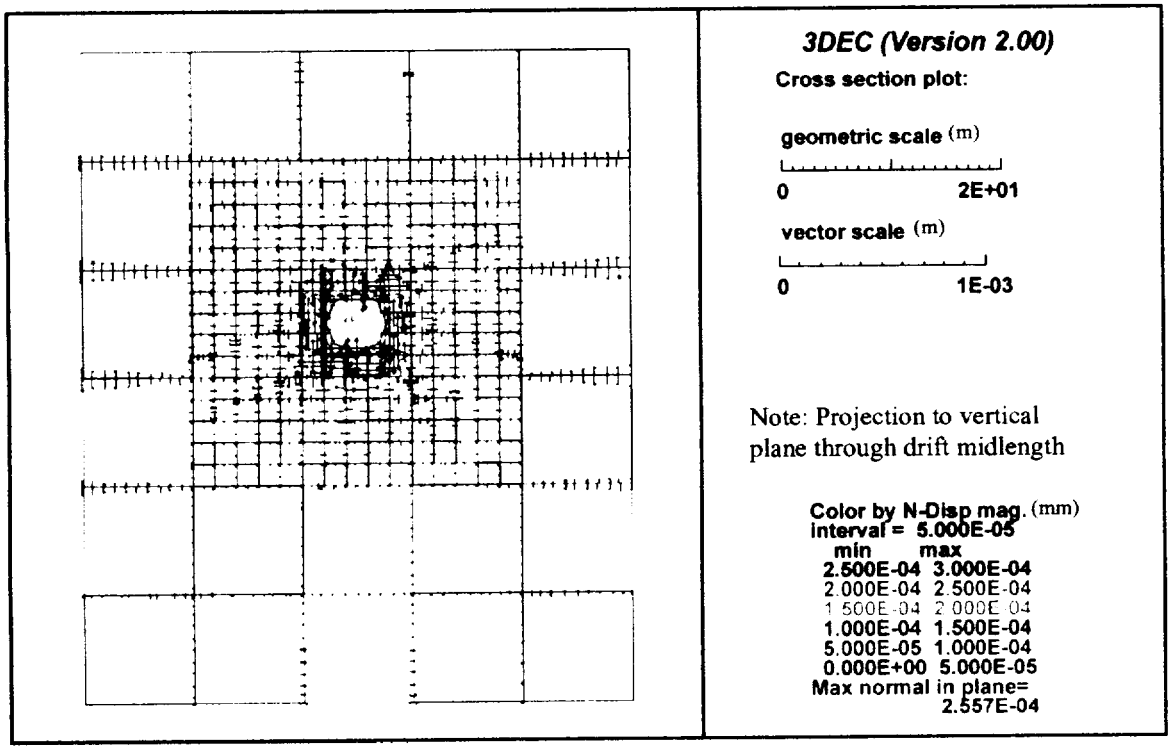


DTN: LL000313504243.036

(b) YZ Plane

Figure III-3. Joint normal displacements at 55 years, early post-ventilation heating phase

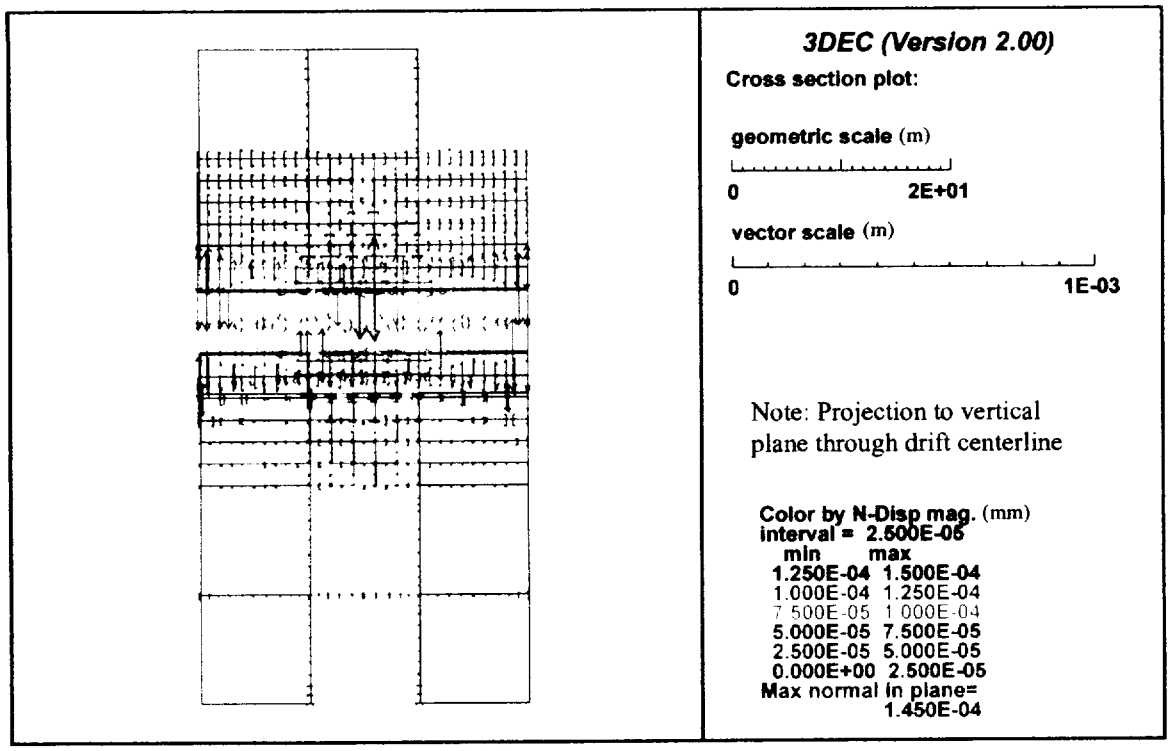


(a) XY Plane

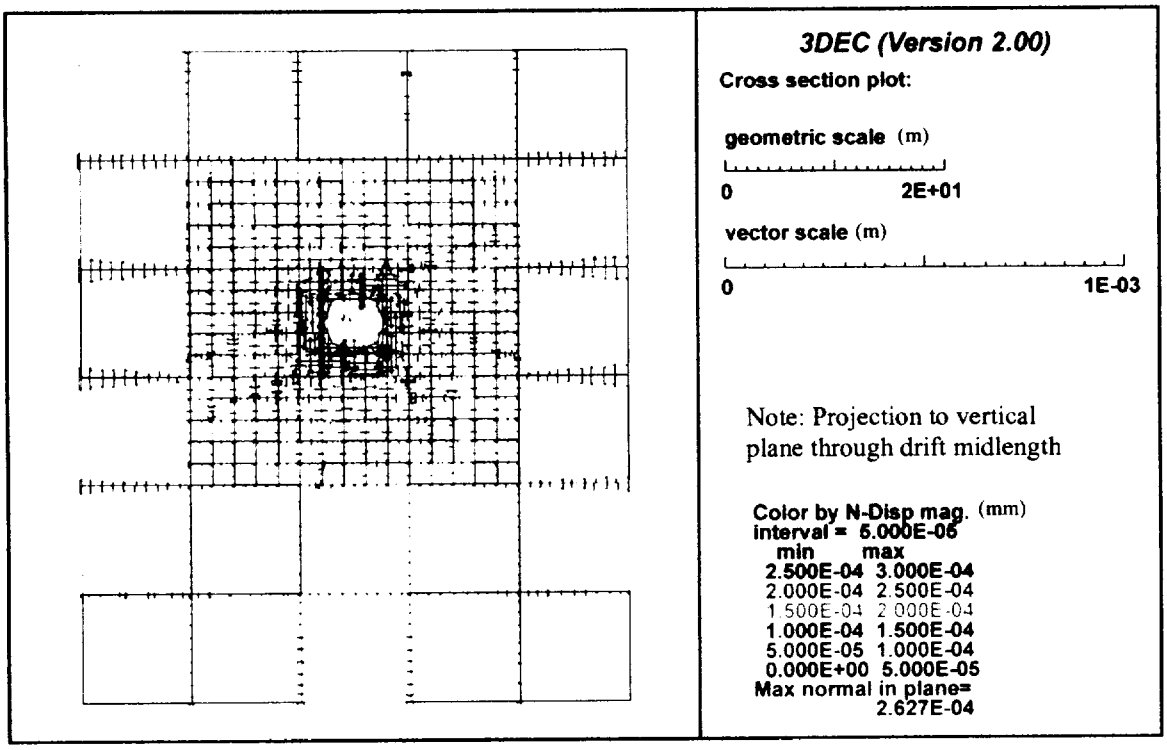


DTN: LL000313504243.036

(b) YZ Plane

Figure III-4. Joint normal displacements at 150 years, late post-ventilation heating phase

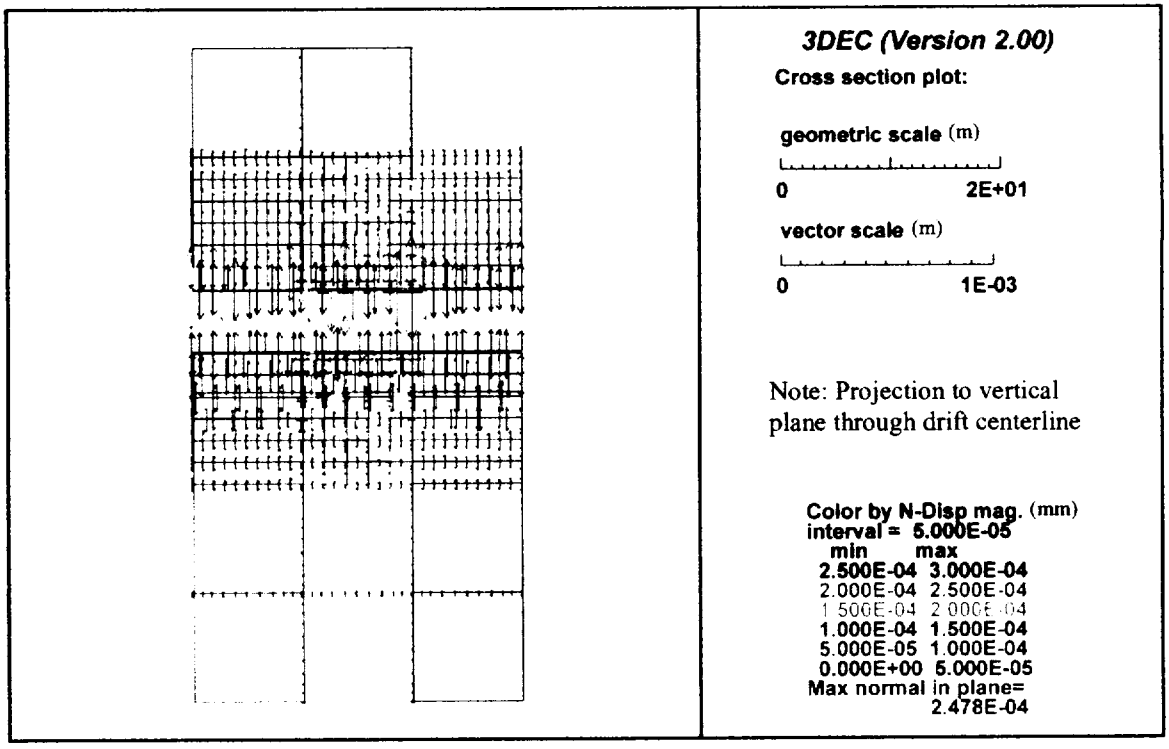


(a) XY Plane

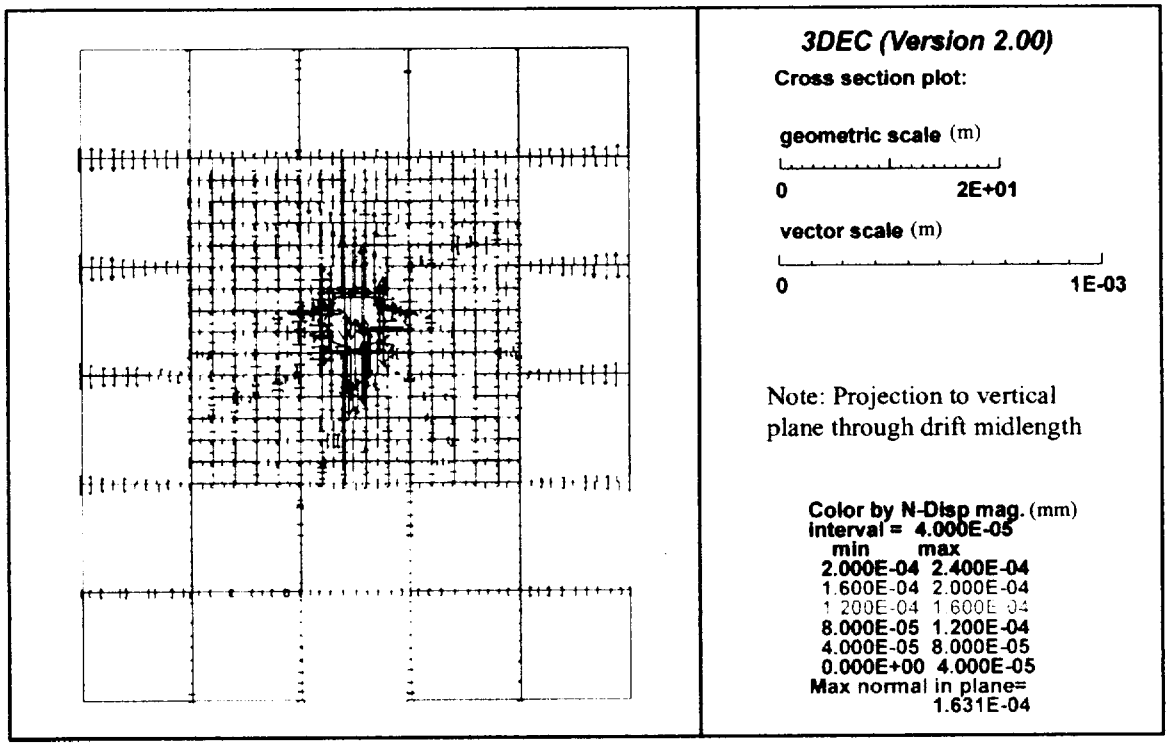


(b) YZ Plane

DTN: LL000313504243.036

Figure III-5. Joint normal displacements at 155 years, early cool-down phase

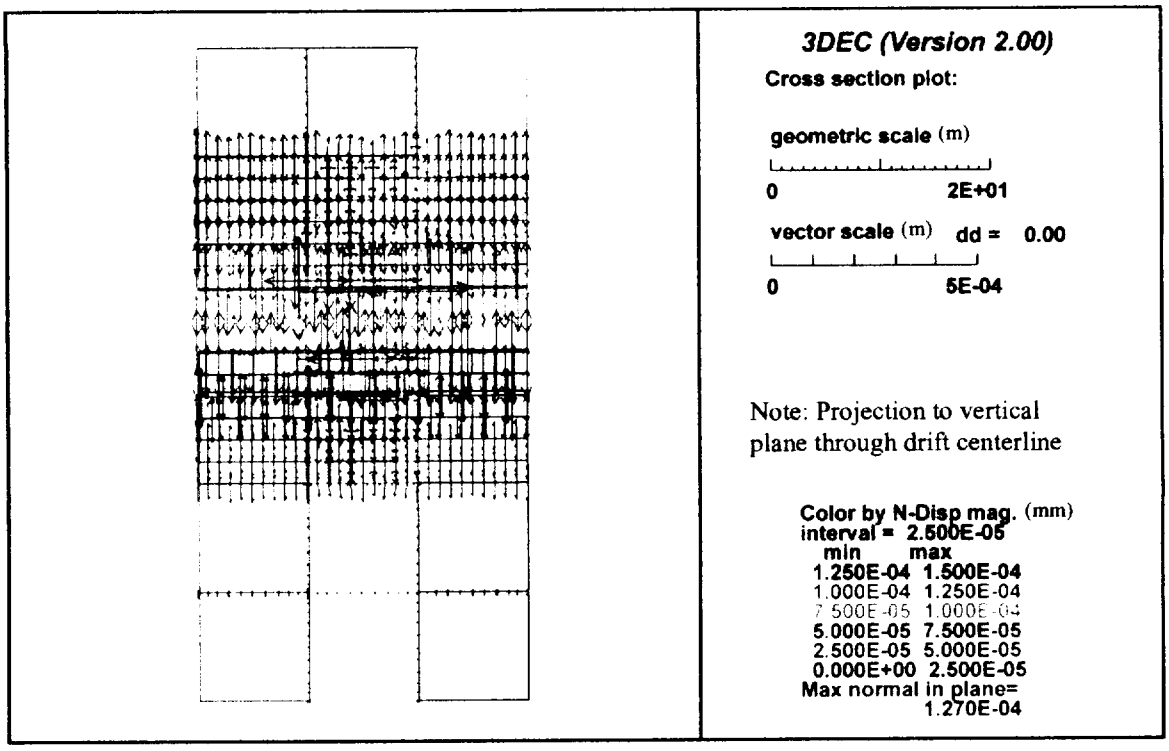


(a) XY Plane

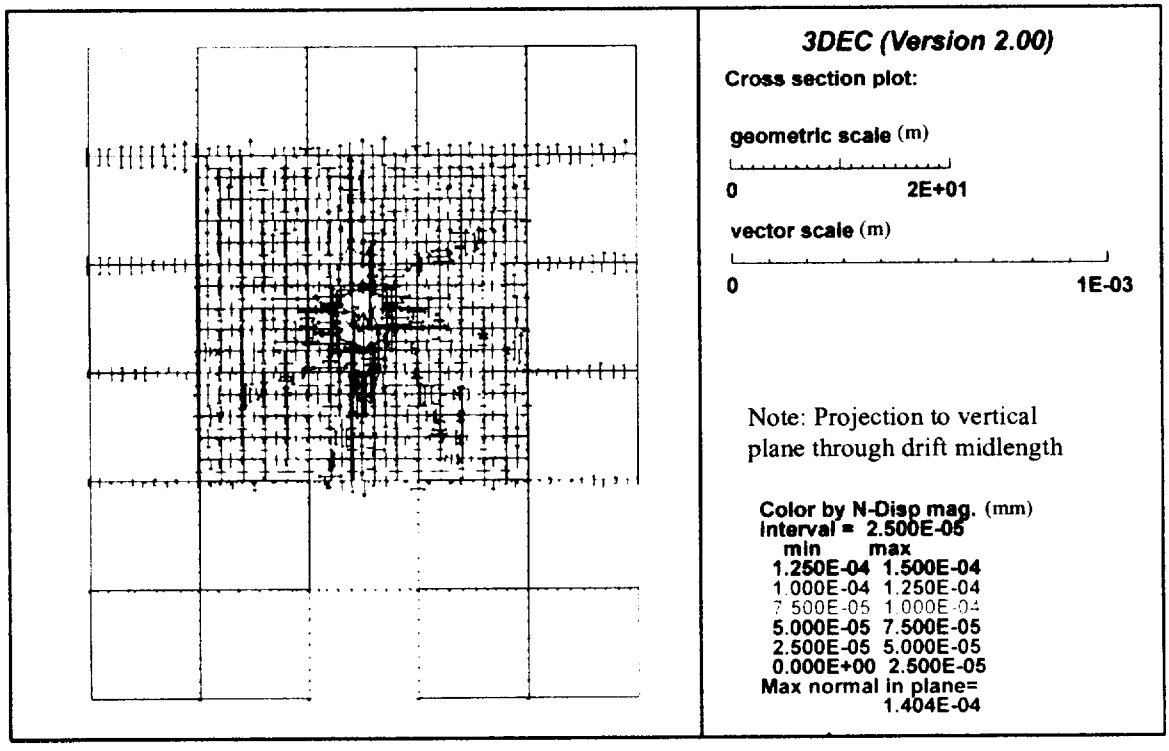


(b) YZ Plane

DTN: LL000313504243.036

Figure III-6. Joint normal displacements at 200 years, middle cool-down phase

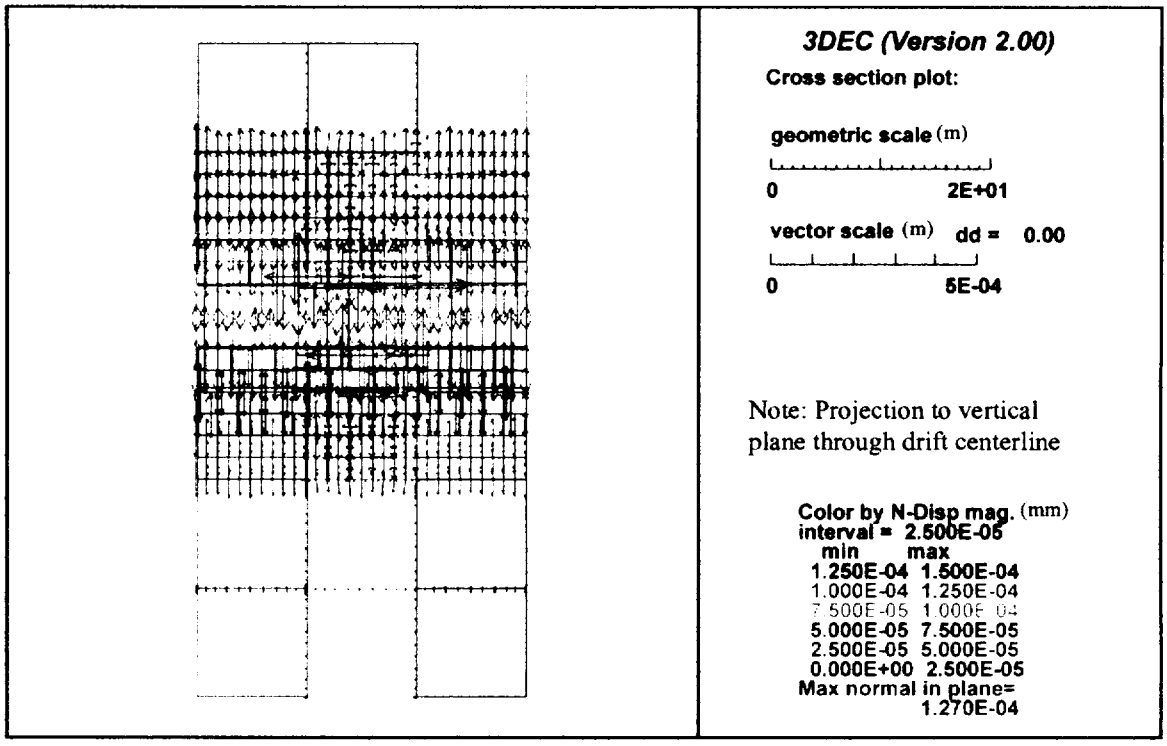


(a) XY Plane

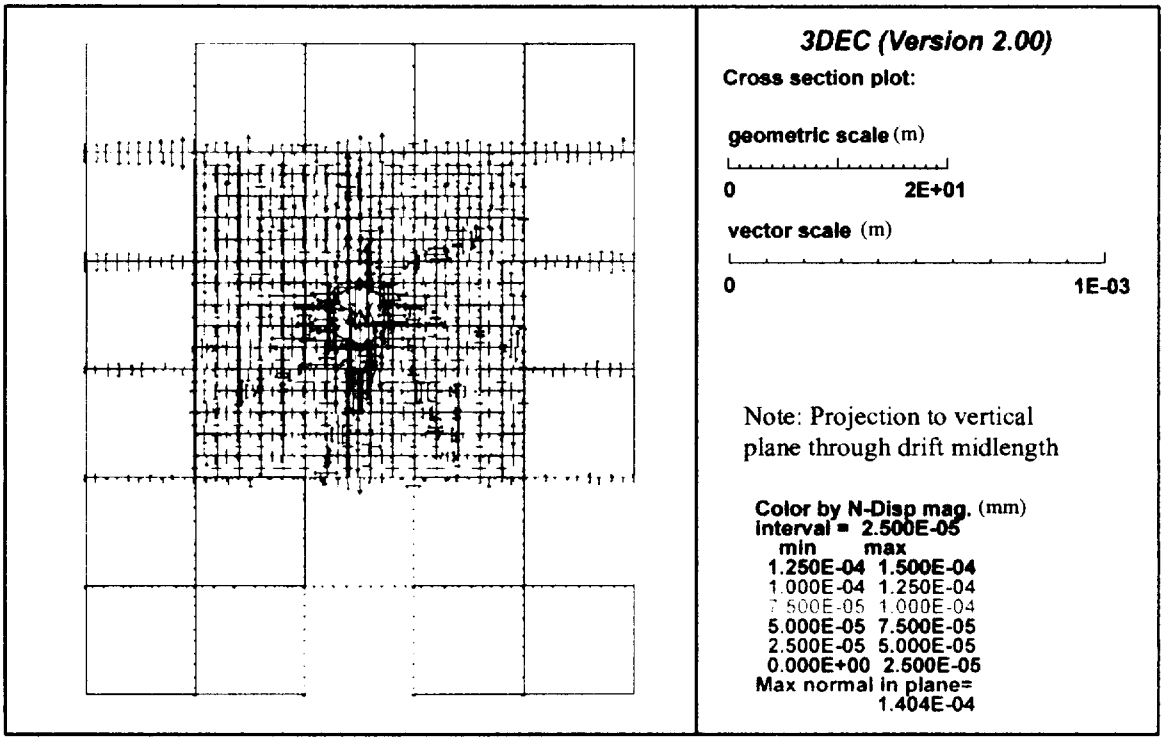


DTN: LL000313504243.036

(b) YZ Plane

Figure III-7. Joint normal displacements at 1000 years, late cool-down phase

## ATTACHMENT IV

## JOINT SHEAR DISPLACEMENTS (PAGES IV-1 TO IV-8)

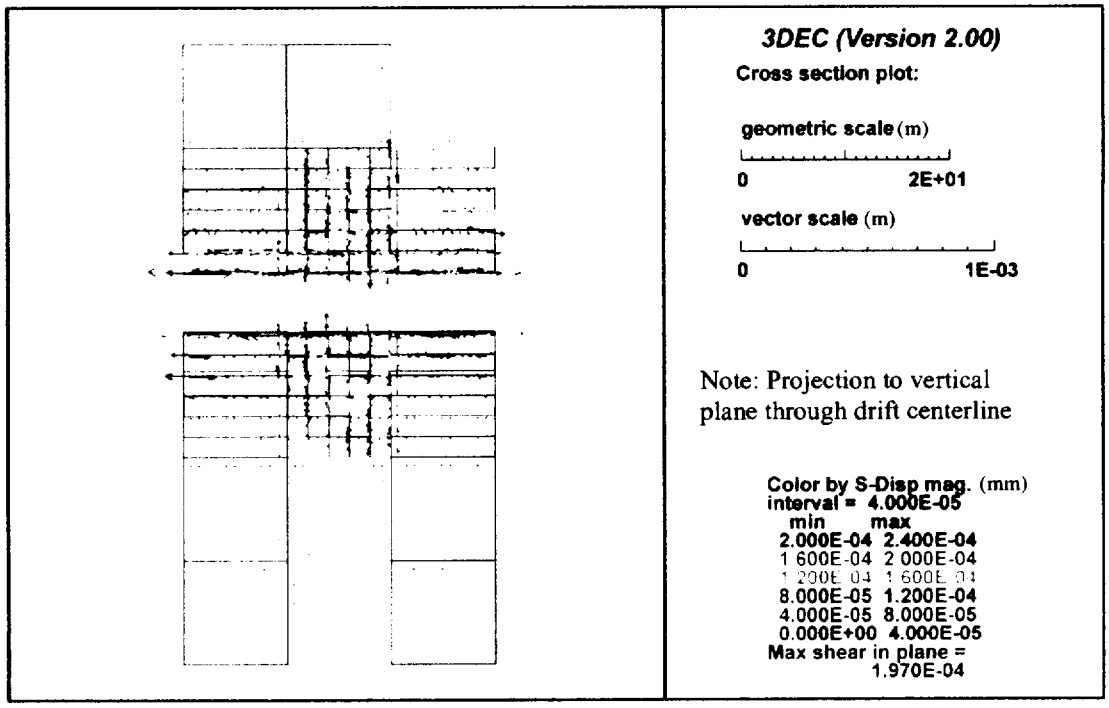


(a) XY Plane

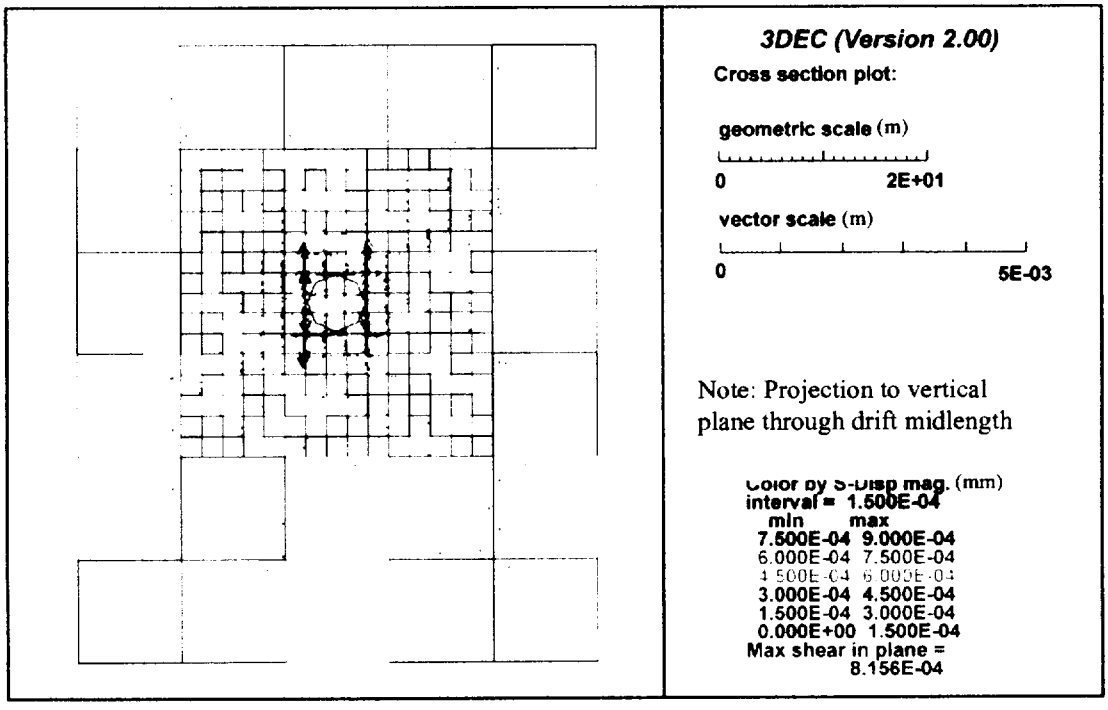


(b) YZ Plane

DTN: LL000313504243.036

Figure IV-1. Joint shear displacements at 10 years, early ventilation phase

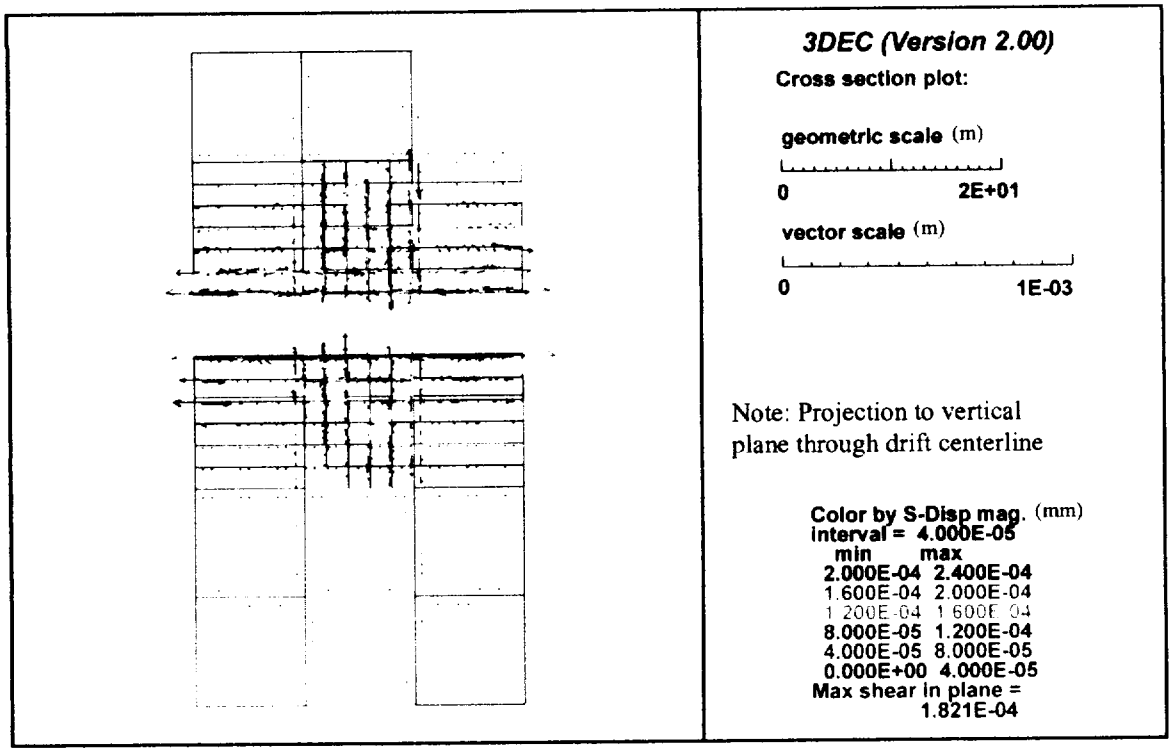


(a) XY Plane

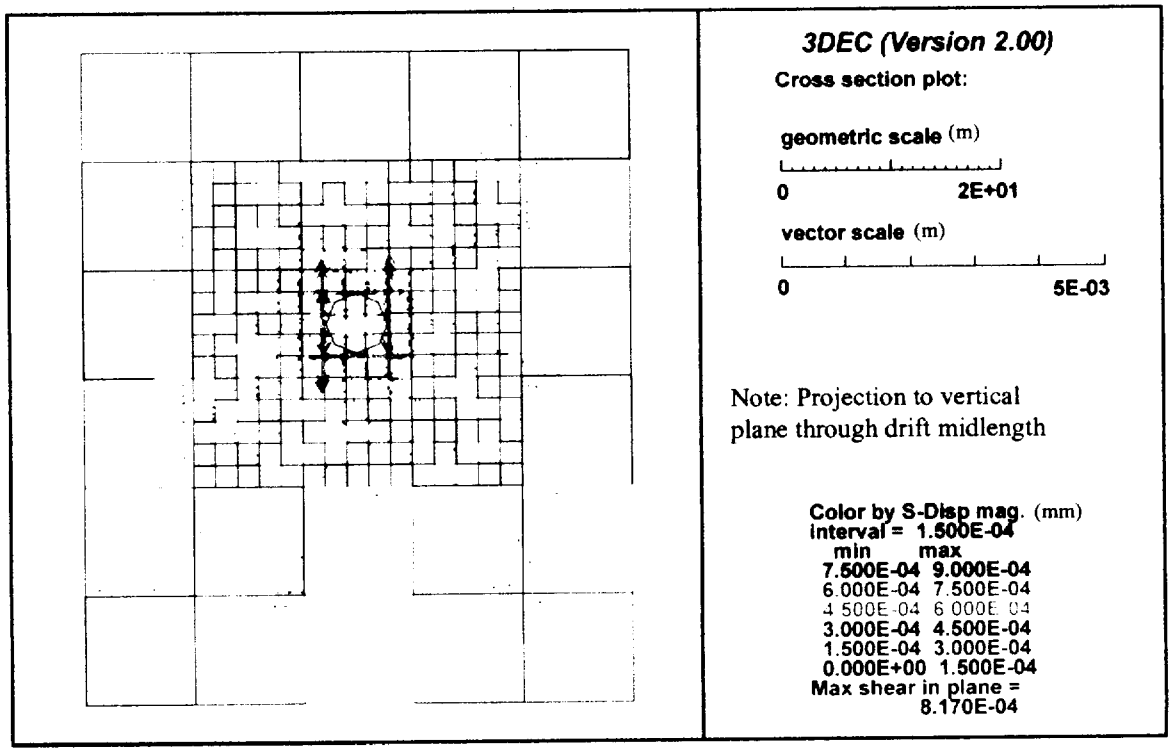


(b) YZ Plane

DTN: LL000313504243.036

Figure IV-2. Joint shear displacements at 50 years, late ventilation phase

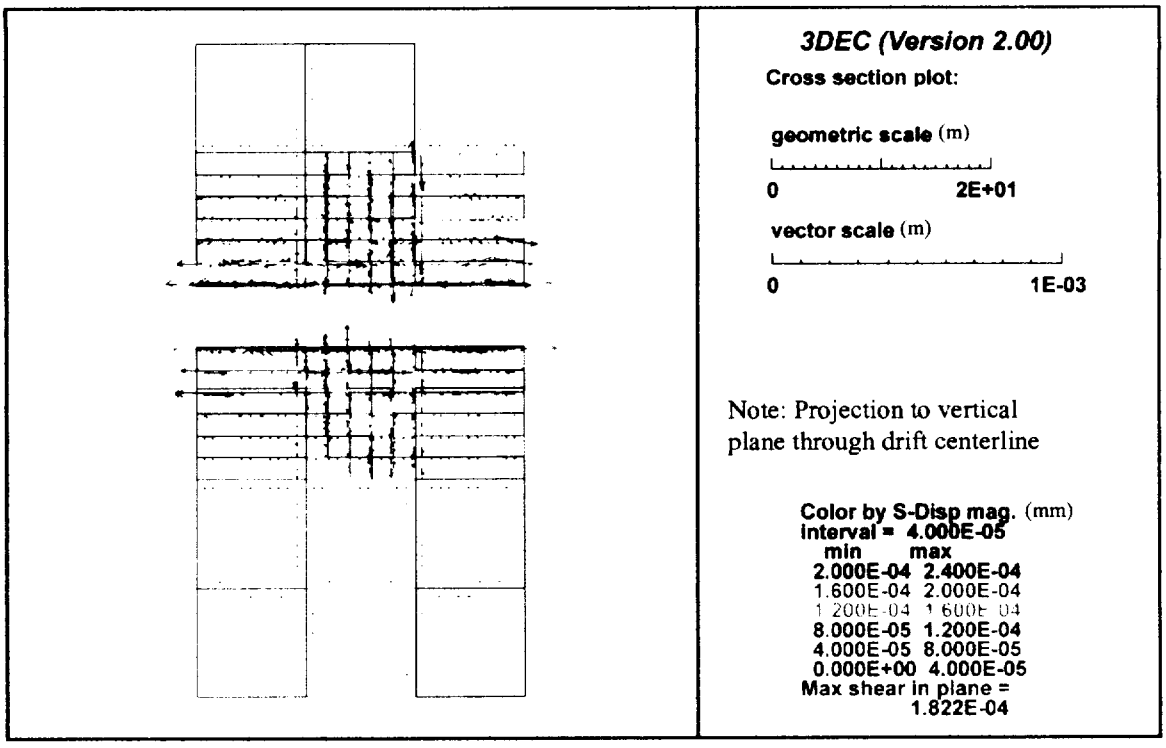


(a) XY Plane

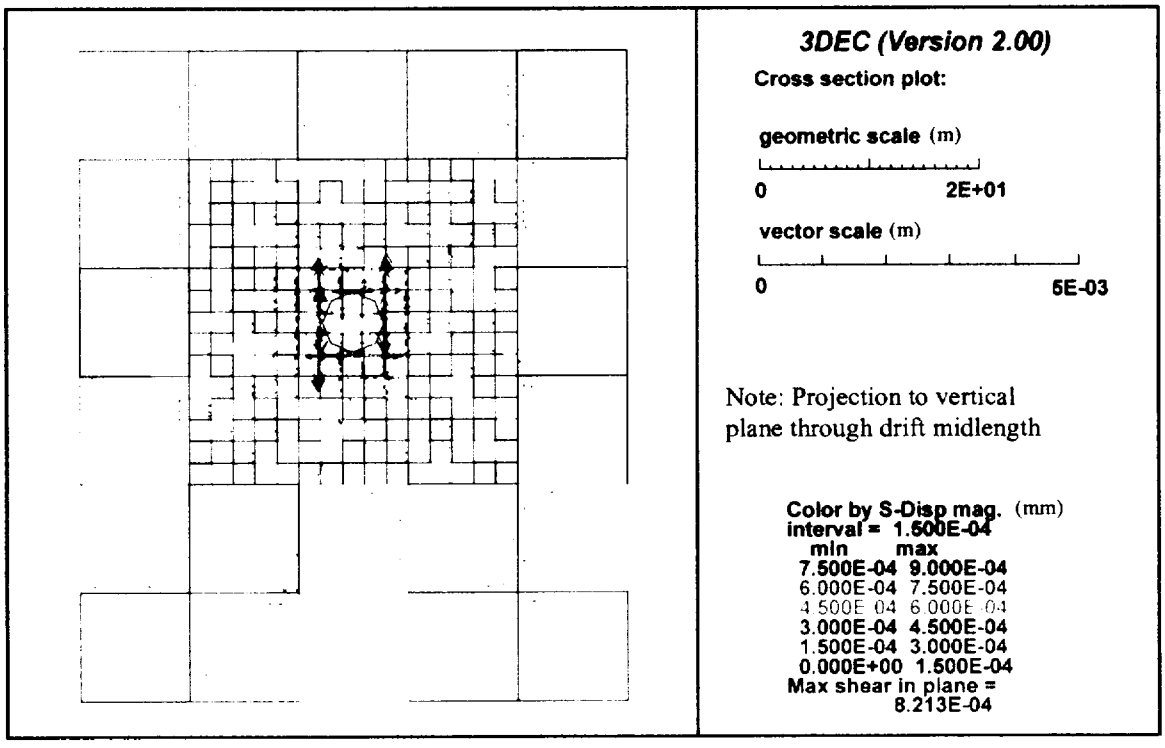


(b) YZ Plane

DTN: LL000313504243.036

Figure IV-3. Joint shear displacements at 55 years, early post-ventilation heating phase

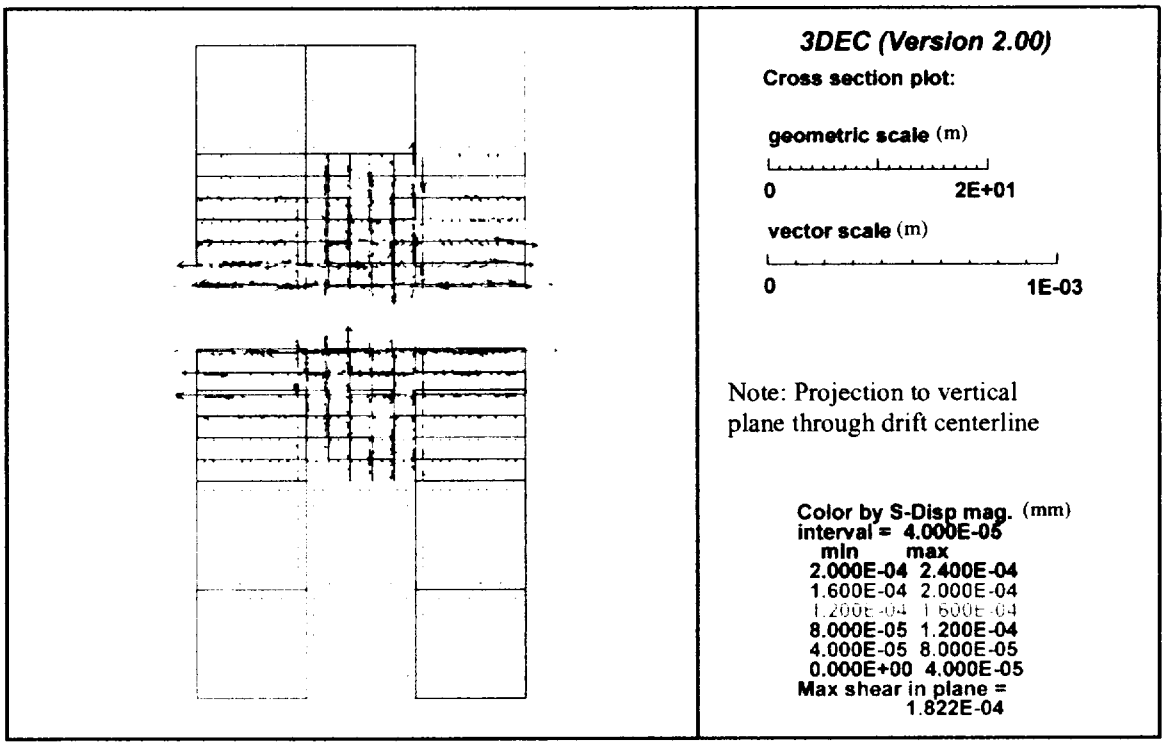


(a) XY Plane

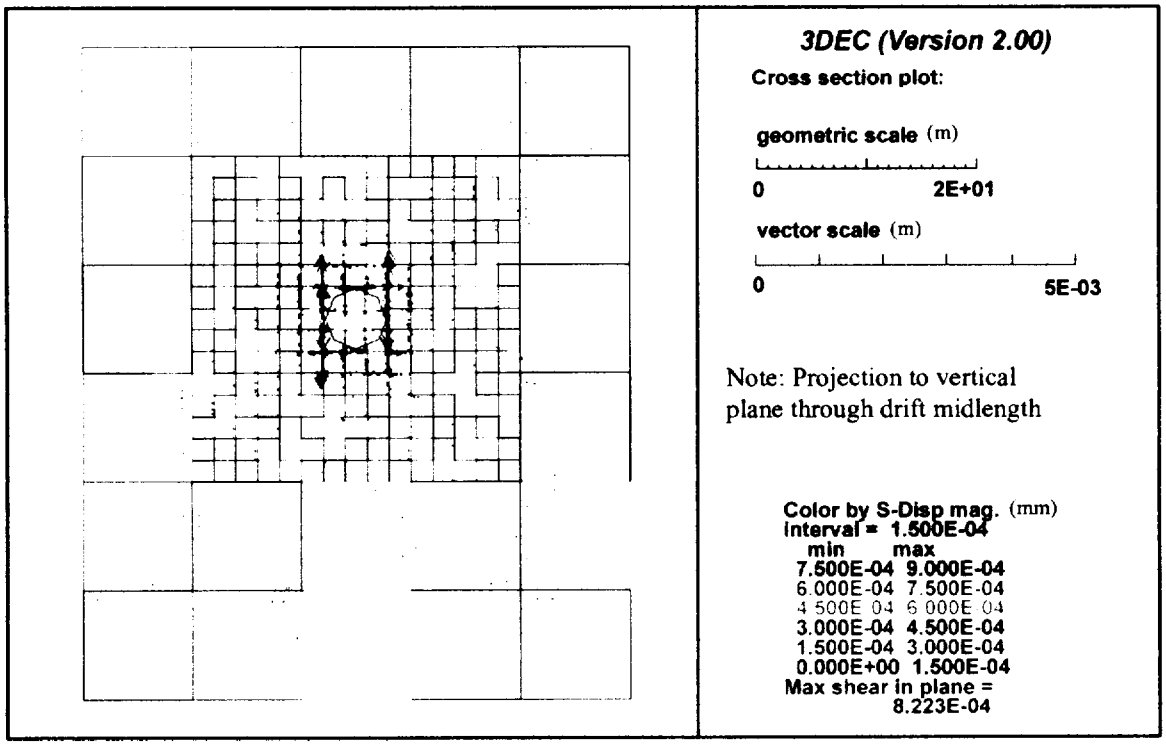


(b) YZ Plane DTN: LL000313504243.036

Figure IV-4. Joint shear displacements at 150 years, late post-ventilation heating phase

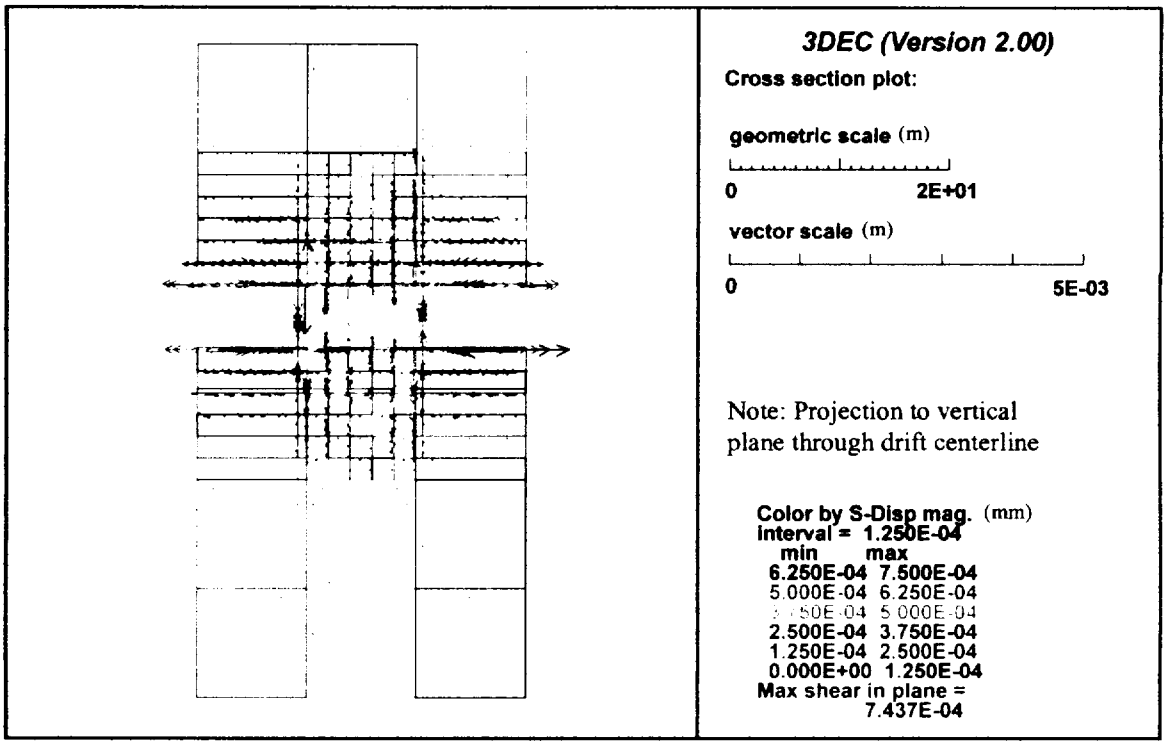


(a) XY Plane

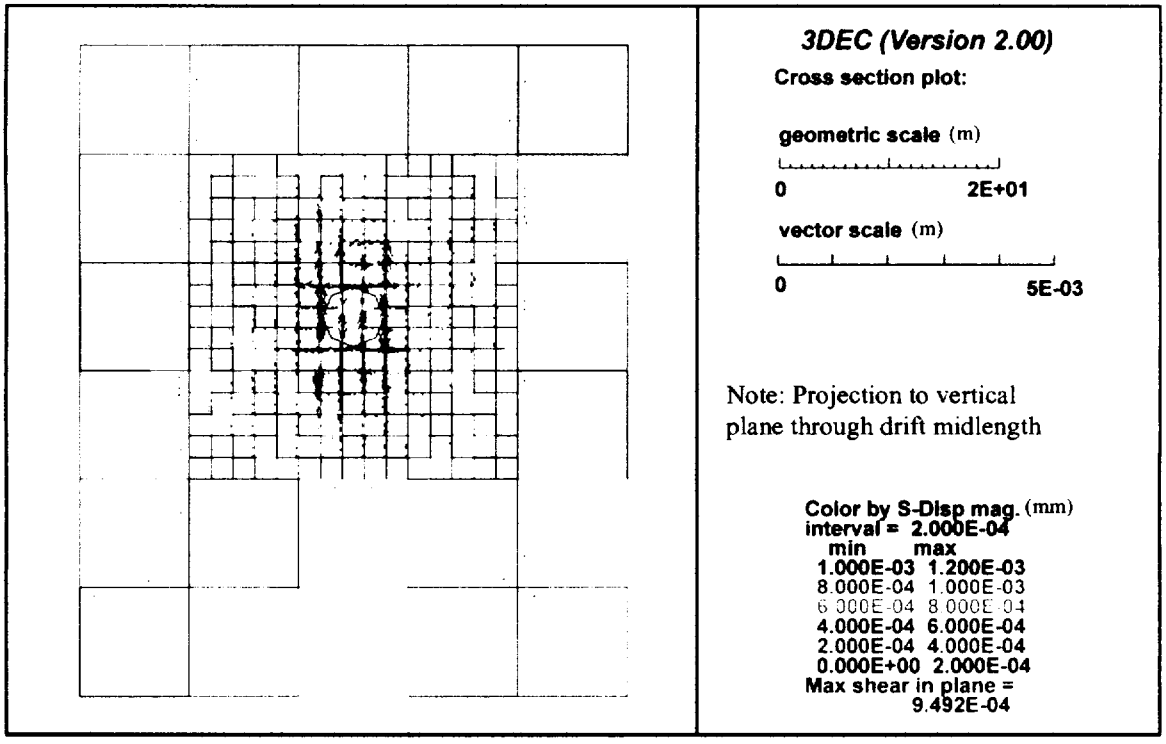


(b) YZ Plane

DTN: LL000313504243.036

Figure IV-5. Joint shear displacements at 155 years, early cool-down phase

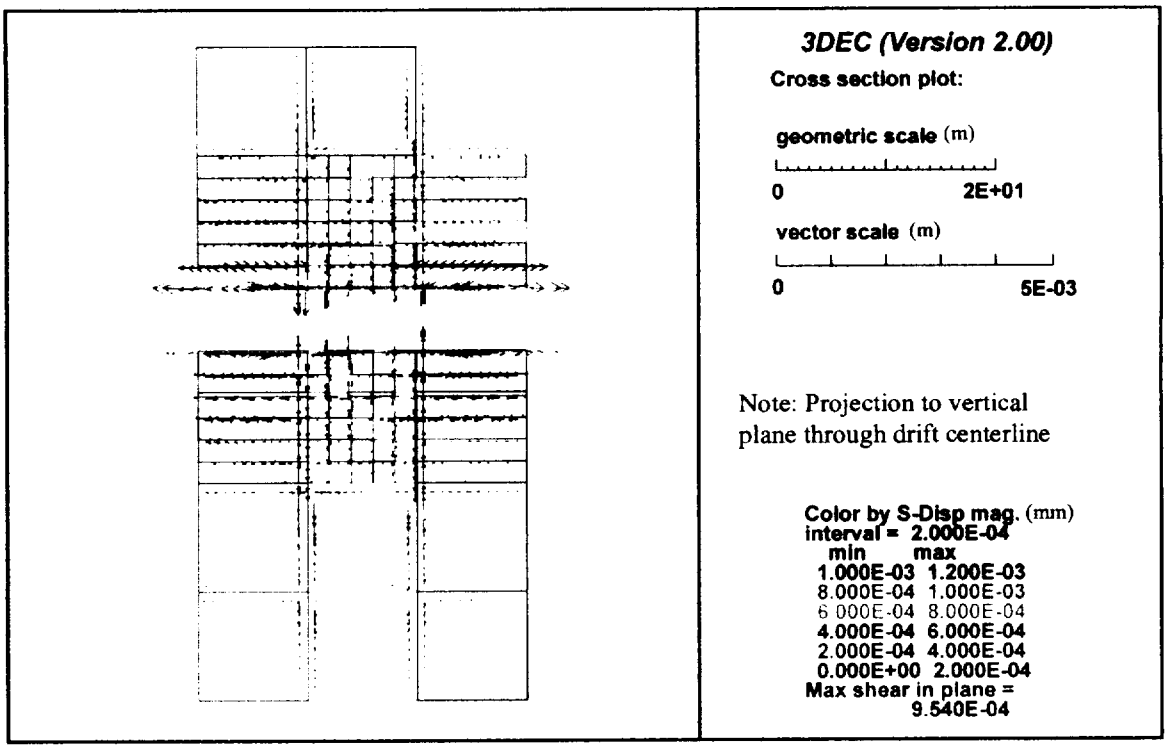


(a) XY Plane

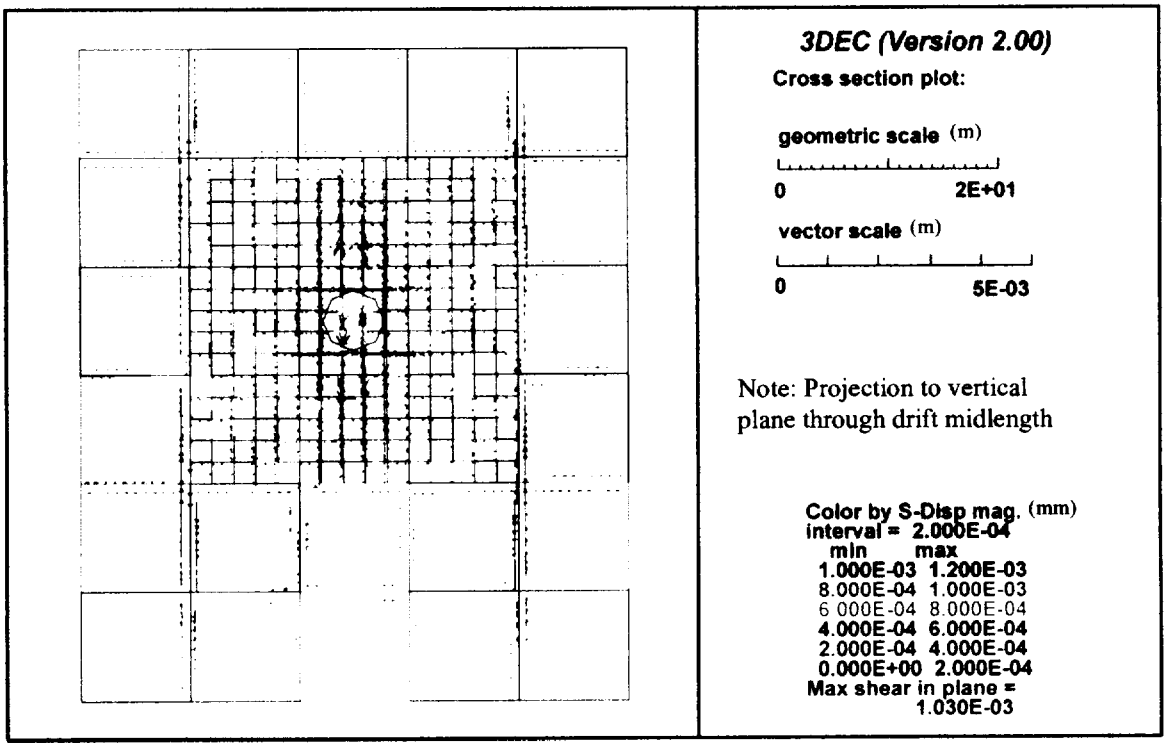


(b) YZ Plane

DTN: LL000313504243.036

Figure IV-6. Joint shear displacements at 200 years, middle cool-down phase

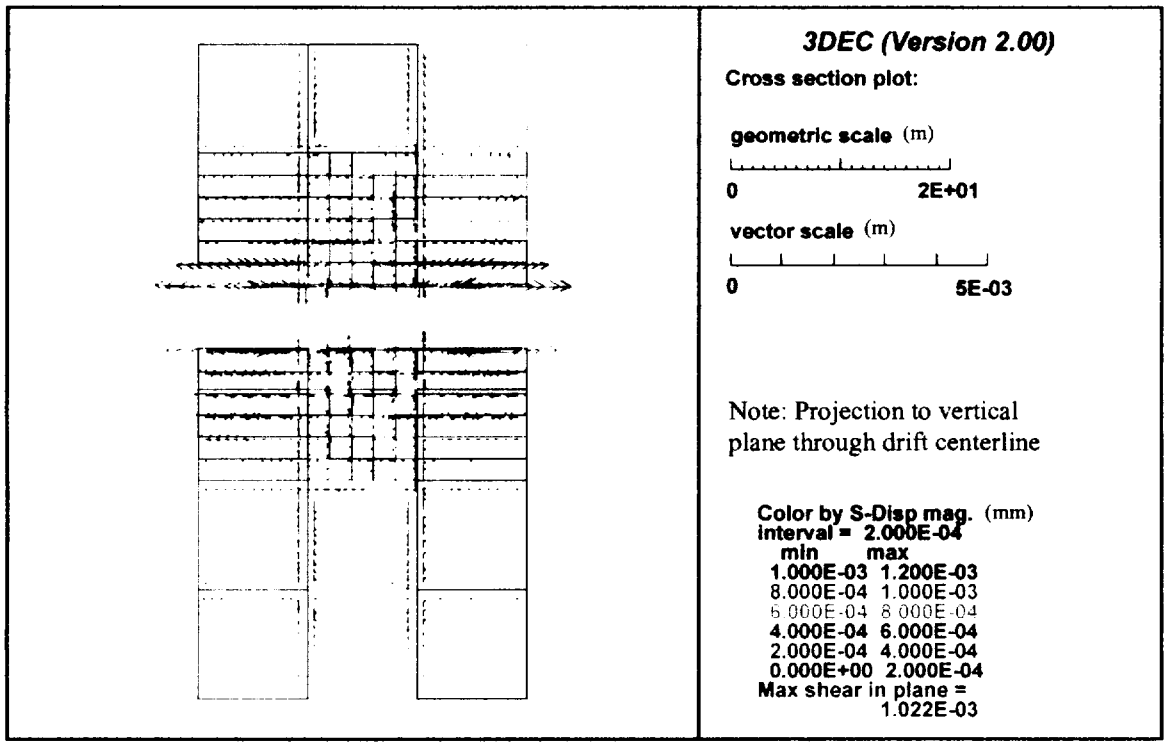


(a) XY Plane

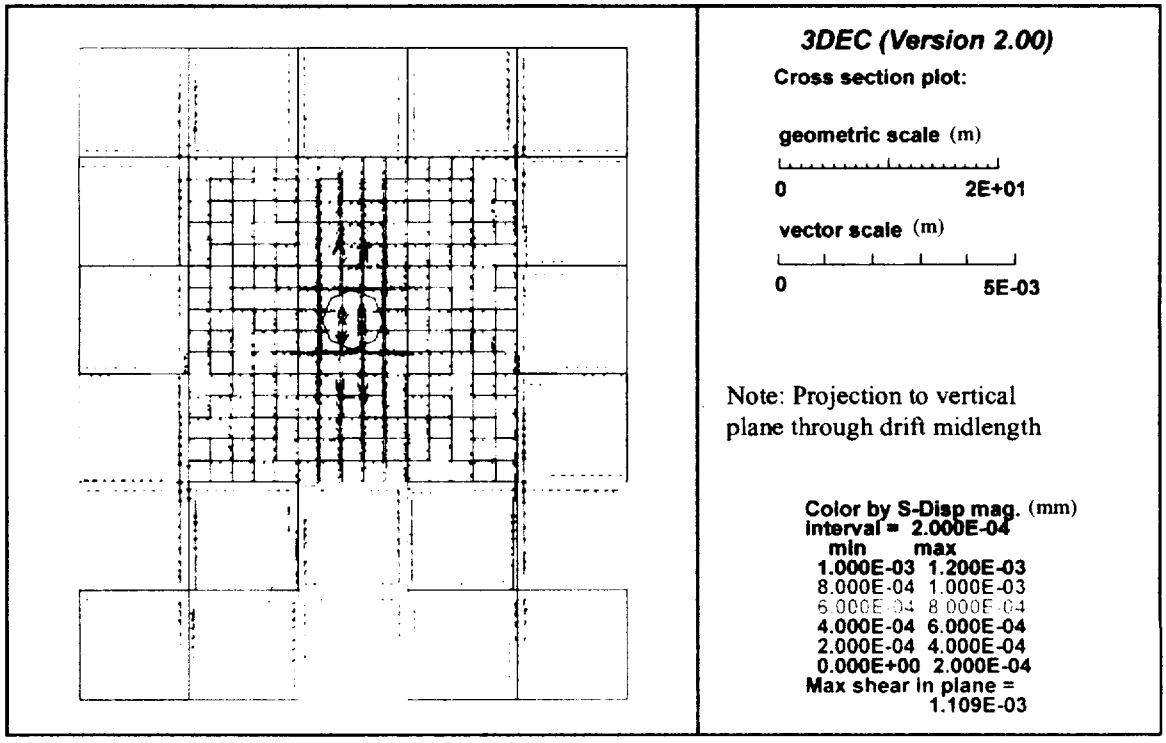


(b) YZ Plane

DTN: LL000313504243.036

Figure IV-7. Joint shear displacements at 1000 years, late cool-down phase